PhD degree in Molecular Medicine

Curriculum in Molecular Oncology

European School of Molecular Medicine (SEMM),

University of Milan and University of Naples “Federico II”

Faculty of Medicine

The study of Snap29 in mitosis and in CEDNIK pathogenesis

Valeria Mastrodonato

IFOM, Milan

Registration n. R10735

Supervisor: Prof. Thomas Vaccari

IFOM, Milan

Academic year 2017-2018

Table of contents

List of abbreviations

AP Autophagosome

CEDNIK Cerebral Dysgenesis, Neuropathy, Ichthyosis and Keratoderma

CLEM Correlative-light electron microscopy

CME Clathrin mediated endocytosis

CNS Central Nervous System

COPI Coated Complex I

COPII Coated Complex II

EE Early Endosome

ER Endoplasmic Reticulum

ERGIC ER Golgi Intermediate Compartment

ESCRT Endocytic Sorting Complex

GA Golgi Apparatus

IC Intracellular Compartment

INM Inner Nuclear Membrane

ISV Intersegmental Vessel

KMN Knl-1 complex, Mis12 complex, Ncd80 complex

KT Kinetochore

LE Late Endosome

MT Microtubule

MTC Multisubunit Tethering Complexes

MVB Multi Vesicular Body

NE Nuclear Envelope

NPC Nuclear Pore Complex

NSF *N*-ethymaleimide Sensitive Fusion

ONM Outer Nuclear Membrane

PNS Peripheral Nervous System

PM Plasma Membrane

RE Recycling Endosome

SAC Spindle Assembly Checkpoint

SNAP Synaptosomal Associated Protein

SNARE Soluble NSF Attachment Protein REceptor

Syb Synaptobrevin

SV Synaptic Vesicle

TGN *Trans*-Golgi Network

VAMP Vesicle Associated Membrane Proteins

Figures Index

During my phD I have contributed to the following publications:

Horner, D.S. et al., 2017. ESCRT genes and regulation of developmental signaling. *Seminars in Cell & Developmental Biology*, 74, pp. 29–39.

Mastrodonato, V. et al., 2016. Autophagy in Nonmammalian Systems. In *eLS*. Chichester, UK: John Wiley & Sons, Ltd, pp. 1–6.

Morelli*, E., Mastrodonato*, V., et al., 2016. An essential step of kinetochore formation controlled by the SNARE protein Snap29. *Embo Journal*, 35(20), pp.1–40.

Morelli, E. et al., 2014. Multiple functions of the SNARE protein Snap29 in autophagy, endocytic, and exocytic trafficking during epithelial formation in Drosophila. *Autophagy*, 10(12), pp.2251–2268.

* Co-first authorship

Figures 21A and 29 were made by Elena Morelli

Electron microscopy was performed in collaboration with Galina Beznoussenko and Alexander Mironov.

Zebrafish embryo microinjections were performed with the help of Gianluca Deflorian and Laura Ferrari (IFOM zebrafish facility).

Hematoxylin and eosin staining on paraffin sections were performed by Federica Pisati (IFOM tissue processing facility).

1. Abstract

Intracellular trafficking includes a series of regulated events that allow the transport of proteins and macromolecules. A key step of intracellular trafficking is the fusion between a containing-cargo vesicle and a target membrane, mediated by Soluble *N*-ethylmaleimide-sensitive fusion Attachment protein REceptor (SNARE) proteins. Snap29 is a cytosolic SNARE protein containing two SNARE domains required for fusion, whose specificity and activity is unclear. During the last few years, we and others have discovered that Snap29 is a key regulator of autophagy required for fusion of autophagosomes with lysosomes, the last trafficking step before cargo degradation. During the first part of my PhD, I contributed to uncover a novel function of Snap29 using *Drosophila melanogaster*, as a model system. We demonstrated that during mitosis Snap29 is repurposed as an outer kinetochore component, and that its localization depends on known kinetochore proteins, but does not require membranes or the autophagy process. Depletion of Snap29 in *Drosophila* S2 cells leads to cell division defects, such as failure to form a proper metaphase plate and segregate chromosomes correctly, or formation of aberrant mitotic spindles, ultimately leading to generation of micronuclei, aneuploidy and cell death. In addition, we observed that Snap29 is fundamental to determine correct tissue development and homeostasis in *Drosophila*, since its depletion or mutation determines disorganization and multilayering in the follicular epithelium, and tumor-like tissue alterations in eye imaginal discs. Since mutations affecting autophagy genes are not sufficient *per se* to induce such disruptions in the epithelial architecture, we hypothesize that these defects might be due to loss of Snap29 activity during mitosis.

Mutations of *SNAP29* human gene cause a rare neurocutaneous syndrome called CEDNIK (Cerebral Dysgenesis, Neuropathy, Ichthyosis and Keratoderma), which causes

severe neurological and dermatological congenital manifestations associated with short life expectancy. So far, the most investigated aspects of this syndrome are dermatological alterations, likely caused by the impairment of SNAP29 activity during membrane trafficking. Other symptoms such as neonatal feeding impairment, muscle hypotonia, and neurological defects were never investigated neither in human patients nor in CEDNIK animal models. To study uncharacterized CEDNIK traits, in the second part of my PhD, we took advantage of an uncharacterized *snap29* mutant in zebrafish. The presence of CEDNIK traits in homozygous mutant fish, such as keratoderma and microcephaly, indicated that *snap29* zebrafish mutant could be a valid CEDNIK disease model. Importantly, by studying the homozygous fish, we found that they display trigeminal nerve formation and axon branching defects, suggesting the requirement of Snap29 for correct nervous system development. Such alterations correlate with mouth opening problems and swimming difficulties, as well as feeding impairment. In addition, we are currently characterizing defects in muscle fibers organization and angiogenesis and we are assessing whether Snap29 plays a role in autophagy and cell division *in vivo*.

Overall, our findings demonstrate that Snap29 is a key regulator of cell division and shed light on uncharacterized aspects of CEDNIK syndrome, highlighting a pivotal role of Snap29 in nervous system development.

2. Introduction

2.1. SNARE proteins and regulation of membrane trafficking

2.1.1 Intracellular trafficking

Intracellular trafficking involves a series of events that allow transport of proteins and macromolecules between intracellular organelles or to and from the plasma membrane (PM). Based on transport direction, it is possible to distinguish two main different pathways, the endocytic and the exocytic pathways (reviewed by Bonifacino & Glick 2004). The endocytic pathway involves vesicles internalization from the PM to intracellular compartments (ICs), while exocytosis involves the transport of vesicles containing recycled or newly synthesized molecules from IC to the PM and the extracellular space (Fig. 1) (reviewed by Gould & Lippincott-Schwartz 2009).

During endocytosis, internalized vesicles are delivered first to the early endosome (EE), which can matures into a multi vesicular body (MVB) or late endosome (LE). The MVB (or LE) is the organelle that ushers endocytic cargoes to the degradation pathway. Indeed, the MVB fuses with a lysosome, in which cargoes are degraded by specific enzymes called hydrolases (reviewed by Rohrer & Kornfeld 2001). An alternative degradation pathway is that of autophagy, which allows degradation of long-lived cytoplasmic proteins and of entire organelles. In the final step of autophagy, the mature autophagosome (AP), a double-membrane organelle that generates from the endoplasmic reticulum (ER), also fuses with the lysosome to degrade its content (Hamasaki et al. 2013).

Exocytic vesicles mainly originate from EEs and from the Golgi apparatus (GA). The GA is composed by different regions, such as *cis*-Golgi, the *medial*-Golgi and the *trans*-Golgi network (TGN). The *cis*-Golgi is the portion facing the ER, while the TGN faces the PM

(Kinseth et al. 2007). Transmembrane or membrane-associated proteins that are newly synthesized in the ER are, for the most part, transported to the GA, where they are post-translationally modified, and from there to the PM to be finally secreted (Spang et al., 2013). In addition, cargoes reaching the EE during endocytic internalization not only undergo degradation, but can also be redirected to the PM, by being routed to recycling endosomes (RE) (reviewed by Fader & Colombo 2009).

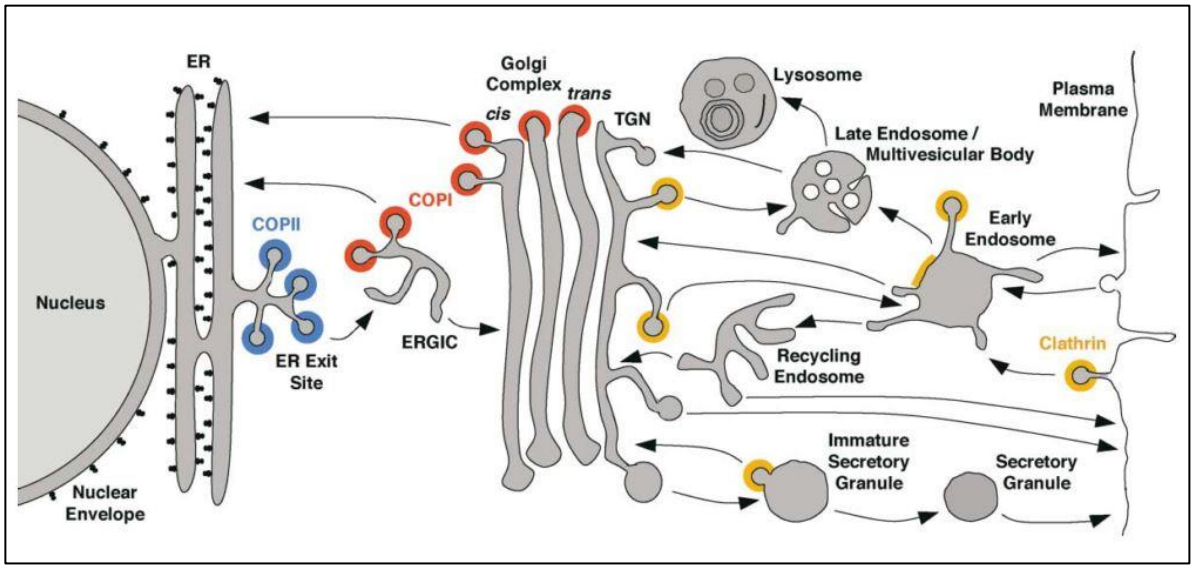

Figure 1. Intracellular trafficking pathways. Adapated from Bonifacino & Glick, 2004.

2.1.2 SNARE proteins promote membrane fusion

The two key events of intracellular trafficking are vesicle budding and vesicle fusion. Vesicle budding requires protein coats, such as clathrin and coated protein complex I and II (COPI and COPII). In particular, clathrin is involved in coating membranes that are endocytosed from the plasma membrane and those that bud from TGN directed to EE or LE (Fig. 1) (reviewed by Le Roy & Wrana 2005). COPI proteins promote budding and retrograde transport of vesicles between Golgi stacks and from *cis*-Golgi to the ER. COPII proteins regulate vesicle budding and anterograde transport from the ER toward the intermediate

compartment between ER and Golgi apparatus (ERGIC), and ultimately toward *cis*-Golgi. Moreover, protein coats also play an active role in cargo recognition and selection (reviewed by Brandizzi & Barlowe 2013).

The fusion between a vesicle and a target membrane is mediated by the interaction between Soluble *N*-ethylmaleimide sensitive fusion Attachment Protein REceptor (SNARE) proteins (reviewed by Rizo & Südhof 2002). SNAREs are a superfamily of proteins characterized by the presence of at least one coiled coil α-helical domain called SNARE domain. Most of the characterized SNARE proteins possess a transmembrane domain (TM), but few of them associate with membrane through palmitoylated cystein residues (reviewed by Ungar & Hughson 2003).

SNARE proteins, such as vesicle-associated membrane proteins (VAMP) or synaptobrevins, associate either to vesicles (v-SNAREs), or to target membranes (t-SNAREs), as in the case of syntaxins and SNAPs (SyNaptosomal Associated Proteins) (Fig. 2). The prevailing paradigm posits that transport vesicle carrying a single SNARE domain binds a target membrane carrying three SNARE domains (one provided by a syntaxin and two provided by SNAP protein family members) forming a four-helix bundle called *trans*-SNARE complex or SNAREpin (reviewed by Jahn & Scheller 2006).

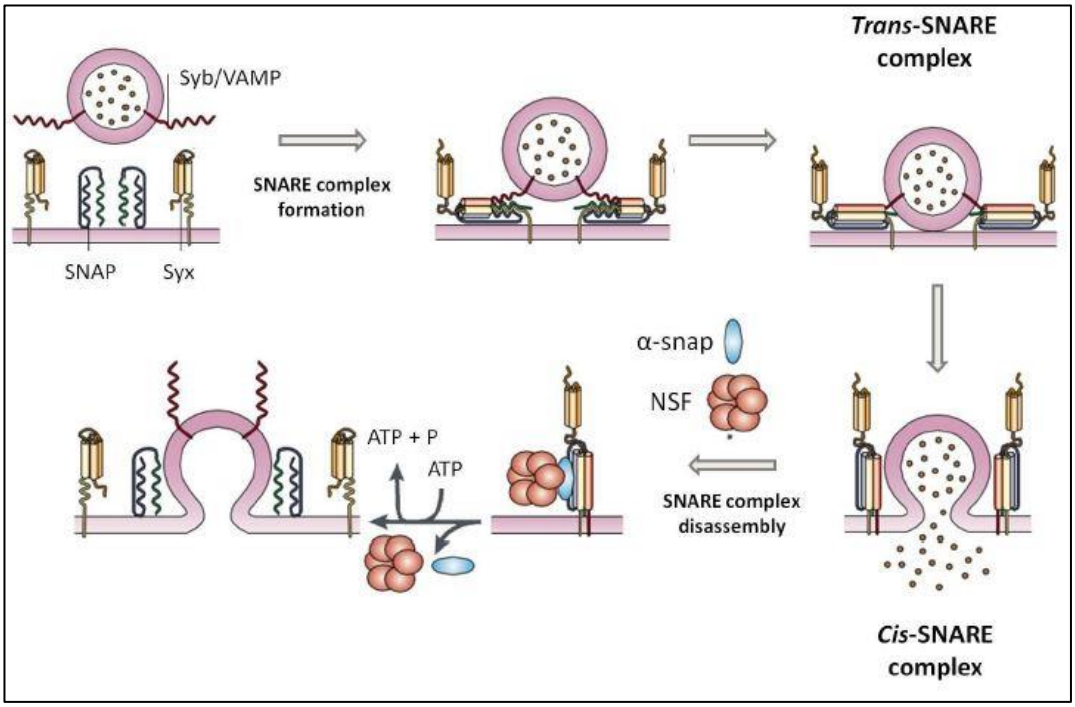

Figure 2. SNARE complex formation mediates membrane fusion between a vesicle and a target membrane. SNARE proteins associate in a *trans*-SNARE complex, which induces the opening of a fusion pore. After membrane fusion, the *trans*-SNARE complex assumes a *cis* conformation and it is disassembled by the NSF ATPase and its adaptor α-SNAP. SNARE proteins are recycled and available for a new fusion process. Adapted from Rizo & Südhof, 2002.

The *trans*-SNARE complex assumes a conformation that allow membrane fusion by opening a fusion pore between the two membranes. Once fusion occurs, the *trans*-SNARE complex becomes a *cis*-SNARE complex, since all SNAREs now reside on the same membrane. After fusion, the disassembly of the *cis*-SNARE complex is achieved through the activity of the ATPase *N*-ethylmaleimide-sensitive fusion protein (NSF) and its adaptor α-SNAP. This event, together with the re-delivery of v-SNAREs to their originating compartment, ensures that SNARE proteins are available for repeated vesicle fusion processes (Zhao et al. 2007; Rotem-Yehudar et al. 2001).

SNARE proteins have been also classified according to structural features of the SNARE complex (Fig. 3). Crystallographic analysis of the four-helix bundle highlighted that it

is held together mainly by several layers of hydrophobic interactions. These are centered around a single hydrophilic interaction, called '0' or 'ionic' layer, composed by one arginine residue (R) often carried by the v-SNARE, called in this case R-SNARE, and three glutamine (Q) contributed by t-SNAREs, called Q-SNAREs (including Qa, Qb and Qc) (reviewed by Jahn & Scheller 2006).

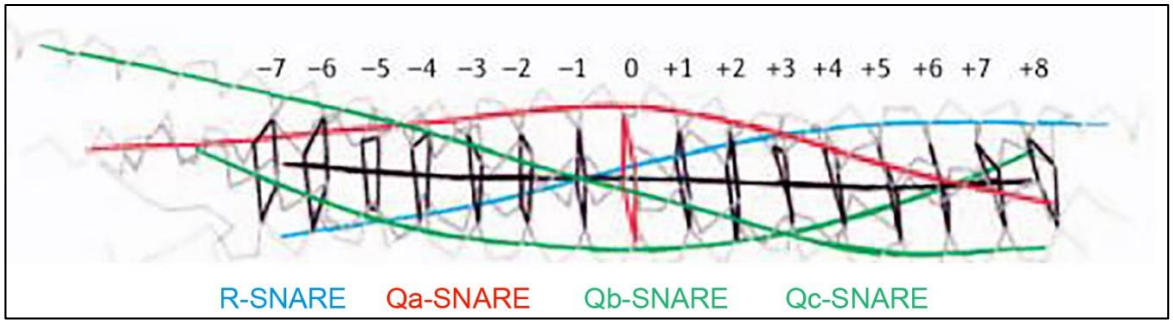

Figure 3. SNARE four-helix bundle. Hydrophobic interactions between R-, Qa-, Qb and Qc SNARE are represented in black, while the unique hydrophilic interaction, constituting the '0' or 'ionic' layer is shown in red. Adapted from Jahn & Scheller, 2006.

Combination of different R- and Q-SNAREs confers specificity to each membrane fusion event. Further specificity and efficiency of the fusion process are also ensured by Rab proteins, Sec1/Munc18 (SM) proteins and tethering factors (Carpp et al. 2006).

2.1.3 Rab proteins, SM proteins and tethering factors confer specificity to SNARE-mediated fusion events

Rab proteins constitute the largest family of Ras GTPase proteins, with more than 60 members identified in humans (revieweded by Zerial & Mcbride 2001). The GTP-bound forms of Rab proteins interact with Rab effectors, which are an heterogeneous group of proteins that confers specificity to intracellular membrane trafficking events (reviewed by Zhen & Stenmark 2015; Gillingham et al. 2014). For instance, Rab5 and its effectors Rabaptin-5, Rabex-5 and early

endosome antigen 1 (EEA1) form an oligomeric complex on the membrane together with NSF. This complex confers high efficiency to EE fusion process, since it allows vesicle docking through EEA1 that transiently interacts with the t-SNARE syntaxin 13, thus promoting fusion pore opening (McBride et al. 1999).

SM are evolutionary conserved proteins that envelope the assembling SNARE complex, allowing correct positioning of SNAREs and ensuring appropriate timing to fusion events. Indeed, recent data suggest that Munc18-1 interacts with the t-SNAREs syntaxin 1 and the SNAP protein SNAP25, thus constituting a ternary complex, which is both protected from NSF/α-SNAP disassembly and highly prone to bind the v-SNARE synaptobrevin. This SNARE configuration occurs during neuronal exocytosis, mediating the fusion between synaptic vesicles and the axonal presynaptic membrane (Jakhanwal et al. 2017).

Tethering factors can be divided in multisubunit tethering complexes (MTCs) or long coiled coil proteins like Golgins, p115 and GM130 (reviewed by Dubuke & Munson 2016; Cheung & Pfeffer 2016). However, both MTCs and long coiled coil tethering factors promote SNARE proteins interaction, by bridging vesicles with target membranes, but while long coiled coil tethering factors are involved in the initial stage of tethering, MTCs mediate *trans*-SNARE complex assembly (reviewed by Hong & Lev 2014; Chen et al. 2007). For example, the heterohexameric homotypic fusion and vacuole protein-sorting (HOPS) is a MTC complex required for vacuoles fusion in *Saccharomyces cerevisiae* (Wickner 2010). The SM proteins Vps33 is subunit of the HOPS complex that binds SNARE proteins Vam3 and Nyv1 to form an early SNARE complex intermediate, in which the two SNAREs are correctly oriented and primed for the full *trans*-SNARE complex assembly with Vam7 (Baker et al. 2015).

2.1.4 The SNAP protein family

The SNAP proteins family comprises four members in mammals, which are SNAP23, SNAP25, SNAP29 and SNAP47 (Fig. 4). The peculiarity of these proteins is the presence of two SNARE domains.

SNAP23 is an ubiquitously expressed SNAP protein, involved in a multitude of exocytosis events occurring in different cellular types, such as adipocytes, mast cells and platelets (Kawaguchi et al. 2009; reviewed by Suzuki & Verma 2008; Polgár et al. 2003). Moreover, in human endothelial cells, SNAP23 associates with syntaxin 4, VAMP3 or VAMP8, thus constituting a SNARE complex required for the exocytosis of von Willebrand factor, which is a glycoprotein required for hemostasis (Zhu et al. 2015).

SNAP25 is so far the most characterized member of the SNAP family proteins and is expressed mainly in the nervous system, where it mediates synaptic vesicles (SVs) fusion and exocytosis (reviewed by Wojcik & Brose 2007). Indeed, SNAP25 is present, together with syntaxin 1, on the axonal presynaptic membrane, where it assembles with synaptobrevin/VAMP2 (Syb2) anchored to the synaptic vesicle membrane into a ternary complex, required for neurotransmitters and peptides release in the intersynaptic space (reviewed by Südhof & Rothman 2009). Both SNAP23 and SNAP25 anchor to the target membrane through post-translational palmitoylations, occurring in one or more cysteine residues located in the linker region between SNARE 1 and SNARE 2 domains (Rapaport et al. 2010).

In contrast to SNAP23 and SNAP25, SNAP47 does not possess any palmitoylated cysteine residue. However, similarly to SNAP25, SNAP47 is a neuronal SNAP expressed mainly in mammalian neurons (Holt et al. 2006). The association of SNAP47 with SNAP25 and VAMP2 is involved in the secretion of the brain-derived neutrophic factor (BDNF) in

mouse, which is essential for axonal growth and maturation. Nevertheless, SNAP47 does not participate in SVs exocytosis and recycling, suggesting a possible modulation role in favoring protein-protein interaction between SNAP25, VAMP2 and syntaxin 1, rather than a direct involvement in SNARE complex formation, considering its lower affinity binding with syntaxin 1 (Shimojo et al. 2015; Holt et al. 2006).

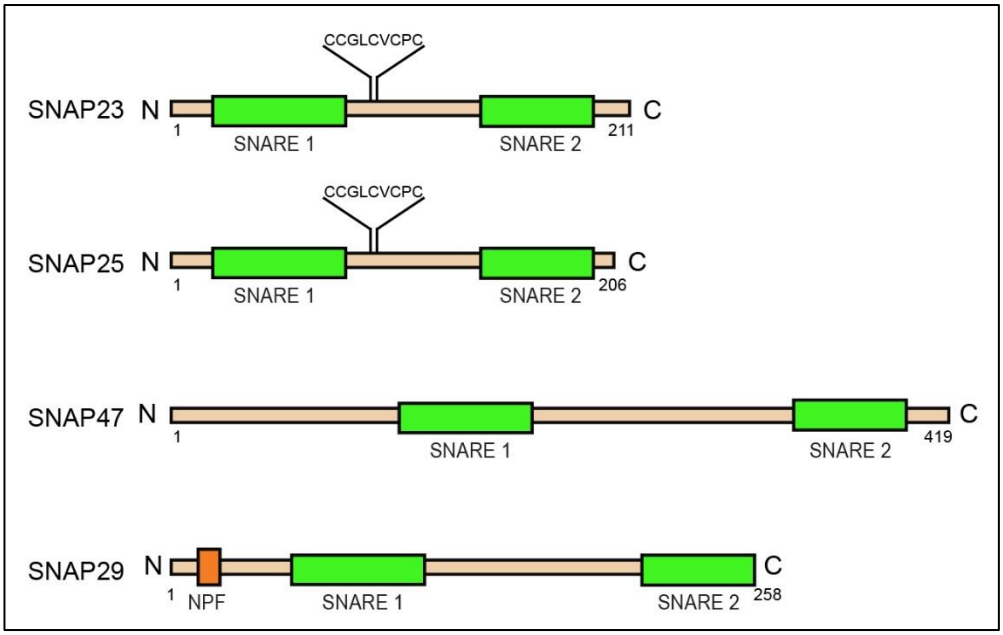

Figure 4. SNAP protein family. All the four members of SNAP protein family possess two SNARE domains. SNAP47 and SNAP29 lack palmitoylated sites that allow membrane anchoring. Differently from others, SNAP29 has a NPF motif, which interacts with endocytic adaptors such as EHD1. Adapted from Rapaport et al., 2010.

Differently from other members of the SNAP family, SNAP29 possesses a short three-amino acids motif at the N-terminus called NPF (asparagine, proline, phenylalanine), but similarly to SNAP47, SNAP29 lacks palmitoylated residues required for membrane anchoring, consistent with a mainly cytoplasmic localization (Rapaport et al. 2010).

2.1.5 SNAP29 functions

SNAP29 is highly conserved and has been proposed to be a ubiquitous SNARE protein (Fig. 5). When associated to membranes, SNAP29 partially localizes with a number of intracellular organelles, such as the PM, EE and RE, with ER and the Golgi apparatus (Morelli et al. 2014).

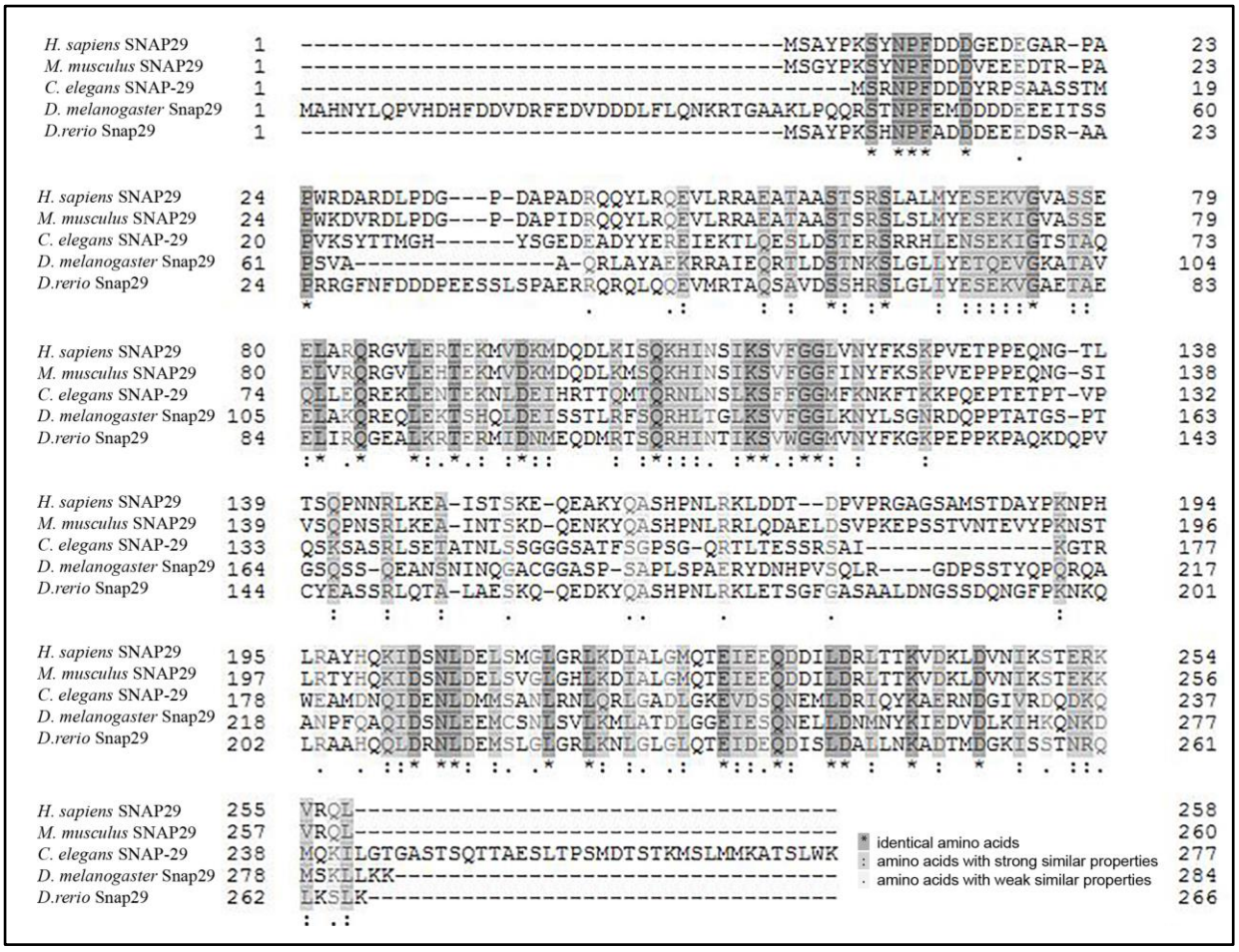

Figure 5. Multiple sequence alignment of SNAP29 protein sequence from different eukaryotic species. Residues are colored according to their conservation. Performed with http://uniprot.com.

The SNAP29 NPF motif was shown to interact with the Eps15 homology domain (EHD) family member EHD1 (Rotem-Yehudar et al. 2001). EHD1 is involved with the lipid modifier phospholipase A2 (cPLA2α) in membrane vesiculation (Cai et al. 2012). The interaction between SNAP29 and EHD1 is required for the assembly of primary cilium (PC), which is an

organelle composed by 9+2 microtubules (MTs) and surrounded by a membrane structure in both human cells and *Danio rerio* (hereafter called zebrafish). In particular, EHD1 is required for vesicles formation from preexisting membranes that fuse together and assemble in a membrane structure that envelopes cilium MTs, through the action of SNAP29-containing SNARE complex (Lu et al. 2015).

Studies in *Caenorhabditis elegans* (*C. elegans*) demonstrated the pivotal role of SNAP29 during the exocytic trafficking in the intestine. SNAP29 was shown to interact with plasma membrane syntaxins 1 and 4, with the endosome/lysosomes syntaxin 17 and with the *cis*-Golgi syntaxin 5. Indeed, upon SNAP29 depletion, the Golgi apparatus becomes fragmented and endosomes lose their morphology, consistent with inability of Golgi vesicles and organelles to fuse with their target membranes and to transport digestive enzymes and molecules required for proper intestinal epithelium development and homeostatis (Sato et al. 2011).

2.1.6 SNAP29 is involved in synaptic transmission

Besides the role that SNAP29 plays in general membrane trafficking events, it was demonstrated that SNAP29 is directly involved in synaptic transmission and in axon myelination process. In particular, SNAP29 was found at synapses of rat hippocampal neurons, where it acts as a negative modulator of synaptic vesicle exocytosis. Indeed, SNAP29 has been found to compete with α-SNAP for the binding with the SNARE complex formed by SNAP25, syntaxin 1A and VAMP2, thus inhibiting SNARE complex disassembly required for SNARE proteins and consequently synaptic vesicles recycling. According with this, overexpression of SNAP29 in presynaptic neurons inhibits synaptic transmission, whereas

knockdown of SNAP29 increases synaptic transmission efficiency (Su et al. 2001; Pan et al. 2005).

In addition, experiments performed using rat glial cells highlighted the role of SNAP29 in myelin biogenesis. Myelin is a highly specialized plasma membrane of glial cells called oligodendrocytes in the central nervous system (CNS) and Schwann's cells in peripheral nervous system (PNS). Myelin is required for electrical insulation of axon neuron projections. Myelin insulation properties rely on formation of a thick sheath full of lipids and proteins. These dock to the plasma membrane via SNARE-mediated vesicles transport, thanks to the interaction of SNAP29 with the GTPase protein Rab3A. Consistent with such function, SNAP29 is upregulated in sciatic nerve and Charcot-Marie-Tooth disease, two pathological conditions in which remyelination is enhanced to counteract the myelin degeneration (Schardt et al. 2009).

2.1.7 SNAP29 as a key regulator of autophagy

Very recently, a requirement for SNAP29 in the regulation of membrane fusion during autophagy has been reported for human and *Drosophila melanogaster* (hereafter *Drosophila*) tissues (Takáts et al. 2013; Guo et al. 2014; Morelli et al. 2014; Itakura et al. 2012). As previously mentioned, macroautophagy (autophagy here after) is a pathway required for the degradation of long-lived organelles and proteins. Differently from microautophagy and chaperone-mediated autophagy, autophagic degradation requires the formation of an intermediate double-membrane organelle called autophagosome that fully engulfs the cargo before fusion with lysosome (reviewed by Mizushima & Komatsu 2011).

Autophagosomes derive from an isolation membrane originating mainly from the ER. Once the material is engulfed, the so-called phagophore will mature in an autophagosome, by sequential recruitment of autophagy related proteins (Atg). The first step for the phagophore

maturation from the isolation membrane requires Atg12 and Atg5, which constitute a dimer that will recruit Atg16. The step required for autophagosome maturation foresees the coupling of microtubule-associated protein 1 light chain 3 (LC3I) with the phospholipid phosphatidylethanolamine, which turns it into LC3-II. Ubiquitinated proteins that need to be degraded are recognized by sequestosome 1 (SQSTM 1/p62), which in turn binds LC3 (Pankiv et al. 2007). The fusion between autophagosome and lysosome occurs via a SNARE complex composed by SNAP29, the autophagosome-associated syntaxin 17 and lysosome-associate SNARE VAMP8 (Fig. 6) (Itakura et al. 2012).

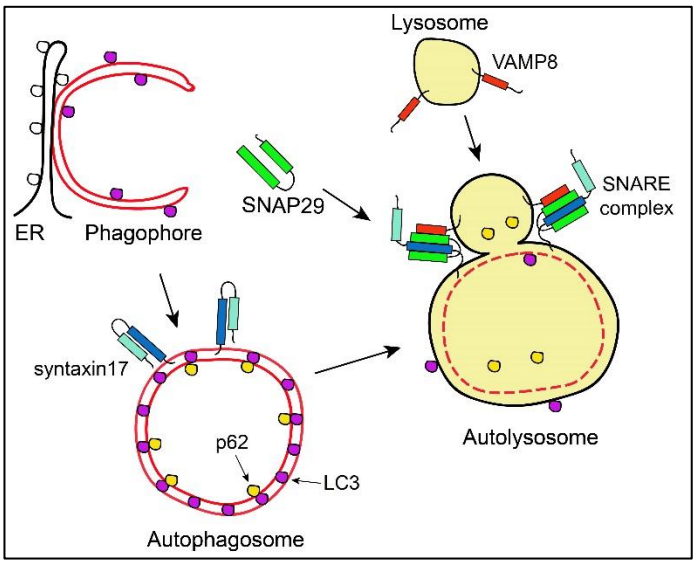

Figure 6. SNAP29 controls the fusion between an autophagosome and a lysosome. SNAP29 mediates the interaction between autophagosome and lysosome through the formation of a SNARE complex with the t-SNARE syntaxin 17 and the v-SNARE VAMP8. Adapted from Itakura et al., 2012.

The first interaction occurs between SNAP29 and syntaxin 17 through the tethering factor Beclin-1 (or Atg14). Beclin-1 possesses cysteine residues that favor oligomerization, thus stabilizing the binary interaction between SNAP29 and syntaxin 17, before the assembly with VAMP8 (Diao et al. 2015). Moreover, SNAP29 was recently demonstrated to be post-

translationally modified by an *O*-linked β-*N*-acetylglucosamine (O-GlcNAc) transferase on serine and threonine residues in both *C. elegans* and mammalian cells. Such modifications work as nutrient sensor, since upon normal feeding conditions, they are proposed to create a steric hindrance that prevents SNARE complex formation and that blocks autophagic degradation. On the contrary, upon starvation O-GlcNAc transferase activity is reduced, thus inducing the autophagic flux that works as a compensatory mechanism to recover nutrients (Guo et al. 2014).

The importance of fusion between autophagosomes and lysosomes mediated by SNAP29 was demonstrated by the accumulation of autophagosomes occurring in Snap29 depleted *Drosophila* tissue (Morelli et al. 2014; Takáts et al. 2013). Impairment in this late autophagy step can hit also viral replication in human cells. Indeed, autophagy works also as a primary immune response that the host cell uses to eliminate virus particles. Human parainfluenza virus type 3 (HPIV3) blocks autophagosome-lysosome fusion by competing with the coiled coil SNARE 1 domain of both SNAP29 and syntaxin 17 and inhibiting their binding, thus favoring virus particle retention (Ding et al. 2014).

Recent findings demonstrated the involvement of SNAP29 not only in degradative autophagy, which implies the fusion of autophagosomes with lysosomes, but also in secretory autophagy. Secretory autophagy occurs in response to lysosomal stress, which can be triggered by inflammatory stimulation. This pathological condition implies the secretion of pro-inflammatory molecules such as interleukin-1β (IL-1β), which after its proteolytic cleavage activation, binds its receptor TRIM16 residing on the lysosomal membrane. IL-1β is sequestered within the autophagosome through the binding of its receptor TRIM16 with the SNARE Sec22b, residing on the autophagosome membrane. Autophagosomes containing IL-1β- fuse with the plasma membrane through the formation of a SNARE complex involving Sec22b, syntaxin 3 or 4 and SNAP29 (Kimura et al. 2017).

2.1.8 Mutations in *SNAP29* human gene cause CEDNIK syndrome

Inactivating mutations in human *SNAP29* gene are responsible for CEDNIK (Cerebral Dysgenesis, Neuropathy, Ichthyosis, palmoplantar Keratoderma), a rare autosomal recessive syndrome characterized by congenital neurological and dermatological alterations, including palmoplantar keratoderma and ichthyosis, microcephaly, neurogenic muscle atrophy, reduced peripheral nerve conduction, corpus callosum abnormalities and cortical dysplasia. The severity of the traits determines a radical shortening of lifespan (between 5 and 12 years) (Fuchs-Telem et al. 2011; Rapaport et al. 2010; Sprecher et al. 2005). Skin biopsy of CEDNIK patients revealed a thickened stratum corneum (hyperkeratosis), compared to control patients. Further ultrastructural analysis of the skin of CEDNIK mouse models and zebrafish embryos transiently depleted of Snap29, show the accumulation of empty lamellar granules in upper epidermal layers (Sprecher et al. 2005; Schiller et al. 2016; Li et al. 2011). In physiological conditions, these granules are required for lipids and proteins transport from the GA to the surface of the epidermis, to ensure normal skin development and homeostasis (Fartasch 2004). Consistent with the role that SNAP29 plays in membrane fusion, CEDNIK patient-derived fibroblasts show a fragmented Golgi and an altered morphology of EE and RE (Rapaport et al. 2010).

Besides skin defects, CEDNIK patients present severe nervous system development defects, including psychomotor retardation, pachygyria and polymicrogyria. The last two manifestations refer respectively to abnormal neuronal migration in developing brain and to a brain cortex malformation, due to an excessive number of small and fused cortical convolutions (Sprecher et al. 2005). Since CEDNIK patient-derived neural tissue was not available and nervous system defects were not investigated in established CEDNIK models, the consequences of loss of SNAP29 in nervous system development remain elusive.

2.2 Membrane trafficking and the regulation of mitosis

2.2.1 Cell cycle and mitosis

The cell cycle is a highly regulated series of events that ensures correct DNA replication and its partition in two daughter cells, through four different phases called G1, S, G2 and M. During G1, cells grow and synthesize proteins and enzymes required for DNA replication occurring during S phase. In G2, cells continue to grow and start to synthesize molecules required for replicated DNA segregation as sister chromatids. G1, S, G2 are defined as interphase. The M phase, also called mitosis, is the multi-step process leading to correct sister chromatids segregation, and to cell content partition (cytokinesis) into two daughter cells (reviewed by Blow & Tanaka 2005).

The mitosis is divided into five stages known as prophase, prometaphase, metaphase, anaphase and telophase. Prophase starts with chromatin condensation into chromosomes and the nuclear envelope (NE) fragmentation. While the first is an ancestrally conserved event, the latter is different among eukaryotic species. In particular, the budding and fission yeast *Saccharomyces cerevisiae* (*S. cerevisiae*) and *Schizosaccharomyces pombe* (*S. pombe*) undergo a "closed" mitosis, in which NE does not break down (Smoyer & Jaspersen 2014). *Drosophila* (as well as *C. elegans*) undergoes a "semi-open" mitosis in which the nuclear envelope partially fenestrate, while in mammals mitosis is defined as "open", since the nuclear envelope completely breaks down (Fig. 7).

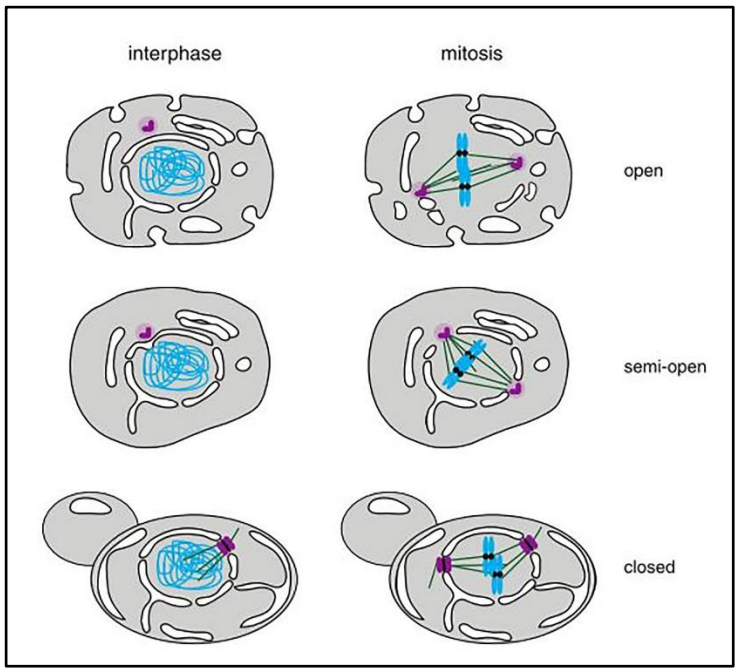

Figure 7. The nuclear envelope encounters different fates at the onset of mitosis. Interphase cells are shown on the left and mitotic cells are shown on the right. Mitotic cells undergo open, semi-open and closed mitosis, according to NE disruption or not at the onset of mitosis, respectively in mammals, *Drosophila* and yeast. Adapted from Smoyer & Jaspersen, 2014.

In most metazoans, NE fenestration or breakdown are required for the attachment of mitotic spindle fibers to a specific chromosome region called centromere, by means of a multi-protein plate-like structure assembled on it, which is called kinetochore (KT) (reviewed by Güttinger et al. 2009).

2.2.2 Mitotic spindle and motor proteins

Mitotic spindle consists of fibers of microtubules (MTs), which are highly dynamic polymers of α- and β-Tubulin subunit dimers that grow at their plus ends and depolymerize and shrink at their minus ends. MTs are polymerized from centrosomes, which act as microtubule-organizing centers (MTOCs) as well as, at least in part, from chromatin. In the mitotic spindle, the MT minus ends are anchored to MTOCs, while the plus ends target KTs (Haren et al. 2006). Each centrosome is composed by two orthogonal structures called

centrioles surrounded by an amorphous mass of proteins that include γ-Tubulin, a third variant of Tubulin. γ-Tubulin associates with other proteins to form a circular structure known as γ-Tubulin ring complex (γ-TuRC). This complex acts as a scaffold for α/β-Tubulin dimers that begin polymerization to form the mitotic spindle (Khodjakov & Rieder 1999). With the exception of *S. cerevisiae* and *S. pombe* in which MTOCs are part of the NE or inserted in it, in all other organisms MTOCs are located outside the nucleus and MTs of the developing mitotic spindle do not have access to chromosomes until the nuclear membrane fenestrates or breaks apart (reviewed by Sluder et al., 2014).

At the end of prophase, centrosomes start to migrate toward the opposite poles of the cell, while during prometaphase MTs budding from centrosomes attach to KTs. Metaphase begins when chromosomes align and form the metaphase plate, in which the two sister chromatids, which are attached to spindle MTs, are bi-oriented toward opposite spindle poles (Fig. 8). Chromosome alignment at the metaphase plate requires kinesin motor proteins, which move chromosomes toward the plus-end of MTs that are located at the center of the spindle plate. MT motors exert their activity in an ATP-dependent manner. In particular, kinesins are composed by two heavy chains in their motor head, which are responsible for the movement. Differently from kinesins, dynein motor is composed by a large protein complex comprising its adaptor Dynactin and moves toward minus-end MTs localizing mostly around centrosomes (reviewd by Hirokawa et al. 2009; Höök & Peter 2010). In addition, Dynein is involved in the stabilization of the binding between occurring chromosomes and MTs (Varma et al. 2008; Wu et al. 2006).

In anaphase, sister chromatids segregate toward opposite poles of the mitotic spindle. Sister chromatids separation occurs thanks to the degradation of cohesin molecules, that hold sister chromatids together, by the action of a protease called separase. In particular, during anaphase A, chromatids migrate by exploiting the pulling forces generated by KT-associated

MTs (kMTs), while during anaphase B the mitotic spindle is subjected to elongation occurring as a consequence of sliding forces, generated by motor proteins, between antiparallel MTs located between separating sister (reviewed by Goshima & Scholey 2010; Scholey et al. 2016). Moreover, experiments performed in *Drosophila* spermatocytes demonstrated that mitotic spindle elongation requires vesicles-derived membrane addition, mediated by the two exocytic complex subunits Exo84 and Sec8 (Giansanti et al. 2015).

During telophase, the mitotic spindle starts to be dismantled and, as soon as chromatids reach the opposite poles of the cell, DNA decondense and starts to be enclosed in a new nuclear envelope (Woodruff et al. 2010; Vas & Clarke 2008; Olmos et al. 2015).

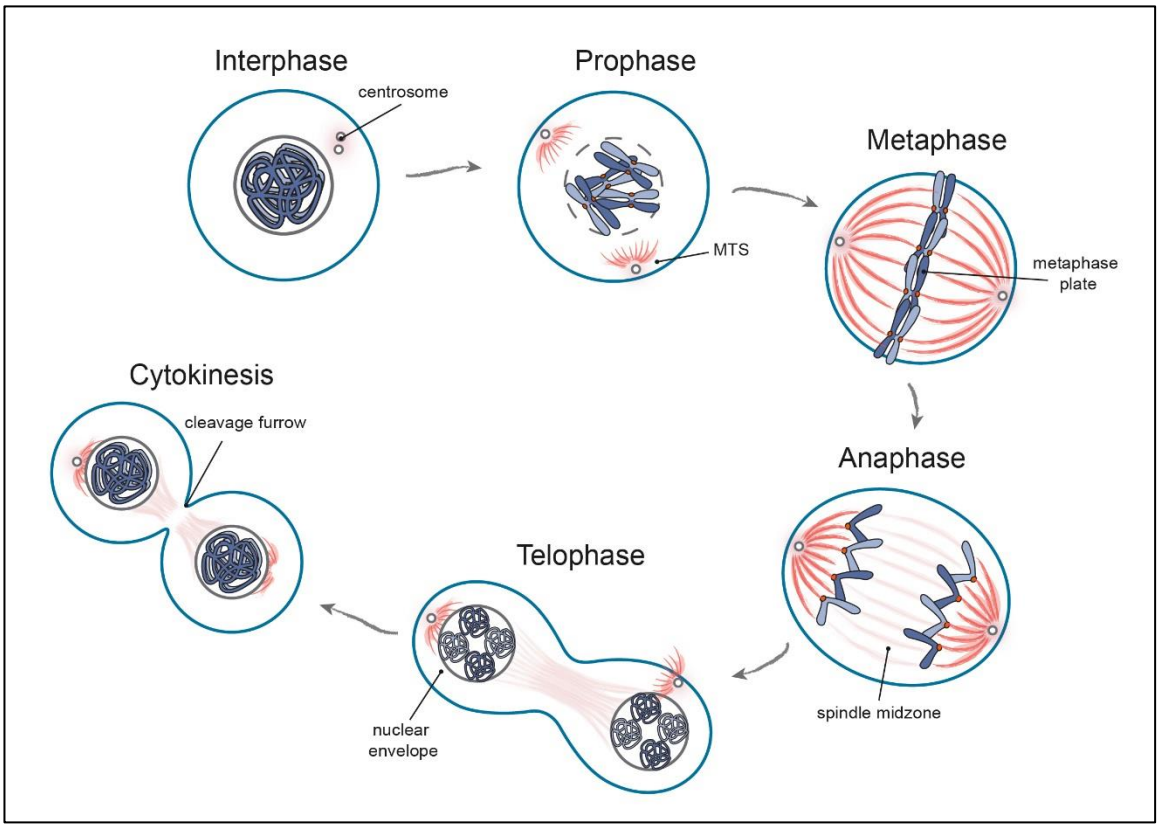

Figure 8. Mitosis and cytokinesis. During interphase, centrosomes are close to each other and chromatin is condensed. In prophase, centrosomes start to migrate toward opposite cell poles and nuclear envelope breakdown occurs. In metaphase, chromosomes form the metaphase plate, while the mitotic spindle extends in its entire length. In anaphase, sister chromatids migrate toward opposite spindle poles. In telophase, the nuclear envelope starts to form around decondensing nuclei of the two daughter cells and mitotic spindle disassembles.

During cytokinesis, the cytoplasm of daughter cells divides through the formation of a cleavage furrow.

2.2.3 Cytokinesis involves membrane trafficking proteins

Cytokinesis is a complex membrane-orchestrated process, which immediately follows mitosis and ensures equal distribution of the cytoplasm in the two daughter cells. Cell division is achieved through the positioning of an actin-myosin contractile ring that leads to the formation of a cleavage furrow (reviewed by Neto et al. 2011). Trafficking vesicles constitute a membrane reservoir for the formation of the cleavage furrow and require the GTPase Rab11 and exocyst subunits for fusion with one other (Giansanti et al. 2015; Arden et al. 2007). Concomitant to furrow formation, remnants of the disassembled mitotic spindle MTs become organized in an interconnecting bridge between the two daughter cells called midbody. Here, the SNARE protein VAMP8 mediates the fusion of Rab11-positive vesicles, producing a second ingression furrow (Schiel & Prekeris 2013). In addition, the midbody serves as an assembly platform for the endosomal sorting complex required for transport III (ESCRT-III) subunit CHMP4B, which promotes the final abscission of the two nascent daughter cells (Elia et al. 2011). Interestingly, recent works uncovered the role of autophagy for midbody residues clearance after the final abscission, according to two possible mechanisms (reviewed by Jongsma et al. 2014). The first requires asymmetrical inheritance of the midbody in one daughter cell, in which its components undergo ubiquitination and association with p62 for subsequent degradation (reviewed by Pohl & Jentsch 2009). The second mechanism posits a symmetrical inheritance of the midbody, which remains on the cell surface where is subsequently phagocytosed and degraded (Crowell et al. 2014)

2.2.4 Organelles inheritance during mitosis

In the last decade, complex and diverse mechanisms of inheritance of cytoplasmic organelles during mitosis have begun to come into focus. Here, we will only focus on those pertaining inheritance of the ER, NE and Golgi apparatus.

The NE is a specialized district of the ER comprising two distinct membrane bilayers, the inner and the outer nuclear membrane (INM and ONM). ONM can be considered as an ER extension, since they share a similar morphology, while the INM is directly associated with chromatin through integral membrane proteins (Jongsma et al. 2015). INM and ONM are interconnected by points of fusion containing the nuclear pore complexes (NPCs), which are multisubunit complexes mainly composed by 30 different proteins named nucleoporins (Nups) (Katsani et al. 2008; Strambio-De-Castillia et al. 2010). To be inherited by daughter cells, the ER is fragmented into cisternae or tubules at prophase (Puhka et al. 2012). This event is triggered by the activity of several kinases, such as vaccinia-related kinase 1 (VRK1), which in prophase phosphorylates BAF (barrier to auto-integration factor) (reviewed by Brachner & Foisner 2011). In interphase, BAF interconnects chromatin with INM integral proteins and, as soon as becomes phosphorylated, it promotes the release of chromatin from INM (Nichols et al. 2006). Another process required for ER fragmentation involves CLIMP63 (cytoskeleton-linking membrane protein 63 kDa), which upon phosphorylation allows ER collapse (Vedrenne et al. 2005). In metaphase, ER cisternae and tubules are cleared from the space between the spindle poles by the action of receptor accessory proteins 3 and 4 (REEP3/4), thus allowing chromosomes movement toward the metaphase plate on cleared routes (Schlaitz et al. 2013). In addition, the phosphorylation of Stromal Interaction Molecule-1 (STIM-1), which becomes unable to bind MT plus end-binding protein 1 (EB-1), results in loss of interaction between the mitotic spindle and the ER (Smyth et al. 2012). During anaphase and telophase,

when segregated chromosomes start to decondense, the ER reassembles. This event includes NE reformation around chromatin and is promoted by a series of dephosphorylations mediated by different factors, such as the protein phosphatase 1A and 2A (PP1A and PP2A), which dephosphorylates respectively BAF and serine residues of histone H3, thus restoring interactions between INM and chromatin (Vagnarelli et al. 2011).

The Golgi apparatus (GA) is a complex and wide membrane structure located in close proximity of nucleus and MTOCs that undergoes extensive remodeling during the cell cycle (reviewed by Yadav & Linstedt 2011). The most characteristic shape of GA is that of mammalian cells, where it is composed by flat cisternae interconnected by tubular structures, constituting the Golgi ribbon (Lowe 2011). However, different GA shapes exist across species (Stanley et al. 1997). For instance, in *Drosophila* Golgi stacks are not interconnected by tubules, but they are scattered in the cytoplasm, even though assembly and disassembly processes are strongly conserved with mammals, but regulated by different mechanisms and proteins (reviewed by Kondylis & Rabouille 2009). GA disassembly starts in G2, when in mammals Golgi stacks are disconnected from tubules and in *Drosophila* Golgi pairs become separated in a process called unstacking (Fig. 9). The unstacking in mammals occurs through the actions of BARS proteins and by GRASP55/65 (Golgi Reassembly And Stacking Proteins 55 and 65) phosphorylation, while in *Drosophila* it is dependent on actin depolymerization (Wei & Seemann 2017). Further Golgi fragmentation (called vesiculation) is required for the equal distribution of the GA in two daughter cells. Vesiculation is promoted by the abrogation of different fusion events, including SNARE complex formation impairment, occurring by ubiquitination and degradation of the *cis*-Golgi SNARE syntaxin 5 (Huang et al. 2016). Correct GA reformation occurring in telophase is also ensured by inheritance of specific Golgi proteins, which during mitosis are transported to the ER (Sengupta et al. 2015).

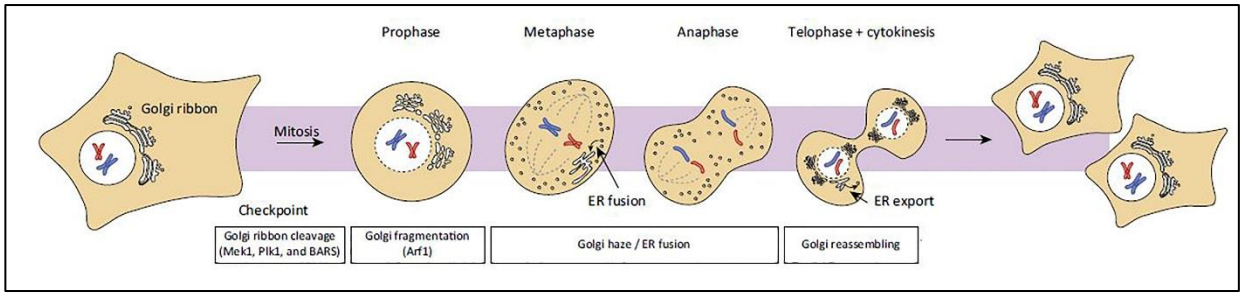

Figure 9. Golgi apparatus inheritance dynamics during mitosis. During mitosis, Golgi undergoes fragmentation processes, which allow the inheritance of membranes and proteins required for its reformation during telophase. Adapted from Jongsma et al, 2015.

2.2.5 Moonlighting functions of trafficking proteins during mitosis

Whether intracellular trafficking is abrogated or not during mitosis has been debated for long time (Schweitzer et al. 2005; Boucrot & Kirchhausen 2007). However, strong evidence suggest that endocytosis is reduced from prophase to cytokinesis. During mitosis, cell undergoes osmotic changes that determine an increase in plasma membrane tension, a condition that would imply a higher amount of energy to induce clathrin-mediated endocytosis (CME). So, shortfall of energy can explain the shutdown of CME during mitosis (Kaur et al. 2014). Interestingly, an increasing number of trafficking proteins have been shown to possess moonlighting functions during mitosis, such as clathrin, epsin, Rab5, Rab11 and ESCRT-III, which control different mitosis aspects (reviewed by Royle 2013).

In interphase, clathrin forms a triskelion structure composed of three heavy chains and three light chains allowing membrane invagination toward the cytoplasm. During mitosis clathrin concentrates at the mitotic spindle. Here, clathrin binds to TACC3 (Transforming Acidic Coiled coil protein 3) and ch-TOG (colonic and hepatic Tumor Overexpressed Gene), forming a complex that stabilizes connections between mitotic spindle MTs and KT required for proper chromosome segregation (Royle et al. 2005; Hood et al. 2013).

Epsin is an endocytic adapter protein, which directly binds and shapes membranes through its epsin NH2-terminal homology (ENTH) domain. In mitosis, epsin is thought to influence mitotic spindle morphology to regulate the formation of a highly interconnected membrane network, which acts as an elastic support for mitotic spindle assembly (Liu & Zheng 2009).

During mitosis, the small GTPase Rab5, which in interphase regulates the formation of early endosomes, is required for proper chromosomes alignment at the metaphase plate. In *Drosophila*, Rab5 associates with the nuclear lamina and with a protein complex called Mud (Mushroom body defect), which is the homolog of the mammalian NuMA (nuclear mitotic apparatus protein). In particular, Rab5 was demonstrated to be required for NE disruption in prophase, for the accumulation of Mud at the spindle poles, which drives correct mitotic spindle formation, and for the correct distribution of key components for spindle structure maintenance (Capalbo et al. 2011). Moreover, experiments performed in human cells demonstrated the essential role of Rab5 in the localization of CENP-F, a transient kinetochore component required for chromosome segregation, which during interphase resides in the nuclear matrix. Indeed, depletion of Rab5 leads to misaligned chromosomes, unstable MT-KT connections, prometaphase delay and aberrant chromosome segregation. Such defects, were also observed in CENP-F depleted cells and in cells simultaneously depleted of Rab5 and CENP-F, indicating that the two proteins act in the same pathway (Serio et al. 2011).

In addition to the trafficking role that it plays during cytokinesis (Giansanti et al. 2015), the small GTPase Rab11 has recently been found in murine oocytes to drive the formation of an actin network involved in the positioning of asymmetric mitotic spindle, which is required for asymmetric cell division (Holubcová et al. 2013).

2.2.6 Kinetochore composition

Sister chromatids segregation toward opposite poles occurs when spindle MTs are fully attached to chromosomes by means of a multi-protein structure called kinetochore (KT) (Fig. 10) (Chan et al. 2009). The KT is an evolutionary conserved platform that assembles on a specific chromosome region called centromere, which possesses a histone H3 variant named CENP-A (or CID in *Drosophila*) (Erhardt et al. 2008). CENP-A is responsible for the recruitment of CCAN (constitutive centromere-associated network) proteins, which include up to 16 proteins (Izuta et al. 2006). The most representative member of CCAN complex is CENP-C, which is also the largest subunit (Screpanti et al. 2011). Since both CENP-A and CENP-C are constitutive components of the kinetochore, their levels half at each cell division and their pools need to be replenished. Experiments performed using *Drosophila* cells showed that newly synthesized CID is recruited to centromeres during metaphase, while CENP-C incorporates in both interphase and mitosis (Mellone et al. 2011). CCAN associates to CENP-A and it constitutes the inner part of the KT. The outer KT, connected to CENP-C recruits the KMN (Knl-1, Mis12, Ndc80) network, composed by the multisubunit Knl-1, Mis12, Ndc80 complexes (Cheeseman & Desai 2008).

The Ndc80 complex (also named HEC1 complex) consists of two protein heterodimers each composed by two globular head terminations and by an internal coiled coil structure. One heterodimer includes the Ndc80 and Nuf2 subunits, which directly bind MTs, while the other includes the Spc24 and Spc25 (Mitch in *Drosophila*) subunits, which interact with Knl-1 and Mis12 complexes (Varma et al. 2013; Ciferri et al. 2008).

The Mis12 complex consists of four subunits, Mis12, Nnf1, Dsn1 and Nsl1, aligned to form a rod-shape complex that bridges inner and outer KT, by interacting with CENP-C and the Ndc80 and Knl-1 complexes. The Mis12 complex, defined as a “hub” for KT assembly

and stability is evolutionary conserved, even though some differences among species have emerged (Petrovic et al. 2010). For instance, in *Drosophila* Dns1 protein is not present, Nsl1 is replaced by Kmn1 and Nnf1 gene has been duplicated, resulting in the synthesis of two redundant proteins, Nnf1a and b (Przewloka et al. 2007; Liu et al. 2016).

In mammals, the Knl-1 complex consists of KNL-1, which directly binds the Ndc80 and Mis12 complexes with its C-terminal domain, and a coiled coil protein, which pairs to the coiled coil N-terminal tail of KNL-1. Both of them are involved in the recruitment at the KT of a multiprotein complex called spindle assembly checkpoint (SAC), which surveys KT-MT interactions, avoiding precocious and incorrect chromosome segregation (Musacchio 2015). Similarly to the Mis12 complex, also Knl-1 complex composition diverges in *Drosophila*, in which ZWINT-1 is absent, and only the KNL-1 subunit ortholog, named Spc105-related (Spc105R) is found (Schittenhelm et al. 2009).

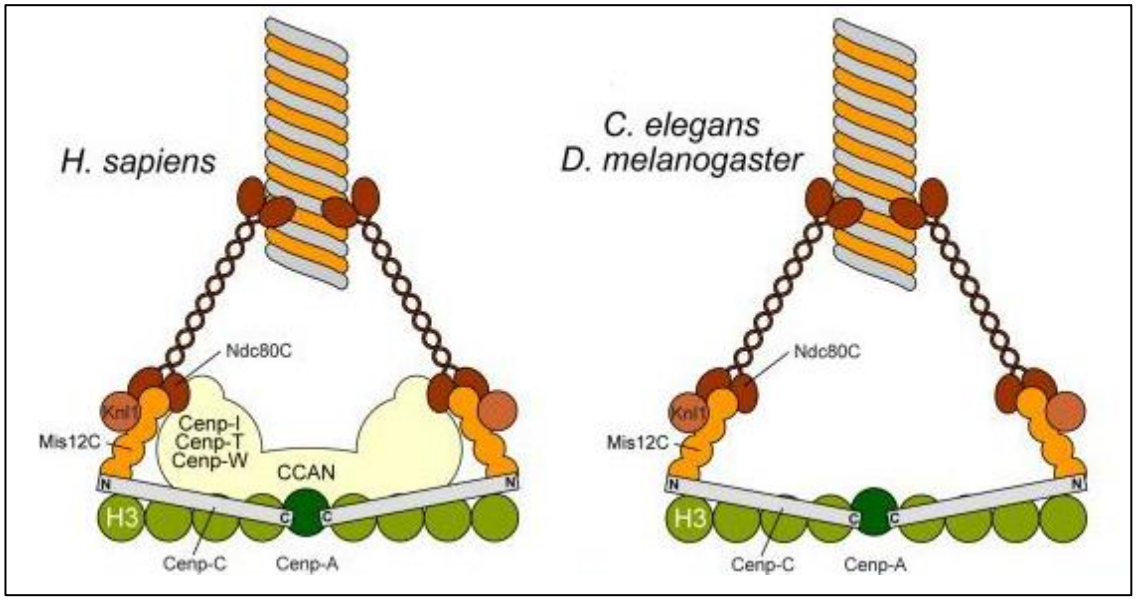

Figure 10. Schematic representation of *H. sapiens*, *D. melanogaster* and *C. elegans* kinetochore structures. The majority of KT components are evolutionary conserved, except for CCAN, which in *D. melanogaster* and *C. elegans* is represented only by Cenp-C subunit. Adapted from Screpanti et al., 2011.

2.2.7 Spatiotemporal dynamics of kinetochore assembly

Drosophila proved a useful organism to study KT formation *in vivo*, since early stages of development are characterized by synchronous mitotic waves and KT complexity is reduced (Glover 1989; Liu et al. 2016). In *Drosophila*, the only representative of the CCAN complex, CENP-C, shows a strong dependence on CID for centromere localization in interphase, but a weak dependence for association with centromeres or kinetochores in mitosis (Fig. 11). Differently from human cells, in which the entire Mis12 complex is associated to KT also during interphase, in *Drosophila* the Mis12 complex component Kmn1 associates to KT only in prophase (Venkei et al. 2012; Przewloka et al. 2011; Kline et al. 2006).

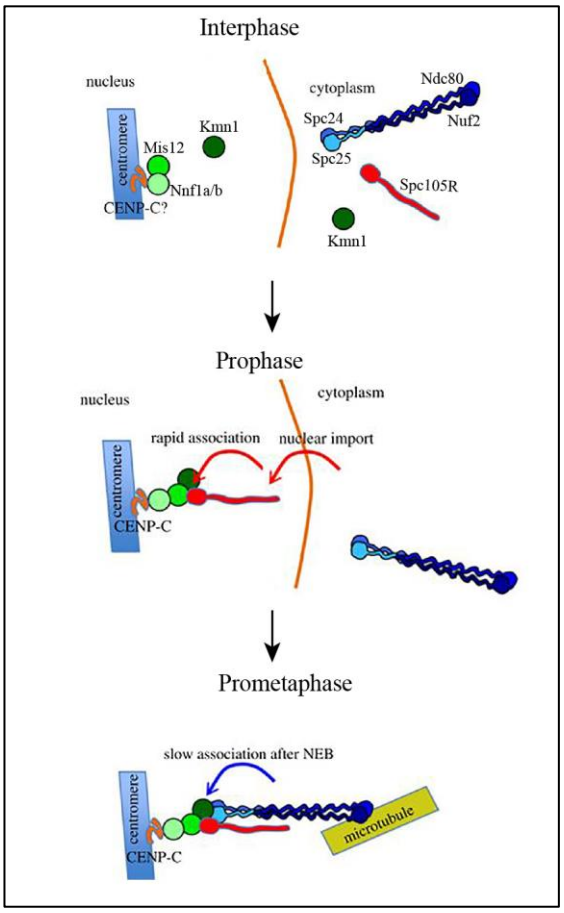

Figure 11. *Drosophila* kinetochore assembly. During interphase the Ndc80 complex and Spc105R are excluded from the nucleus. At the onset of mitosis, Spc105R is imported in the

nucleus and rapidly associates to Mis12, Nnf1a, Nnf1b and Kmn1subunits at the KT. After nuclear envelope fenestration, the Ndc80 complex associates to the KT and binds MTs. Adapted from Venkei et al., 2012.

In early prophase, the accumulation of Cyclin dependent kinase 1 (CDK1) bound to Cyclin B, (also named maturation promoting factor or MPF) triggers the nuclear import of Spc105R. The nuclear import of Spc105R in early prophase and the immediate association of Kmn1 with the Mis12 complex on centromeres are thus the first steps in kinetochore assembly. During interphase, the Ndc80 complex is excluded from the nucleus, albeit its subunits Spc24 and Spc25 are small enough to diffuse through nuclear pores. This suggests that the Ndc80 complex, which allows the interaction between KTs and MTs through Ndc80 and Nuf2 heterodimer, might be assembled in the cytoplasm only to be incorporated at the KT and only when NEB occurs (Venkei et al. 2012). Despite the differences between humans and *Drosophila*, both species share a conserved KT spatial organization (Joglekar et al. 2009; Wan et al. 2009). By reconstituting both kinds of KTs *in vitro*, it was demonstrated that assembly relies more on the interdependency of subunit and complex recruitment, than on post translation modification (Venkei et al. 2012; Screpanti et al. 2011).

2.2.8 The spindle assembly checkpoint

The correct succession of events during the cell cycle is ensured by mechanisms of checkpoint. Their function is to verify whether key steps have been accurately carried out before progression into the next phase. The SAC (Spindle Assembly Checkpoint) is a mitotic checkpoint active during prometaphase that blocks sister chromatid segregation in case of incorrect MTs binding to KTs preventing premature anaphase onset. Checkpoint activity heavily relies on post translation modifications (Fig. 12). Prior to MT attachment, KTs provide a platform for the docking of MAD1-MAD2 (mitotic arrest deficient 1 and 2) heterodimers.

When the these reach the KT, MAD2 shifts its conformation from a closed (C-MAD2) to an open (O-MAD2) one (De Antoni et al. 2005; Yu 2006). The latter possesses high affinity for Cdc20 and together they are able to recruit BUB3 (budding uninhibited by benzymidazole 3) and BUBR1, together constituting the mitotic checkpoint complex (MCC). The MCC impairs the activity of the E3-ubiquitin ligase anaphase promoting complex/Cyclosome (APC/C), which is thus unable to ubiquitinate and degrade securin and Cyclin B. Securin inhibits the protease activity of separase, which is unable to cleave cohesins, the ring-like proteins that hold sister chromatids together, while cyclin B remains bound to the mitotic kinase CDK1, thus preventing mitotic exit (Musacchio & Salmon 2007).

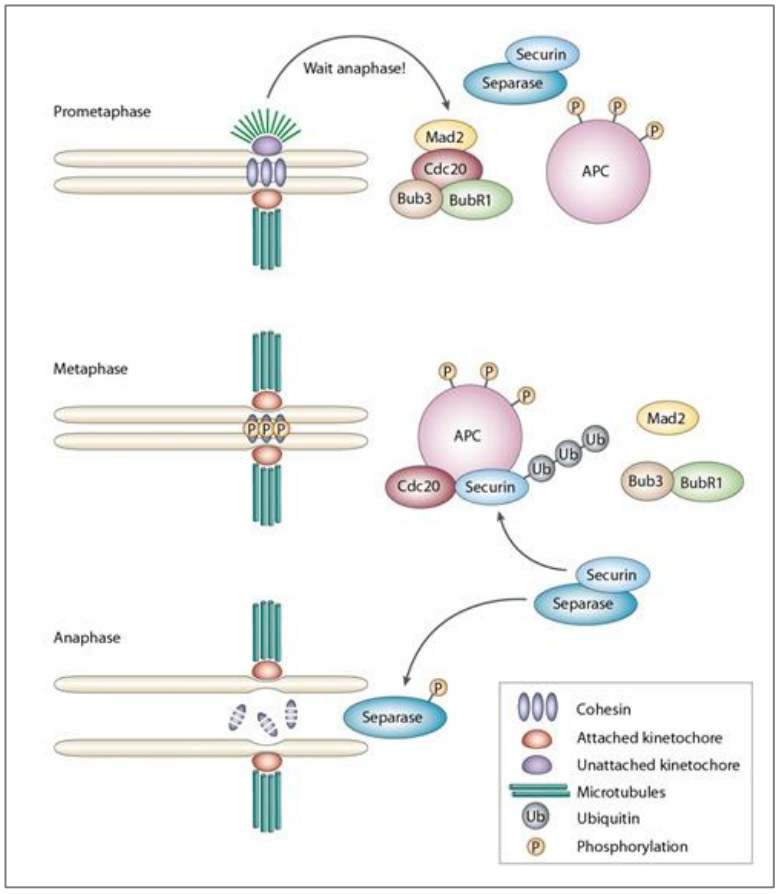

Figure 12. **SAC assembly promotes securin degradation and allows sister chromatid separation.** KTs not properly attached to MTs promotes mitotic checkpoint assembly (MCC). MCC complex inhibits APC/C, which loses the ability to degrade securin. When MTs are properly attached to KTs, APC/C degrades securin, allowing separase to degrade cohesins and allowing sister chromatid to segregate. Adapted from Musacchio & Hardwick, 2002.

SAC efficacy is ensured also by the activity of two kinases, Mps1 and Aurora B. Mps1 is involved in the recruitment at KT of MAD1, MAD2, BUB1, BUB3 and BUBR1 (Lan & Cleveland 2010). In particular, BUB1 and BUB3 localization at the KT, relies on the ability of Mps1 to phosphorylate KNL-1 (Shepperd et al. 2012). Moreover, Mps1 is required for the O-MAD2 recruitment to the MAD1-MAD2 heterodimers associated to KTs (Hewitt, 2010). In turn, Mps1 recruitment at the KT depends, in both human cells and in *Drosophila,* on interaction with Ndc80 proteins (Santaguida et al. 2011; Saurin et al. 2011). Aurora B promotes outer KT-MTs binding by phosphorylating the globular domain of Ndc80 protein, is involved in recruitment of Mps1 to the KT, and promotes stability of the inhibited APC/C complex (Santaguida et al. 2011; Maldonado & Kapoor 2011). In addition, Aurora B is part of the chromosomal passenger complex (CPC) together with three regulatory proteins INCENP (inner centromere passenger protein), survivin and borealin (Fig. 13). The CPC localizes to inner centromere region during early mitosis, while during anaphase it is found at the central portion of the mitotic spindle, the midzone, where it promotes recruitment of proteins required for telophase and cytokinesis. During cytokinesis, the CPC is involved in the assembly of the actin-myosin ring required for abscission and promotes the disassembly of midbody intermediate filaments to allow cleavage furrow formation. Further studies proved that Aurora B is also implicated in the cytokinesis checkpoint that delays abscission in case of presence of lagging chromosomes at the level of the cleavage furrow (Capalbo et al. 2012; Carmena et al. 2012)

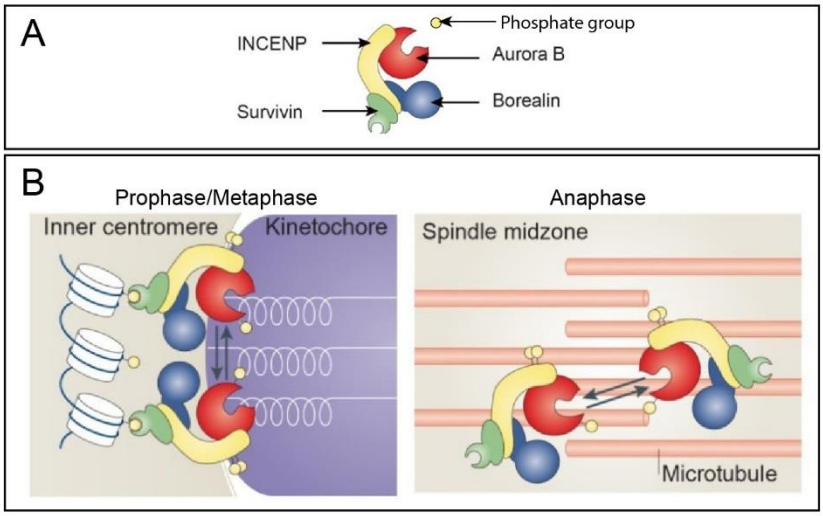

Figure 13. CPC relocalizes from the centromere to the spindle midzone (A) Schematic representation of chromosomal passenger complex (CPC) subunits: Aurora B, INCENP, borealin and surviviv. (B) During prophase and metaphase, CPC localizes at the centromere, while during anaphase it moves to the midzone of mitotic spindle. Adapted from Carmena et al, 2012.

The SAC is highly conserved from yeast to mammals, even though some differences among species have emerged. One of the most consistent discrepancies resides in the role of Mad2 in *Drosophila*. Indeed, *Drosophila* Mad2 mutants do not show abnormal mitosis, aneuploidy and lethality and cells divide normally (Basu et al. 1999; Buffin et al. 2007). It has been proposed that Mad2 is dispensable for proper cell division in *Drosophila*, because it is not involved in KT stabilization. Thus, *Drosophila* might have evolved to by-pass mild perturbations perhaps to allow rapid cell divisions occurring during early embryonic development (Buffin et al. 2007).

2.2.9 The RZZ complex

The RZZ complex, with composed of Zw10, Rod and Zwilch, is associated to the KMN network and is involved in the recruitment of the motor protein Dynein and of SAC proteins (Fig. 14) (Basto et al. 2004). Zw10 and Rod were first identified in *Drosophila*, in a screen to identify genes involved in cell division (Smith et al. 1985; Karess & Glover 1989). Indeed, depletion or downregulation of RZZ components result in defective chromosome segregation including sister chromatids nondisjunction and lagging chromosomes during anaphase (Karess 2005). Importantly, dynein/dynactin complex interacts with Zw10 through the adaptor protein Spindly and is involved in RZZ complex and SAC proteins removal from the KT after corrects MT-KT interaction thus allowing anaphase onset (Schmitt 2010). Besides the function that it plays with the RZZ complex during mitosis, Zw10 is involved in vesicular trafficking during interphase. Indeed, it interacts with Rint-1 (Rad50-interacting protein), with syntaxin 18 and p31, two ER membrane SNARE proteins, and with NAG (neuroblastoma-amplified gene protein). *Drosophila* does not encode NAG and its role is exerted by Rod (Civril et al. 2010; Varma et al. 2006; Wainman et al. 2012). The NRZ (NAG, Rint-1, Zw10) complex acts as a tethering factor for vesicles association to the ER and GA in anterograde and retrograde trafficking, and is crucial for maintenance of GA architecture (Hirose et al. 2004; Sun et al. 2007; Varma et al. 2006; Wainman et al. 2012).

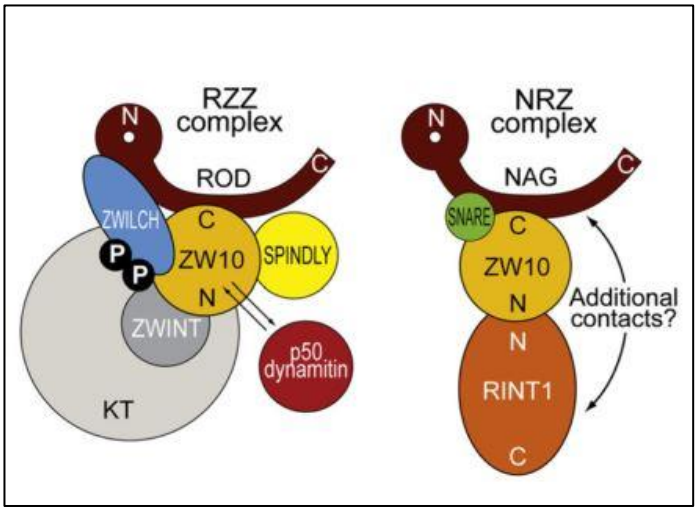

Figure 14. Schematic representation of RZZ and NRZ complexes. RZZ acts during mitosis, by recruiting Dynein at the KT through Spindly, while NRZ is involved in vesicular trafficking processing between Golgi and ER during interphase. Adapted from Çivril et al. 2010.

In addition, experiments performed in *Drosophila* spermatocytes highlighted an essential role of Zw10 and Rint-1 for cytokinesis during meiosis. Since vesicles act as a membrane reservoir for midbody expansion, Zw10 and Rint-1 mutants lead to cytokinesis failure ,because of defective vesicle trafficking (Wainman et al. 2012).

3. Aim of the work

The SNARE protein Snap29 has been extensively characterized in both humans and *Drosophila* for its role in membrane trafficking and in particular for regulation of fusion between an autophagosome and a lysosome (Morelli et al. 2014; Takáts et al. 2013; Itakura et al. 2012). Preliminary observations in our lab demonstrated that, unexpectedly, during mitosis Snap29 associates to the kinetochores of dividing *Drosophila* S2 cells. Thus, the aim of the first part of my PhD project has been to investigate whether Snap29 plays a role during cell division.

Mutations in *SNAP29* human gene are associated to a rare neurocutaneous syndrome called CEDNIK, which is characterized by congenital skin and central nervous system defects (Fuchs-Telem et al. 2011; Sprecher et al. 2005). Since the most investigated aspects of CEDNIK concern dermatological symptoms, during the second part of my PhD I have begun to investigate uncharacterized aspects of CEDNIK, including those in the nervous system, using a zebrafish genetic model that I have established.

4. Materials and methods

4.1 Experiments performed in *Drosophila melanogaster*

4.1.1 Cell cultures and treatments

S2 cells (a gift of B. Mellone) and H2B-GFP-mCherry-α-Tubulin S2 cells (a gift of Sylvia Erhardt) were cultured in Schneider's medium (Life Technologies) supplemented with 1% glutamine and 20% fetal bovine serum (FBS) at 28°C (Erhardt et al. 2008). To depolymerize MTs, S2 cells were incubated with 0.5 μg/ml colcemid (Sigma-Aldrich) for 2 hours.

4.1.2 *Drosophila* strains

Flies were maintained on standard yeast/cornmeal/agar medium. All experiments were performed at 25°C. Fly strains used from Bloomington *Drosophila* Stock Center were w; BxMS1096-GAL4 (8860), UAS-Ndc80 RNAi (38260), UAS-Nuf2 RNAi (36725), UAS-Mis12 RNAi (38535 and 35471), UAS-Spc105R RNAi (35466), UAS-Vamp7 RNAi (43543), UAS-Syntaxin 17 RNAi (29546) and UAS-Snap25 (51997). Fly strains used from Vienna *Drosophila* RNAi Center (VDRC) were UAS-Snap29 RNAi (107947) and UAS-Zw10RNAi (34933). Kyoto Stock Center provided traffic jam-GAL4 strain (1624). Other strains used were w; FRT42 Snap29 B6-21, UAS-ΔSNARE1, UAS-ΔSNARE2, UAS-NPF>AAA (Morelli et al. 2014), eyGal4; UAS FLP; UAS p35 (gift of S. Cohen). Mosaic eye imaginal discs were generated using yw eyFLP; ubiGFP[w+] FRT42 (Morelli et al. 2014).

4.1.3 Immunostaining of *Drosophila* cells and tissue

S2 cells were plated on coverslips and let adhere for one day before starting the immunostaining. Before fixation, S2 cells were rinsed two times with PBS 1X and treated with 3.7% paraformaldehyde (PFA) (Polyscience) for 15 minutes. Then, cells were rinsed three

times in PBS 1X and permeabilized with 0.1% Triton-X100 in PBS 1X (PBS-T) for 20 minutes. In order to minimize aspecific antibodies interactions, PBS-T 1% BSA (blocking solution) was added for 30 minutes and incubated with primary antibodies diluted in PBS-T 0.1% BSA for two hours at room temperature (RT). After three washes in PBS 1X to remove the excess of antibody, cells were incubated with secondary antibodies diluted in PBS 1X for 2 hours at RT. To mark lectins, wheat agglutinin gearm (WGA) Alexa Fluor 555 1:100 (Thermo Scientific) was added together with secondary antibodies. Cells were washed three times in PBS 1X. To label nuclei, 4',6-Diamidine-2'-phenylindole dihydrochloride (DAPI) (Sigma-Aldrich) diluted 1:5000 in PBS 1X was added to cells for 10 minutes at RT and then washed once in PBS 1X. Coverslips were mounted on slides using Mowiol Mounting Medium (Calbiochem) or glycerol 70%.

For *Drosophila* tissue staining, L3 stage larvae were dissected in cold M3 medium (Shields and Sang M3 insect medium). Carcasses were fixed using 4% PFA for 20-30 minutes at RT. After fixative removal, samples were washed three times with PBS-T and permeabilized with 1% Triton X-100 diluted in PBS 1X for 10 minutes. Carcasses were incubated with blocking solution (5% BSA in PBS-T) for 30 minutes at RT and then primary antibodies diluted in blocking solution were added following incubation O/N at 4°C. The following day, samples were washed 3 times with PBS-T solution, incubated with secondary antibodies diluted in PBS 1X for 2 hours at RT and washed three times in PBS 1X. To label nuclei, DAPI was added to samples for 10 minutes at RT and washed once in PBS 1X. To mark cytoskeleton actin, TRITC-conjugated Phalloidin 1:100 (Sigma-Aldrich) was added together the secondary antibodies.

For *Drosophila* tissues and S2 cells experiments, primary antibodies against the following antigens were used: rabbit anti-Snap29 1:1000 (Morelli et al. 2014), mouse anti-Phospho-

HistoneH3 1:1000 (Abcam), rat anti-α-tubulin 1:100 (AbD SeroTech), rat anti-INCENP 1:400 (gift of K. McKim), guinea pig anti-Cenp-C 1:5000 (gift of S. Erhardt), sheep anti-Spc105R 1:1000 (gift of D. Glover), mouse anti-Lamin A (Developmental Studies Hybridoma Bank), rabbit anti-Cleaved Caspase 3 1:200 (Cell Signaling). Alexa conjugated secondary antibodies (Invitrogen) and rabbit Atto594 (Sigma) were used. For all confocal imaging, we used a Leica SP2 microscope with ×40/NA 1.25 or ×63/NA 1.4 oil lenses. For super resolution images, we used a Leica TCS SP8 STED microscope with ×100/NA 1.4.

4.1.4 Correlative-light electron microscopy (CLEM)

$3x10^6$ growing S2 cells were plated on Matek previously coated with Polyornithine (Sigma Aldrich) and let adhere for 2 hours. Cells were fixed with 4% PFA, 0.05% Glutaraldehyde in Hepes 0.15 M adjusted to pH 7.2-7.4 for 5 minutes and then fixed with 4% PFA in Hepes 0.15 M adjusted to pH 7.2-7.4 3 for 10 minutes. This passage was repeated three times. Cells were quickly washed three times with Hepes 0.2 M and incubated with blocking solution (0.005 g/ml BSA, 0.001 g/ml saponin, 0.0027 g/ml NH4Cl in Hepes 0.2 M) for 30 minutes. Cells were then incubated for 2 hours with primary antibodies (anti-Snap29 1:1000, anti-pH3 1:1000) diluted in blocking solution, washed three times with Hepes 0.2 M and incubated with secondary antibodies diluted in blocking solution, in turn diluted 1:10 in PBS 1X. Cells were finally washed 3 times with Hepes 0.2 M. Imaging was performed using a DeltaVision Elite imaging system (Applied Precision) driven by softWoRx software and equipped with a phase-contrast 60× oil immersion objective (Olympus, NA 1.25). Images were edited with ImageJ. Sample were processed for CLEM according to (Beznoussenko & Mironov 2015) using Nanogold-anti-rabbit Fab' Kit Gold Enhance EM (GEEM) for signal enhancement.

4.1.5 Protein extraction and Western blot

Cells were collected and centrifuged at 1200 rmp for 5 minutes at 4°C. After supernatant removal, the pellet was washed and resuspended with 1 ml of PBS 1X, and centrifuged at 1200 rmp at 4°C for 5 minutes. The supernatant was aspirated accurately and the pellet was lysate using RIPA Buffer (10 mM Tris-Cl, 1 mM EDTA, 0.5 mM EGTA, 1% Triton X-100, 0.1% sodium deoxycholate, 0.1% SDS, 140 mM NaCl) supplemented with Proteinase Inhibitors (PI) (1:200) for 20 minutes. Samples were centrifuged at 13400 rpm for 10 minutes at 4°C and the supernatant was collected in a new tube and stored at -20° C. Protein extracts were quantified by BiCinchonic acid Assay (BCA Assay, Thermoscientific) according with manufacturer procedure.

For Western blot, proteins were denatured with Laemmli Buffer 2X (6.25 mM Tris-HCl pH 6.8, 1% glycerol, 2% SDS, 2% β-mercaptoethanol, 0.0012% bromophenol blue) and boiled for 5 minutes. Proteins were then separated by Mini-PROTEAN Precast Gel (Biorad). After running, the gel was enclosed with a nitrocellulose Transfer Membrane (Whatman) between 4 sheets of blotting paper and 2 sponges forming a "sandwich" and transferred with a voltage amplifier at 100V for 1 hour in transfer buffer supplemented with 20% methanol at 4°C. Membranes were incubated with 5% milk diluted in 50 mM Tris, 150 mM NaCl, 0.01% Tween (TBS-T) for 30 minutes at RT with a gentle shaking and were washed with TBS-T three times for 5 minutes. Membranes were then incubated with primary antibodies diluted in milk 5% in TBS-T for 2 hours at RT or O/N at 4°C. Membranes were washed three times in TBS-T and incubated with secondary antibodies HPR-conjugated for 30 minutes. The excess secondary antibody was washed three times in TBS-T. Immunoblots were visualized with SuperSignal West pico or femto chemioluminescent substrate (Thermo Scientific) using Chemidoc (Biorad). Primary antibodies used were rabbit anti-Snap29 (Morelli et al. 2014) and

mouse anti-β-Tubulin 1:8000 (Amersham). Secondary antibodies used were rabbit and mouse HRP-conjugated 1:8000 (Amersham).

4.1.6 Immunoprecipitation

S2 cells were collected and centrifuged for 10 minutes at 800 rpm at 4°C. After discarding supernatant, cell pellet was washed with PBS 1X and centrifuged for 10 minutes at 800 rpm at 4°C. Cell pellet was homogenized in JS lysis buffer (50 mM Hepes pH 7.4, 150 mM NaCl, 10% Glycerol, 1% Triton X-100, 1.5 mM $MgCl_2$, 5 mM EGTA, 0.1 M Na pyrophosphate pH 7.5, 0.1 M PMsF in ethanol, 0.5 M Na Vanadate pH 7.5 in Hepes, 0.5 M NaF, proteases inhibitor cocktail 1:200) and incubated 20 minutes at 4°C on a wheel. Cell suspension was centrifuged for 10 minutes at 13200 rpm 4°C and the supernatant was collected and quantified using the BCA assay. 1 mg of proteins was incubated with 1 μg of antibody O/N at 4°C on a wheel. The antibodies used were anti-Snap29, anti-Ndc80 (gift of P. Somma) and yeast anti-Mad2 antibody (gift of A. Ciliberto) as negative control. The following day, protein G-sepharose beads (Amersham) were added to immunoprotein complexes and incubated for 3 hours at 4°C. After incubation, samples were centrifuged 1 minute at 3000 rpm at 4°C. Supernatants were washed 3 times with JS buffer and finally centrifuged 1 minute at 3000 rpm 4°C. Laemmli buffer 3X was added to samples and they were boiled 5 minutes at 98°C to allow protein denaturation. Proteins were centrifuged for 2 minutes at 13200 rpm to separate the protein G-Sepharose Beads (Bottom) from the immunoprecipitate (Top). The supernatant containing proteins of the immunocomplexes were subjected to Western blot as previously described.

4.1.7 Double stranded RNAs interference in S2 cells

A cDNA library from S2 cells was used as template to amplify regions of genes of interest by PCR using T7- and T3-tagged primers. PCR products were purified using QIAquick PCR purification kit (QIAGEN), transcribed in vitro with T3 and T7 polymerases (Promega) according to manufacturer instructions. To generate double stranded RNAs (dsRNA), T3 and T7 transcripts were annealed at 68°C for 15 minutes and at 37°C for 30 minutes. For dsRNA treatments, S2 cells were starved for 30 minutes in serum-free medium. Medium with 20% serum and dsRNA at a final concentration of 15 μg/10^6 cells were added and cells were incubated for 96 hours.

4.1.8 Real time PCR

S2 cells were collected and centrifuged at 1200 rpm 4°C for 5 minutes. Cell pellets were washed with PBS 1X and centrifuged at 1200 rpm 4°C for 5 minutes. This step was repeated two times. RNA was extracted and purified respectively using TRIZOL reagent (Invitrogen) and RNAase Mini KIT (QIAGEN). Concentration and purity was determined by measuring optical density at 260 and 280 nm using a Nanodrop spectrophotometer. cDNA was retrotranscribed from 1 μg of RNA using SuperScript VILO cDNA Synthesis kit (Invitrogen), according to the manufacturer protocol. 500 ng of cDNA was used as template for real time PCR (qPCR) reactions performed by IFOM-Cogentech quantitative PCR service.

4.1.9 Time-lapse analyses

Control and dsSnap29 treated HB2-GFP-mCherry-α-Tubulin S2 cells were recorded using DeltaVision Elite imaging system (Applied Precision) equipped with a phase-contrast 60x/NA 1.25 oil immersion objective (Olympus). Cells were plated into glass-bottomed dish (Matek) and placed onto a sample stage within an incubator chamber set at 28°C. Images were

acquired using 8 and 80 ms exposure for GFP and mCherry tags respectively, every 2 min for 3 hours, keeping the laser intensity at 2% for GFP and at 5% for mCherry. Image Z-stacks were collected every 0.5 μm for a total of 10 μm thickness. 20 fields with 20 stacks were automatically acquired using a high-precision motorized stage.

4.1.10 Measurements

Quantification of Snap29 localization at KTs in *Drosophila* tissue and in S2 cells was performed using a plugin developed by Emanuele Martini (IFOM Imaging Facility). Briefly, a mask was drawn automatically around Cenp-C signal of pH3-positive cells and Snap29 signal colocalizing with Cenp-C was quantified in >20 cells for each condition. For colcemid experiment, a mask was drawn manually on pH3 positive nuclei and applied to Snap29 in >20 cells for each condition.

All experiments were repeated at least 3 times for quantification and the average of 3 experiments with standard deviation is shown, unless otherwise noted. Quantifications were performed with ImageJ and Prism was used for statistical analyses.

4.1.11 Oligonucleotides used for *Drosophila* experiments

Oligonucleotides used for double-stranded RNAs synthesis:

T3-Snap29 5'- taatacgactcactatagggagaAACCCAGGAGGTGGGTAAG - 3'

T7-Snap29 5'- aattaaccctcactaaagggagaATGTTATCCAGCAATTCATTTTG - 3'

T3-ZW10 5'- taatacgactcactatagggagaCCGGACATATTTCTGGAGGA - 3'

T7-ZW10 5'- attaaccctcactaaagggagaTGATGGTCTCGTAGCACTCG - 3'

T3-Rod 5'- taatacgactcactatagggagaTGGTGGAGATCATGGCTAAC - 3'

T7-Rod 5'- attaaccctcactaaagggagaCCTTGGCGCTTTCAATTTG - 3'

T3-Zwilch 5'- taatacgactcactatagggagaAACTCTCATTGAAAATAGCTACC - 3'

T7-Zwilch 5'- attaaccctcactaaagggagaCACATTGGAAGAGCATACTAAA - 3'

Oligonucleotides used for qPCR analysis:

Ndc80 F 5'- TGGAGAAGAGGGAGAAGCAG - 3'

Ndc80 R 5'- GTAGATCCTCGTTCCGTTGC - 3'

Zw10 F 5'- CGAAGTGGCAAACGATCC - 3'

Zw10 R 5'- TGCGGTCCATTAGTTTGACA - 3'

Spc105 R F 5'- GCCATCGAACTCCTTTGAGA - 3'

Spc105 R R 5'- ATTCCTCGTGGCACTATGCT - 3'

Nuf2 F 5'- ATGGCGTTATCAGTCGAAATT - 3'

Nuf2 R 5'- TCGCAGCTCTGTCACTTGACT - 3'.

Mis12 F 5'- CGCGAACATATTGTGCAGGA - 3'

Mis12 R 5'- CACTTTGCTGTCCAGTTCCC - 3'

Snap29 F 5'- AGCAGCGAACTCTGGACTCT - 3'

Snap29 R 5'- TGTGATGTCTTCTCCAGTTGCT - 3'

Vamp7 F 5'- GCGGGCCTTCCTCTTCT - 3'

Vamp7 R 5’- TGTCTTTAAGCTCGTCAAATCT- 3’

Syntaxin 17 F 5’- GAATTTGCGGAGCTCCAACT- 3’

Syntaxin 17 R 5’- TGAAGCCGAGGATGCCACAT- 3’

4.2 Generation of human disease models in the *Danio rerio* (zebrafish)

Danio rerio (or zebrafish) is an upcoming model to study human syndrome pathogenesis. It is an intensely studied vertebrate, which displays extensive genetic conservation with mammals. Indeed, around 70% of human genes have clear orthologues in zebrafish (Howe et al. 2013). Because of its external development and eggs transparency, early stages of development are more accessible compared to *in utero* mouse development. In addition, zebrafish can lay 200-300 eggs/week and their development is very rapid, with formation of the majority of organs occurring within the first 24 hours post fertilization (hpf). Finally, compared to mice, zebrafish rearing costs and space are strongly reduced (Dooley & Zon 2000; Santoriello & Zon 2012).

4.2.1 Zebrafish life cycle

The zebrafish life cycle can be subdivided into four main stages (Fig. 15):

- **Embryo.** Eggs are considered embryos immediately after fertilization until 72 hfp. The embryo stage comprises the following periods:
    - Zygote (0 – 0.75 hpf). After fertilization, the cytoplasm moves toward the animal pole to form the blastodisc, determining the transition from 1 to 2 cells stage.
    - Cleavage (0.75 – 2.25 hpf). Cell divisions from 2 to 64 cells occur rapidly and synchronically.
    - Blastula (2.25 – 5.25 hpf). Cell divisions become asynchronous and the blastodisc begins to round up. Then, cells acquire the ability to move and migrate to cover 50% of the embryo surface (defined as 50% of epiboly).

- Gastrula (5.25 – 10.33 hpf). This period involves formation of the three germ layers (endoderm, mesoderm and ectoderm). At the end of gastrula, the embryo reaches 90% of epiboly.
- Segmentation (10.33 – 24 hpf). Primary organogenesis starts and somites, pharyngeal arches, and neuromeres begin to develop.
- Pharingula (24 – 48 hpf). Pharyngeal arches develop rapidly during this stage, the nervous system becomes hollow, the brain develops 5 lobes and melanophores start to differentiate. The circulatory system develops and the heart starts to beat.
- Hatching (48 – 72 hpf). The timing of zebrafish embryo hatching from chorion is variable depending on environmental conditions.

- **Larva.** An individual is defined larva from 72 hpf until it starts to develop adult phenotypic traits. After 72 hpf, the swim bladder inflates and at 120 hpf the yolk is consumed and the larva starts to feed autonomously and to swim.
- **Juvenile.** During this stage, most of the phenotypically adult traits have been acquired, except sexual maturity. Conventionally, this period lasts from 4 weeks post fertilization until 12 weeks post fertilization.
- **Adult.** At this stage, sexual dimorphism traits become apparent and individuals are able to produce gametes (Kimmel et al. 1995; Parichy et al. 2011).

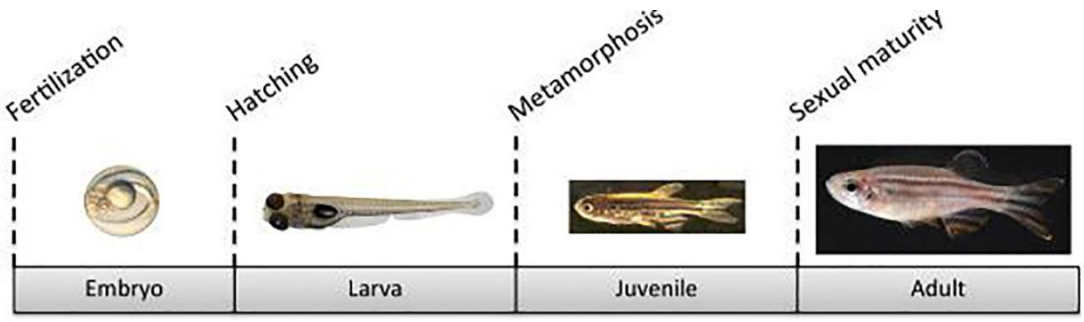

Figure 15. Zebrafish life cycle stages. http://biologycorner.com

4.2.2 ENU induced mutagenesis

Human disease models in zebrafish have been generated using different approaches. One of them involves the exposition of zebrafish males to the mutagen ethylnitrosourea (ENU), which induces point mutations in the male pre-meiotic germ cells by alkylating bases on a single DNA strand (Fig. 16). The high resistance of zebrafish to ENU toxicity allows a high rate of mutagenesis. Pre-meiotic germ cells encounter several rounds of DNA replication before their maturation into mature spermatocytes, during which the mutation become fixed. To derive homozygous fish for a specific mutation, ENU-treated males are crossed with wild type females, producing F1 mosaic heterozygous progeny. F1 fish are then crossed with sibling or wild types generating the F2 progeny, composed by 50% of wild type and 50% of heterozygous fish. Heterozygous derived from F2 are crossed, producing F3 progeny composed by 25% wild type, 50% heterozygous and 25% homozygous mutants (Solica-Kretzel, 1994; Patton, 2001). Moreover, ENU induced mutagenesis has been used as an efficient tool to perform forward genetic screen. The random nature of mutations caused by ENU allows generation of a multitude of mutants, some of which mimic human diseases phenotypes, thus enabling identification of disease-related genes (reviewed by Lieschke & Currie 2007).

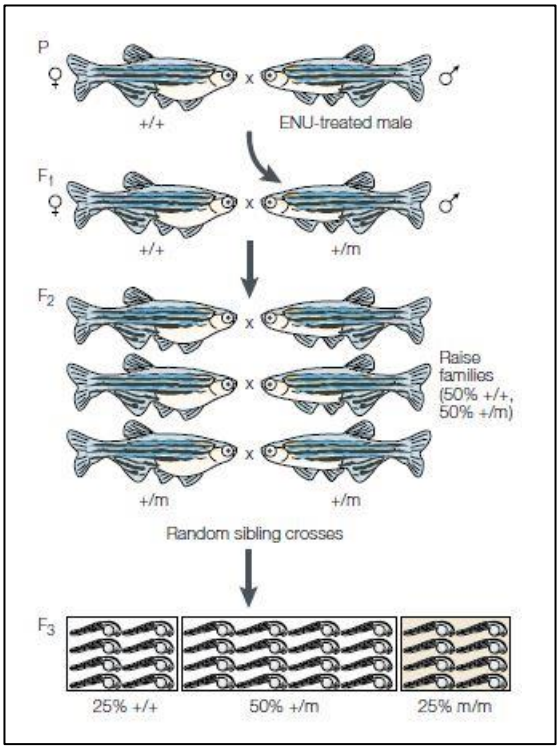

Figure 16. Schematic representation of ENU-derived zebrafish mutants. Zebrafish males are exposed to the mutagen ethylnitrosourea (ENU). Males are crossed with wild type females and they generate the F1 progeny. F1 progeny is genotyped and heterozygous animals are crossed with wild type animals. The derived F2 progeny contains 50% wild type and 50% heterozygous animals. Heterozygous animals are crossed with sibling to derive homozygous mutants. +/+ represent wild type individuals, +/m represent heterozygous individuals and m/m represent homozygous mutants. Adapted from Patton & Zon, 2001.

4.2.3 Available techniques to study a gene of interest in zebrafish

The development of efficient techniques to knockdown or knockout a gene of interest has made zebrafish amenable to reverse genetics. Morpholinos (MOs) are antisense oligonucleotides of approximately 20 bases that pair to a selected region of a gene of interest and inhibit translation. MOs are usually injected in 1 to 4 cells stage embryos, few minutes after fertilization and remain active up to 5 days (Lan et al. 2011). This technique allows studying the effect of transient knockdown *in vivo.*

The need to create targeted stable mutations in zebrafish led to the development of genome editing methods including TALENs (transcription activator-like effector endonucleases), zinc-finger endonucleases (ZFNs) and CRISPR (Clustered Interspersed Short Palindromic Repeats)-Cas9. Both TALENs and ZFNs exploit the DNA cutting property of endonuclease FokI, whose mRNA is injected in 1-cell stage embryos. FokI works as a dimer, in which both subunits are fused with zinc-fingers (ZFs) or with transcription activator-like effector repeat (TALE) domains tailored to recognize a specific DNA regions (Doyon et al. 2008; Zu et al. 2013). Although ZFNs and TALENs have been widely used for genome editing not only in zebrafish, but also in other organisms, both have important limitations. FokI engineering with custom ZF domains have been challenging for many laboratories and ZFNs has been associated to nonspecific ZFN-induced lesions (off-targets) including the ZF transcription factor *gata2* (Sander & Joung 2014; Zhu et al. 2011). In contrast to ZFNs, FokI engineering with TALE domains resulted more accessible (Cermak et al. 2011). However, despite the DNA binding ability of ZFN and TALEN, their mutagenic properties *in vivo* not always result highly efficient (Hsu et al. 2013; Li et al. 2016).

The recent introduction of CRISPR-Cas9 technology among the genome editing options resulted in significant advantages compared to ZFN and TALEN, mainly due to the high efficiency of Cas9 endonuclease *in vivo* and the easy gene targeting. Differently from ZFN and TALEN, CRISPR-Cas9 system exploits the property of Cas9 to bind a small RNA molecule of 20 bases (named short guide RNA or sgRNA), which pairs to a target region. Indeed, while ZFN and TALEN require the synthesis of a new engineered FokI for each single target, Cas9 is suitable for any target and just requires the synthesis of a new RNA oligonucleotide (Li et al. 2016). To be recognized specifically, the target region has to include a protospacer adjacent motif (PAM) sequence, which consists of a nucleotide followed by two guanine nucleotides. The Cas9 nuclease cuts three nucleotides upstream the PAM sequence.

CRISPR-Cas9 (as well as ZFN, TALEN)-induced double-stranded breaks (DSBs) are resolved by cell-intrinsic DNA repair mechanisms, such as non-homologous end-joying (NHEJ), homology directed repair (HDR) or homology independent repair (Fig. 17).

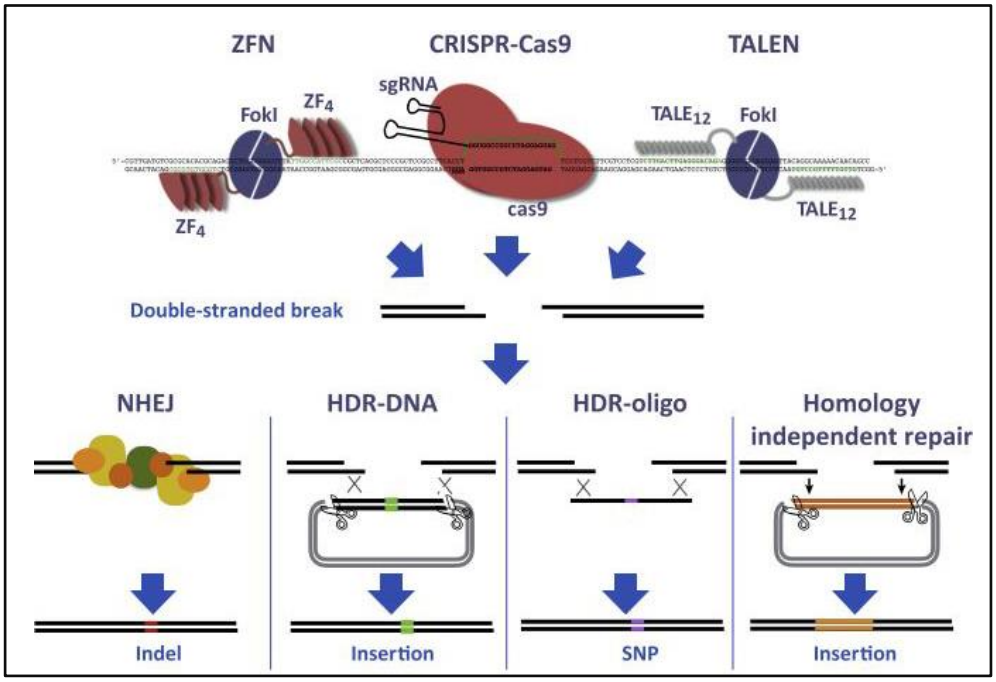

Figure 17. ZFNs, CRISPR/Cas9 and TALENs induce double-stranded breaks that are repaired exploiting intrinsic DNA repair mechanisms. Adapted from Li et al., 2016.

The DSB repair mediated by NHEJ does not require a template and results in base insertions or deletions (Indels), often inactivating the gene of interest. In HDR or homology independent repair, insertions or single nucleotide polymorphism (SNP) can occur using exogenous DNA as template (reviewed by Li et al. 2016).

To raise zebrafish mutants using CRISPR-Cas9, a sgRNA against the gene of interest is injected in 1-cell stage embryos together with Cas9 mRNA or protein (Fig. 18). The mutagenesis efficiency of the resulting F0 progeny is tested by phenotype scoring, sequencing or by T7 endonuclease assay. T7 endonuclease recognizes DNA heteroduplex, formed as a result of mutations induced by CRISPR-Cas9. F0 mutagenized embryos are allowed to grow

to adulthood and crossed with siblings or wild type animals, generating F1 progeny. F1 animals are genotyped and heterozygous animals are selected and crossed to generate homozygous mutants (reviewed by Sander & Joung 2014).

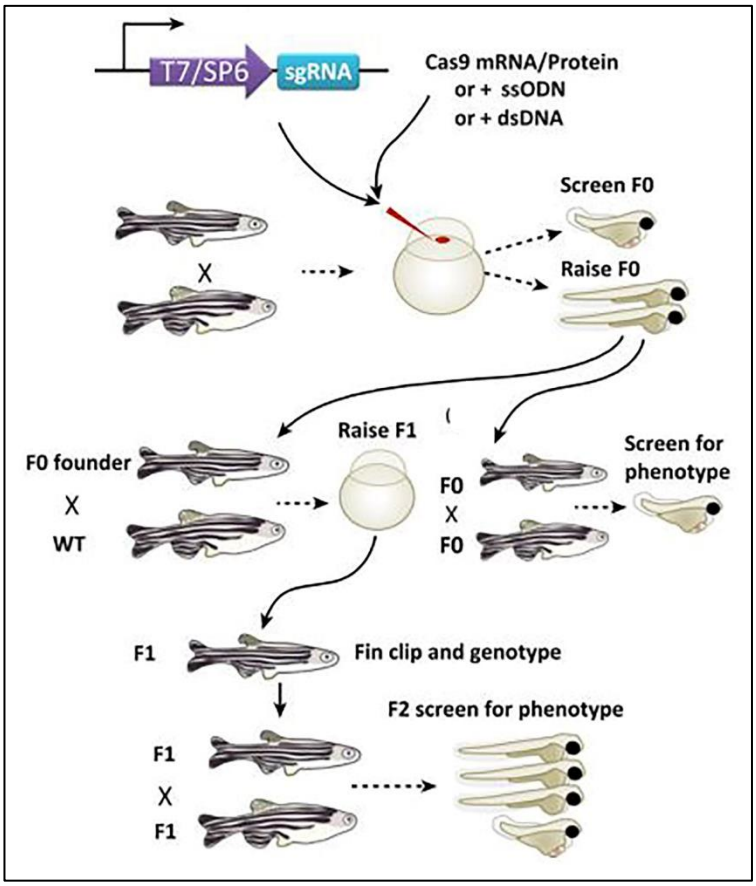

Figure 18. Schematic representation of CRISPR-Cas9-derived zebrafish mutants. The short guide RNA against a gene of interest is injected in one-cell stage embryo. The derived F0 progeny is genotyped and crossed with wild type animals or with siblings. The derived F1 is genotyped and heterozygous animals are isolated and crossed with siblings to generate homozygous mutants (Li et al., 2016).

4.2.4 Zebrafish strains

Adult zebrafish were maintained in a commercial system (Aquatic Habitat) at a water temperature of 28.5°C, pH 7 and conductivity at 500 μS. Zebrafish embryos and larvae not older than 5 dpf are maintained at 28°C in E3 water (50 mM NaCl, 0.17 mM KCl, 0.33 mM CaCl, 0.33 mM $MgSO_4$, 0.05% methylene blue). Zebrafish strains were AB (as wild type strain), *sa13359* (ZIRC), Tg(*kdrl:GFP)* (Jin et al. 2005) and Tg*(islet1:GFP)* (Higashijima et al. 2000).

4.2.5 Morpholino injections and spontaneous motility assay in 24 hpf embryos

Zebrafish zygotes were collected and microinjected through the chorion using an Olympus SZX9 and Picospritzer III microinjector (Parker Instrumentation). Microinjection needles were prepared pulling GC100F-glass capillaries (Harvard Apparatus) with a P-97 puller (Sutter Instrument). Each zygote was microinjected directly into single cell with 2 nl of the following mix, previously incubated 5 minutes at room temperature: Danieau 1X (NaCl 58 mM, KCl 0.7 mM, MgSO4 0.4 mM, $Ca(NO3)_2$ 0.6 mM, HEPES 5.0 mM, pH 7.6), phenol red 0,1%, antisense oligonucleotides Morpholino (MO) (Gene Tools) targeting *snap29* gene in RNAse-free water. 1.7 ng of splice blocking (SB), 3.4 ng of ATG blocking, 8.4 ng of scramble MO and a mixture composed by 0.6 ng of SB and 1.7 ATG blocking MO were injected in each single embryos. Uninjected embryos were used as controls to evaluate lethality at 24 hpf.

Spontaneous motility assay (twitching assay) was performed using 24 hpf embryos, respectively uninjected and injected with a mixture of SB and ATG blocking Morpholino and recorded for 1 minute. Images were acquired with a NIKON DS-5MC digital camera, mounted on a NIKON SMZ-1500 stereomicroscope. 70 individual embryos for each condition were recorded in multiple movies and statistical analysis was performed using Prism.

4.2.6 CRISPR/Cas9 *snap29* mutagenesis in zebrafish and *sa13359* sequencing

The short guide (sg) RNA AGGCCAGTCATCCAAACCTCAGG targeting the exon 4 of zebrafish *snap29* gene, was synthetized in vitro starting from the annealing of two oligonucleotides.

Each oligonucleotides were diluted in annealing buffer (10 mM Tris, pH 7.5-8, 50 mM NaCl, 1 mM EDTA) to reach the final concentration of 100 mM, they were mixed together in equal proportion, heated at 95 °C for 3-5 minutes and cooled at room temperature for 60 minutes. The annealed oligos were cloned in a DR274 vector (Addgene) and the presence of the insertion was verified by sequencing. RNA *in vitro* transcription was performed with a standard kit (MEGAscript T7 Transcription Kit, Ambion) using the linearized DR274 plasmid as template. The sgRNA was injected together with the CAS9 purified protein (prepared by IFOM Biochemistry unit) in one-cell zebrafish embryos and mosaic animals were obtained. To monitor the presence of mutations, mosaic animals were subjected to T7E assay. Briefly, genomic DNA (gDNA) was extracted from caudal fin biopsies (fin clip) of adult animals and a fragment of 500 bp containing the sgRNA complementary region was amplified by PCR with specific primers.

The PCR products were subjected to denaturing/annealing steps (95 ℃ 2min, -2 ℃ /s to 85 ℃, -0.1 C°/s to 25 ℃, 16 C°∞) and digested by the mismatch sensitive endonuclease T7 (T7E) (NEB).

To isolate potential founders animals bearing mutations in the germline, mosaic animals were outcrossed with wild type (AB) animals. Then, a pool of 10 embryos derived from each single cross were subjected to T7E assay. To establish *snap29* mutant strains, founder animals were then crossed with AB animals. When heterozygous offspring reached adulthood, gDNA from 20 animals was extracted by fin clip, amplified with the same primers mentioned above, and sequenced (IFOM Sequencing Facility).

gDNA extracted from heterozygous animals obtained from the outcross of the *snap29* mutant strain *sa13359* (generated with ENU by Zebrafish International Resource Center) with AB animals was sequenced using the procedure and primers described above.

4.2.7 RNA extraction from zebrafish, cDNA synthesis and RT-PCR

Wild type zebrafish larvae (AB strain) were collected at 96 hpf and RNA was extracted using TRIZOL Reagent (Invitrogen) and RNAse Mini kit (QIAGEN). To avoid genomic DNA contamination, samples were digested with RQ1 RNase-Free DNase (Promega). cDNAs synthesis and qPCR were performed as described in 3.1.8.

4.2.8 Genomic DNA extraction from zebrafish embryos

24 hpf embryos were dechorionated with Pronase (Sigma-Aldrich) at a final concentration of 1 mg/ml for 15 minutes at 37°C, collected and put in a sterile tube. 50 µl of lysis buffer (Tris-HCl 10 mM pH8.0, EDTA 1 mM, 0.3% Tween, 0.3% NP40 in distilled water) were added to 50 dechorionated embryos, incubated for 10 minutes at 98°C and then cooled on ice. 5 µl of Proteinase K 10 mg/ml (Sigma-Aldrich) were added and embryos were incubated at 55°C O/N. The second day, 145 µl of sterile water were added, followed by 20 µl of Na Acetate and 200 µl of Phenol. Samples were mixed by inverting them and centrifuged at 13000 rpm for 1 minute. Supernatant was collected and precipitated O/N with 100% ethanol at -20°C. The third day, samples were centrifuged for 30 minutes at 4°C, recovered pellets were washed with 75% ethanol, centrifuged again for 5 minutes and resuspended in 20 µl of DNAse-free water.

4.2.9 Protein extraction from zebrafish larvae

Around 35 larvae of 5 dpf were collected in 1.5 ml tube and resuspended twice with 1 ml of deyolking solution to remove eventual residues of yolk extension. Larvae were washed with PBS 1X and centrifuged at 3000 g. After PBS 1X removal, pellets were homogenized in 150 µl of Laemmli buffer (20% SDS, 50% Glycerol, 0.01% β-Mercapto-ethanol, Tris-HCl 1 M pH 6.8) using a pestle and an insulin needle. Samples were incubated at 98°C and cooled down on ice for three times. Extracts were centrifuged at 13400 rpm for 5 minutes and supernatants were collected in a clean tube. Protein extracts were quantified and samples were analyzed by Western blot as described in 3.1.5. Primary antibodies used for blot were: rabbit anti-LC3 1:1000 (Thermo Fischer), mouse anti-Vinculin 1:5000 (Amersham).

4.2.10 *In situ* hybridization

Zebrafish at different developmental stages were fixed in 4% PFA at 4°C O/N. Digoxigenin (DIG)-labeled antisense probes were synthesized using DIG RNA labelling MIX (Roche) using a DNA template amplified from cDNA using specific primers. After hybridization, detection was performed with an anti-DIG antibody coupled to alkaline phosphatase (Roche) and samples were imaged with Olympus SZX12 stereomicroscope.

4.2.11 Hematoxylin and eosin staining and immunostaining on paraffin sections

Larvae were fixed O/N at 4°C in 4% PFA diluted in PBS and positioned in a 7x7x6 mm plastic base-moulds (Kaltek) containing 1.2 % low-melting agarose in PBS. Before agarose solidification, larvae were correctly orientated. After agarose block solidification, larvae were removed from the base mould and immersed in 70% ethanol. After dehydration, agarose blocks containing larvae were subjected to paraffin embedding by Leica ASP300 S Fully

Enclosed Tissue Processor and 5 μm thick sections were cut using a manual rotatory microtome (Leica) (IFOM Tissue Processing Facility).

Sections were deparaffinized in histolemon for 5 minutes. This passage was repeated twice. Then, sections were hydrated with 100%, 95% and 80% ethanol, respectively for 5 minutes each and repeated three times, and finally rinsed with distilled water.

For hematoxylin and eosin staining (HE), section were stained with Harris hematoxilin solution for 2 minutes, washed in running tap water for 5 minutes, counterstained with eosin-Y solution for 7 seconds and washed in running tap water for 5 minutes. Sections were dehydrated with 95% ethanol and absolute ethanol for 5 minutes two times. Then, they were cleared with xylene for 5 minutes two times and mounted with coverslips in mounting medium. HE sections were imaged using a Nikon Eclipse 9i, respectively with a 20X and a 100X objectives.

For immunostaining, sections were incubated in sodium citrate buffer (2.94 g tri-sodium citrate diluted in 1000 ml of distilled water at 6.0 pH, supplemented with 0.5 ml Tween 20) at 95°C for 45 minutes and cooled at RT for 1 hour under chemical hood. Sections were then incubated with blocking solution (2% fetal bovine serum, 2 g bovine serum albumin, 0.05% Tween 20 in PBS 1X adjusted at 7.2 pH) for 1 hour at RT, with primary antibodies diluted in blocking solution O/N and rinsed in PBS 1X three times for 5 minutes. Secondary antibodies diluted in PBS 1X were added and incubated for 1 hour followed by three washes with PBS 1X for 5 minutes each. Slides were incubated with DAPI for 5 minutes at RT, rinsed in PBS 1X three times for 5 minutes and mounted with coverslips in 50% glycerol. The following primary antibodies were used: rabbit anti-p62 1:1000 (Enzo Life Science), mouse anti- Myosin heavy chain (all-Myo) 1:40 (Developmental Studies Hybridoma Bank). Alexa conjugated secondary antibodies (Invitrogen) rabbit and mouse 488 were used.

4.2.11 Zebrafish whole-mount immunostaining

- Day 1: embryos or larvae were fixed O/N at 4°C with 4% PFA diluted in PBS 1X, rinsed three times with PBS 1X. Embryos older than 24 hpf need to be treated with 0.25% trypsin (Sigma-Aldrich) at RT for a range of time between 2 minutes (for 24 hpf embryos) up to 60 minute (for 5 dpf larvae). Samples were rinsed three times for 5 minutes with washing buffer (1% Triton-X100, 0.2% DMSO in PBS 1X) and incubated for at least 1 hour in blocking buffer (0.1% Triton X-100, 1% DMSO, 5% normal goat serum in PBS 1X) on a shaker. Then embryos were incubated with primary antibodies diluted in blocking buffer O/N at 4°C;
- Day 2: samples were rinsed rapidly two times with washing buffer and at least 3 washes of 1-2 hours each with washing buffer were performed. Samples were incubated in blocking buffer for 30 minutes and with secondary antibodies diluted in blocking buffer O/N at 4°C
- Day 3: samples were rapidly rinsed two times with washing buffer and two washes of 5 minutes each with PBS 1X were performed. Then, samples were incubated 10 minutes with DAPI, rapidly rinsed with PBS 1X and mounted on a slide with 85% glycerol.

The following primary antibodies were used: rabbit anti-phospho H3 (Abcam) 1:1000, rat anti-ds Red (Novus) 1:1000, rabbit anti-cleaved Caspase 3 1:1200 (Cell Signaling), chicken anti-GFP 1:1000 (Cell Signaling). Alexa conjugated secondary antibodies (Invitrogen) were used.

4.2.12 Generation of *GFP-* and *RFP-snap29* mRNA

To generate *GFP-snap29* plasmid, zebrafish *snap29* coding sequence was amplified using as template 24 hpf embryo cDNA and as primers BglII-Snap29 Forward and XhoI-Snap29 Reverse. Both PCR product and pEGFP plasmid (Addgene) were digested using BglII and XhoI restriction enzymes (New England Biolab, NEB), purified using QIAquick Gel Extraction Kit protocol (QIAGEN) and subjected to ligation with T4 DNA ligase (NEB) according with manufacturer protocol. The obtained plasmid was used as a template for a second PCR using as primers BamHI-GFP Forward and XhoI-Snap29 Reverse. Both PCR product and pCS2 plasmid (Addgene) were digested with BamHI and XhoI restriction enzyme, purified and subjected to ligation with T4 DNA ligase (NEB).

To generate the *RFP-snap29* plasmid, zebrafish *snap29* coding sequences was amplified using as template *GFP-snap29* pCS2 and as primers BamHI RFP Forward and BglII RFP Reverse. Both PCR product and pCS2 *GFP-snap29* were digested using BamHI and BglII restriction enzymes, purified and subjected to ligation.

pCS2 *GFP-snap29*, pCS2 *RFP-snap29* and *GFP-gm130* pCS2 (gift of D. Gilmour) were used as templates to synthesize mRNA of *GFP-snap29, RFP-snap29* and *GFP-gm130* with MAXIscript SP6 Transcription Kit (Ambion). 200 pg of each mRNA were injected in single one-cell stage embryos.

4.2.13 Birefringence

AB and *snap29*^{K164*} mutant 5 dpf larvae were anesthetized with Ethyl 4-aminobenzoate (MS-222,Sigma-Aldrich) at a final concentration of 15 mg/l and imaged with Olympus IX81 stereomicroscope through two polarized light filters (Smith et al. 2013) .

4.2.14 Touch-evoked response assay

AB and *snap29*^{K164*} mutant 6 dpf larvae were stimulated with a plastic tip and recorded for 1 minute with a NIKON DS-5MC digital camera, mounted on a NIKON SMZ-1500 stereomicroscope. 5 larvae for each conditions were used and only the first 5 stimuli were considered for quantification. Statistical analysis was performed with Prism.

4.2.15 Alcian blue staining of larval cartilages

6 dpf zebrafish larvae were fixed with 4% PFA O/N at 4°C in PBS1X. Samples were then washed two times with sterile water and incubated in Alcian Blue solution pH 2.5 (Bioptica, cat. 04-163802) O/N at RT. After Alcian Blue staining, larvae were washed 3 times with sterile water and incubated in 3% H_2O_2 solution for 30 minutes at R/T. Larvae were washed with sterile water, gradually dehydrated with ethanol and equilibrated in a solution of glycerol 85% in PBS1X. Splanchnocrania were manually dissected from the heads and imaged with a NIKON DS-5MC digital camera mounted on a NIKON SMZ-1500 stereomicroscope.

4.2.16 Rhodamine Dextran-containing food preparation

Rhodamin-dextran was mixed with two different larval food commonly used for the larval feeding. In particular, we added 100 mg of "Larval AP100 food" (microparticles size < 100 microns), 100 mg of JBL "Novo Tom" lyophilized artemia and 40 µl of 20 mg/ml rhodamin-dextran 10,000 MW (Invitrogen) to 360 µl of Milli-Q water. The mixture was dropped on a glass slide and dried O/N at RT, protected by light exposure. When the solution was dried, it was reduced to a very fine powder by a pestle and administered to larvae, dissolving it on the water surface.

4.2.17 Oligonucleotides used for zebrafish experiments

Oligonucleotides used for sgRNA synthesis:

Oligo 1: TAGGCCAGTCATCCAAACCTC

Oligo 2: AAACGAGGTTTGGATGACTGG

Oligonucleotides used for the screening of *snap29* mutants generated by CRISPR/Cas9 and ENU:

Forward 5'- ACCCCAAATCCCACAATCCT- 3'

Reverse 5'- GGCGTAACTAGGTTCATTAGGG - 3'

Oligonucleotides used for qPCR analysis:

snap29 F 5'- ATCTGGGACAACTTGGGCAACT - 3'

snap29 R 5'- GAGCGTCCAGAGAAATGTCC - 3'

GAPDH F 5'- TCAGTCCACTCACACCAAGTG - 3'

GAPDH R 5'- CGACCGAATCCGTTAATACC - 3'

Oligonucleotides used for *in situ* hybridization:

snap29 T3: 5' – taatacgactcactatagggagaAAACCGCAGAGGAACTGATC - 3'

snap29 T7: 5' – attaaccctcactaaagggagaTCATCATTGTTACTATAAT - 3'

Oligonucleotides used for of *GFP*- and *RFP-snap29* cloning:

BglII-Snap29 Forward: 5'- TCGAGAAGATCTATGTCTGCCTACCCCAAATCCC - 3'

XhoI-Snap29 Reverse: 5'- ATCGCCCTCGAGCTATTTAAGGCTTTTGAGCTG - 3'

BamHI-GFP Forward: 5'- ATCGCGGGATCCATGTGAGCAAGGGCGAGG - 3'

BamHI RFP Forward: 5’- TAGCGCCGGATCCATGGTGTCTAAGGGCGAAGA - 3’

BglII RFP Reverse: 5’- TAGGGAAGATCTATTAACTTTGTGCCCCAGTT - 3’

5. Results

5.1 The role of Snap29 during mitosis

5.1.1 *Drosophila* Snap29 localizes to the outer KTs during mitosis

A specific antibody previously characterized in our lab revealed that Snap29 in *Drosophila* Schneider-2 (S2) cells resides in the cytoplasm of interphase cells, according with the role that Snap29 exerts in membrane trafficking and autophagy (Morelli et al. 2014). Surprisingly, during cell division, Snap29 accumulates in puncta associated with chromosomes, which are particularly evident during prophase, metaphase and anaphase. As soon as chromosomes decondense during telophase, Snap29 is no longer associated with DNA (Fig. 19A).

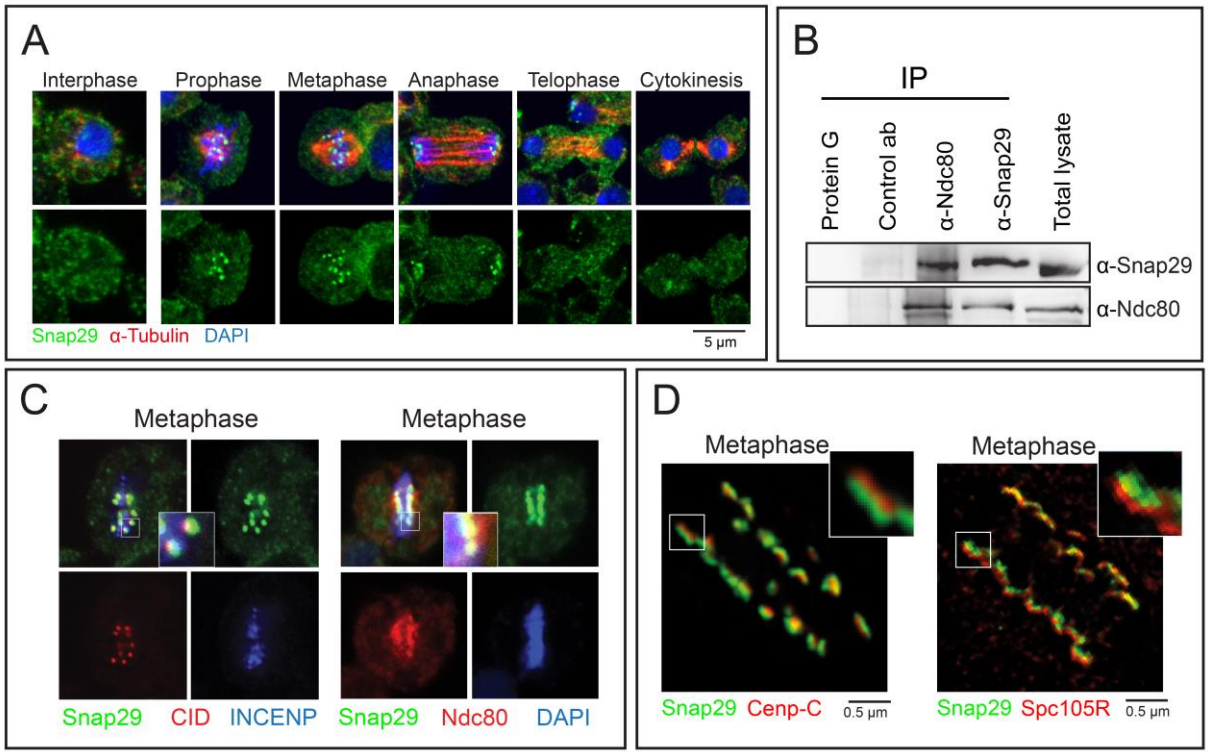

Figure 19. *Drosophila* Snap29 localizes to the outer KT
(A) Single confocal sections of S2 cells at indicated stages, stained with anti-Snap29, anti-Tubulin to mark the mitotic spindle and DAPI to mark DNA. (B) Immuno-precipitations of 1 mg of protein extracts from asynchronous S2 cells using 1 µg of the indicated antibodies. Anti-yeast Mad2 was used as negative control antibody (control ab) (C) Single confocal sections of S2 cells in metaphase. Anti-CID, anti-Ndc80 and anti-INCENP were used

respectively as inner, outer KT and centromeric markers. (D) Maximum projections of S2 cells in metaphase imaged by STED microscopy. Anti-Cenp-C and anti-Spc105R mark the proximal and the distal region of different portions of the outer KT, respectively.

To test whether Snap29 localizes specifically at the KT, we immunoprecipitated S2 cells protein extracts with antibodies against Snap29 or the outer KT component Ndc80. We found Snap29 among Ndc80 co-immunoprecipitants and vice versa, demonstrating that Snap29 is associated with the outer KT in S2 cells (Fig. 19B).

Colocalization analysis of S2 cells in metaphase showed that Snap29 partially overlaps with CID and Ndc80, which are inner and outer components of the KT, but not with the inner centromeric marker INCENP (Fig. 19C). Furthermore, super-resolution confocal microscopy allowed us to establish that Snap29 resides distal to Cenp-C, which connects the inner and the outer part of the KT. In contrast, Snap29 localizes proximal to Spc105R (Fig. 19D). These data indicate that Snap29 resides between the inner and the outer part of the KMN network.

5.1.2 Snap29 recruitment to the KT follows the same spatiotemporal dynamics of recruitment of Spc105R

To investigate the spatiotemporal dynamics of Snap29 assembly to the outer KT, we analyzed the localization of Snap29 relative to two determinant events of the outer KT assembly, which are Spc105R recruitment and nuclear envelope (NE) fenestration. In *Drosophila*, KMN network assembly starts with the nuclear import of Spc105R, which binds to the Mis12 complex (Venkei et al. 2012). As soon as the NE starts to fenestrate, the Ndc80 complex binds to Spc105R and to the Mis12 complex, thus allowing the formed KMN network to bind MTs and eventually to drive chromosome segregation.

Differently from Snap29, which is visible in cytoplasmic puncta, low Spc105R signal is detectable in interphase (Fig. 20A).

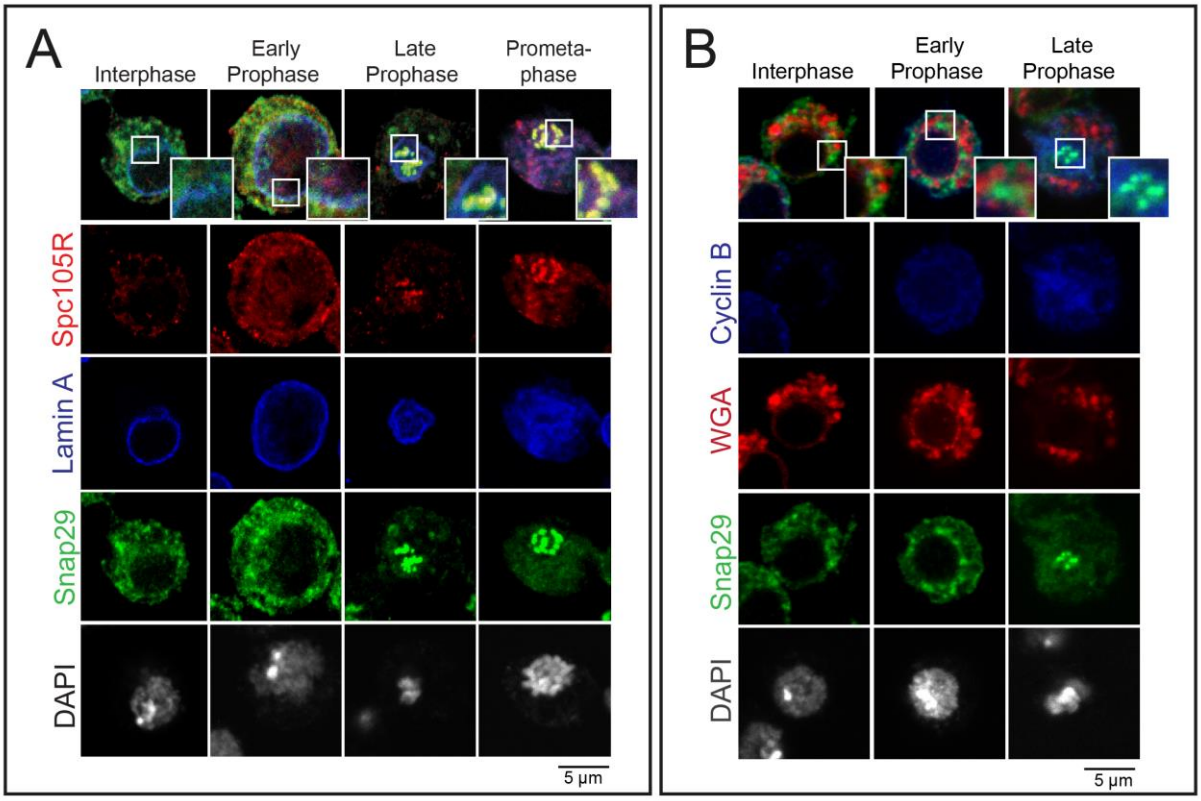

Figure 20. Snap29 follows the same dynamics of recruitment to the KT of Spc105R

(A) Single confocal sections of S2 cells at indicated mitotic stages, stained to detect Snap29, Spc105R and the nuclear lamina (Lamin A). High magnifications of the insets show localization of Snap29 relative to indicated markers. (B) Single confocal sections of S2 cells at the indicated mitotic stages stained with anti-Snap29, labelled wheat germ agglutinin (WGA) and anti-Cyclin B to detect respectively Nuclear Pore Complex (NPC) and cells entering mitosis. High magnifications of the insets show localization of Snap29 relative to the indicated markers.

Starting from early prophase, Spc105R signal increases dramatically and, similar to Snap29, it is found mainly in the perinuclear region external to the nuclear membrane marker Lamin A. As soon as the nuclear lamina starts to disassemble in late prophase, Snap29 and Spc105R are co-recruited to KTs, and chromatin starts to condense. In early and late prophase, when the amount of the mitotic Cyclin B increases, Snap29 localization is distinct from that detected with WGA (wheat germ agglutinin), a lectin that associates with O-linked N-acetyl-

D-glucosamine-modified nuclear pore complex (NPC) proteins (Fig. 20B) (Katsani et al. 2008). These results show that during early prophase Snap29 becomes enriched in a perinuclear region distinct from NPC and is later recruited to KTs together with Spc105, concomitant with NE fenestration.

5.1.3 Snap29 localization to KTs does not depend on the presence of RZZ complex or on microtubules

Several proteins are known to exert a dual role during both trafficking and cell division. Among these, there is Zw10 that, together with Rod and Zwilch, is part of the RZZ complex at KTs. Interestingly, in interphase Zw10 and Rod are present in a different complex, called NRZ, together with RINT-1. The NRZ complex associates with t-SNAREs syntaxin 18 and p31, and is known to regulate anterograde and retrograde transport, respectively between ER and Golgi and vice versa, and to be crucial to maintain Golgi apparatus integrity (Wainman et al. 2012; Civril et al. 2010; Varma et al. 2006). Since RZZ complex components Rod and Zw10 are involved in intracellular trafficking during interphase by interacting with t-SNAREs, we asked whether Snap29 could associate, as a t-SNARE, with Zw10 and Rod during mitosis. In order to test for a possible dependence between Snap29 recruitment at the KT and the RZZ complex, we depleted Rod, Zwilch and Zw10 simultaneously in S2 cells with dsRNAs (Fig. 21A).

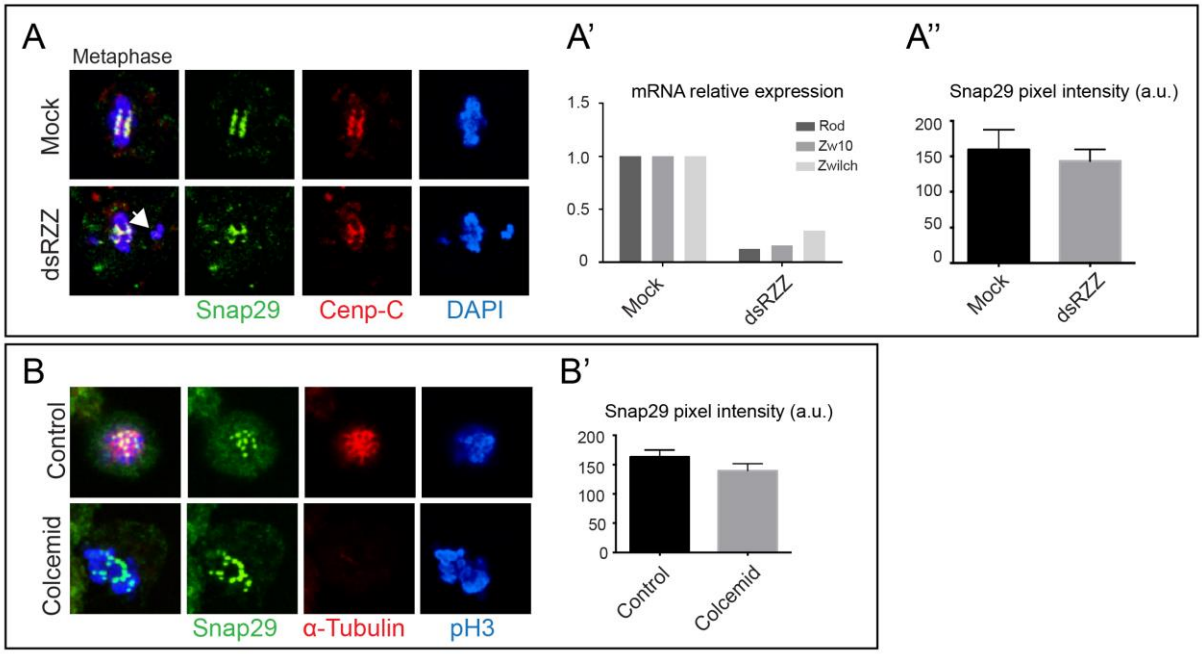

Figure 21. RZZ complex and MTs are not involved in Snap29 localization to the KT

(A) Single confocal sections of S2 cells in metaphase treated with mock or with double strands RNA against Zw10, Zwilch and Rod (dsRZZ). Cells were stained with anti-Snap29, anti-Cenp-C and DAPI. Arrowhead points to chromosome congression defects, indicating the effectiveness of knock-down. (A') qPCR analysis of Rod, Zwilch, ZW10 mRNA levels relative to the experiment shown in A. (A'') Quantification of the average level of Snap29 signal at a single KT, measured relative to Cenp-C. (B) Single confocal sections of cells untreated or treated with 0.5 µg/ml colcemid to depolymerize MTs. (B') Quantification of the total level of Snap29 signal in a single cell, measured relative to pH3. More than 20 cells/sample were considered in A-B'. *P*-values by unpaired t-test indicate no significant differences in A'' and B'.

By qPCR, we confirmed the efficacy of the downregulation for the three genes (Fig. 21A'). Immunofluorescence analysis of RZZ-depleted cells highlighted the presence of chromosome alignment defects at the metaphase plate, as previously reported (Karess et al., 2005). However, quantification of Snap29 signal at KTs, identified by the inner KT marker Cenp-C, did not reveal any difference in RZZ depleted cells, when compared to control (Fig. 21A''). These data suggest that the RZZ complex is not required for the recruitment of Snap29 to the KT.

Next, to investigate whether Snap29 localization at KTs depends on MTs, we treated S2 cells with the MT depolymerizing drug colcemid (Fig. 21B). We identified dividing cells by using the mitotic marker phospho-HistoneH3 (pH3) and we confirmed that colcemid was efficient since α-Tubulin staining was completely lost upon the treatment. Interestingly, quantification of Snap29 signal on chromosomes of dividing cells did not highlight any difference between treated and control cells, indicating that Snap29 docking or retention at KTs is MTs independent (Fig. 21B').

5.1.4 Snap29 localization to the KT does not depend on membranes or autophagy

In interphase Snap29 is associated to membranes, since it mediates their fusion by the formation of a SNARE complex (Jahn & Scheller 2006; Malsam et al. 2008). To investigate whether membranes are involved in Snap29 localization to the KT, we performed correlative light-electron microscopy (CLEM) in S2 cells in collaboration with Galina Beznoussenko and Alexander Mironov (IFOM). We identified mitotic cells by immunofluorescent labelling with pH3 and we processed for immuno-EM with anti-Snap29 interphase and pro-metaphase cells, in which the fenestrated NE is contiguous to the ER (Fig. 22A-B').

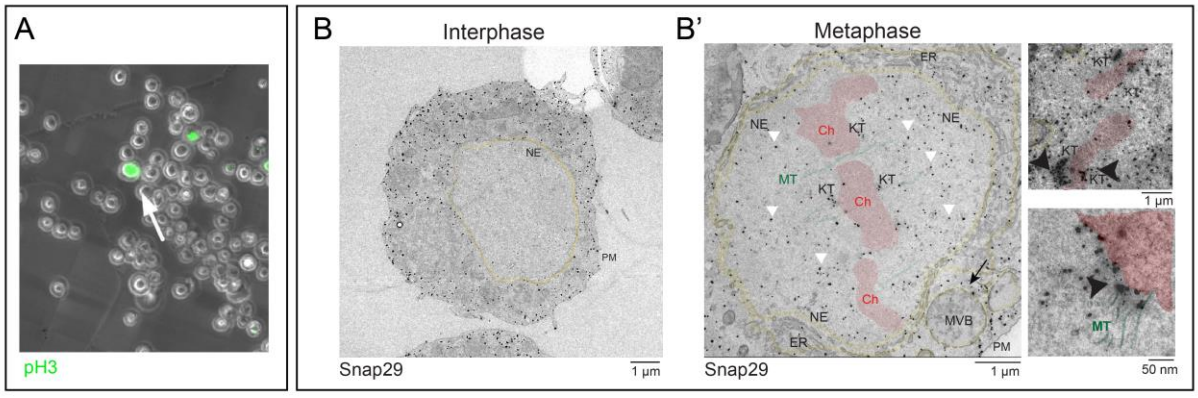

Figure 22. Snap29 localization to the KT does not requires membrane

(A) Confocal image of S2 cells processed for correlative-light electron microscopy (CLEM) and stained with anti-pH3. White arrow indicates a mitotic cell. (B-B') Immuno-gold

localization of Snap29 in interphase and pro-metaphase S2 cells. Pseudo-coloring in red identifies chromosomes (Ch), in yellow organelle membranes and NE and in green MTs. White arrows indicate examples of signal in the nucleoplasm that is not associated to membranes, but rather to electron-dense material. The black arrow indicates intact MVB. High magnifications show Snap29 highly enriched at chromosome sister KT (arrowheads) and in close proximity to MTs (green). MVB: multivesicular body; NE: nuclear envelope; PM: plasma membrane.

We found that sister KTs of dividing chromosomes (Ch) were heavily labeled by Snap29 (Fig. 21B'). At higher magnification, we observed that Snap29 decorates the outer KTs, in close proximity to microtubules (MTs). Importantly, this analysis did not highlight the presence of any membrane associated to Snap29 at the KT or in the nucleoplasm during mitosis. In interphase cells, immune-gold labeling was excluded from the nucleus, indicating that Snap29 signal is specific (Fig. 21B). Membranes of organelles, as for example multi-vesicular bodies (MVB), were also decorated with Snap29 and visible, indicating that membranes were well preserved during CLEM processing (black arrow, Fig. 22B'). Together, our CLEM analysis reveals the absence of membranes associated to Snap29 signal at the KT of dividing cells.

To test whether Snap29 recruitment at the KT depends on autophagy, we took advantage of the UAS-GAL4 system (Brand & Perrimon 1993) to overexpress specific short hairpins in the *Drosophila* wing imaginal disc, which is the epithelial organ precursor of the adult wing (Fig. 23A). Specifically, we overexpressed short hairpins against Syntaxin17 and Vamp7 (*Drosophila* homologue of VAMP8), the two SNARE proteins predicted in *Drosophila* and human cells to partner with Snap29, in regulating autophagy (Takáts et al. 2013; Itakura et al. 2012). In *Drosophila* control and depleted wing disc tissues, Snap29 resides at the KT of dividing cells, identified using pH3 (Fig.23B).

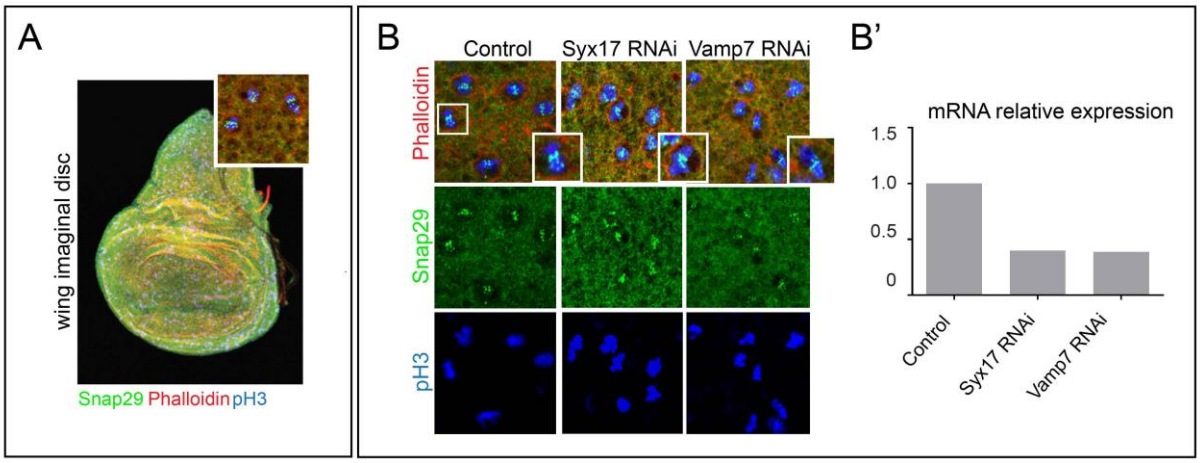

Figure 23. SNAP29 localization at the KT does not rely on its function during autophagy

(A) Maximum projections of confocal sections of third instar larval wing imaginal discs, stained with anti-Snap29, anti-pH3 and Phalloidin to mark F-actin. High magnification shows localization of Snap29 in dividing cells. (B) Comparable maximum projections of confocal sections of the dorsal wing discs in which Syntaxin17 and Vamp7 were downregulated. Anti-pH3 was used to identify mitotic cells. (B') qPCR analysis of Syntaxin17 and Vamp7 mRNA levels relative to the experiment shown in B.

By testing the level of Syntaxin17 and Vamp7 downregulation in wing imaginal discs by qPCR analysis, we found mRNA reduction of 50% (Fig. 24B'). Together, these experiments show that Snap29 at the KT of dividing cells is not associated to membranes or requires autophagy regulators.

5.1.5 Snap29 localization to the KT depends on KMN network components and requires the SNARE1 domain

To investigate whether Snap29 localization at KTs relies on KMN network proteins *in vivo*, we overexpressed short hairpins against KMN network proteins in *Drosophila* wing imaginal discs, using the UAS-GAL4 system mentioned above. We confirmed the effective level of downregulation by qPCR (Fig. 24A-A').

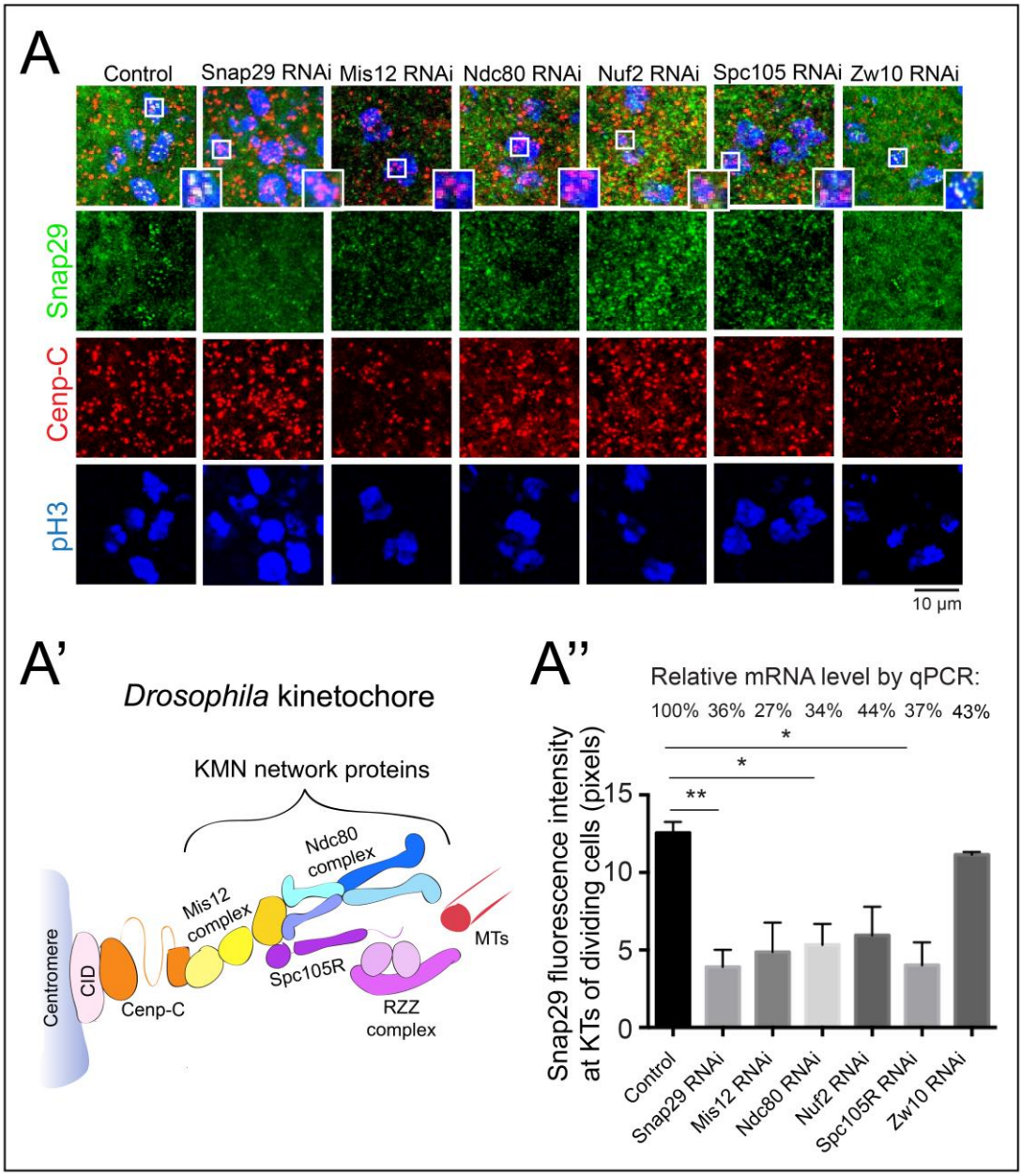

Figure 24. Snap29 localization at KTs depends on outer KT components.

(A) Comparable maximum projections of confocal sections of dorsal wing discs, in which Snap29 and the reported outer KT proteins were downregulated. Anti-pH3 labels mitotic cells and Cenp-C marks KTs. (A') Schematic representation of the *Drosophila* kinetochore. (A'') Fluorescence intensity quantification of Snap29 signal at KTs of dividing cells relative to the experiment shown in panel A, considering >30 KTs for each condition. The signal of Snap29 at KTs is sensitively reduced compared to control upon Snap29, Mis12, Ndc80, Nuf2 and Spc105R downregulation. Relative mRNA expression of reported downregulated genes versus control (expressed in %), measured by qPCR, is shown above the graph. *P*-values are determined by Kruskal-Wallis test with Dunn's multiple comparison analysis. $P^* \leq 0.05$; $P^{**} \leq 0.01$.

Immunofluorescence analysis of KTs of dividing cells, identified respectively by labeling to detect Cenp-C and pH3, revealed a strong reduction of Snap29 KT signal upon Mis12, Ndc80, Nuf2 and Spc105 downregulation, comparable to that measured in Snap29-depleted tissue. Similar to our previous evidence in S2 cells, downregulation of the RZZ component Zw10 *in vivo* did not affect Snap29 localization. Overall, these data suggest that the recruitment of Snap29 depends on KMN network components.

We next identified which portion of Snap29 is required for localization to the KT. To this end, we performed a structure-function analysis by overexpressing three different mutant forms of Snap29 in Snap29-depleted wing imaginal discs and we quantified Snap29 signal at KTs (Fig. 25A).

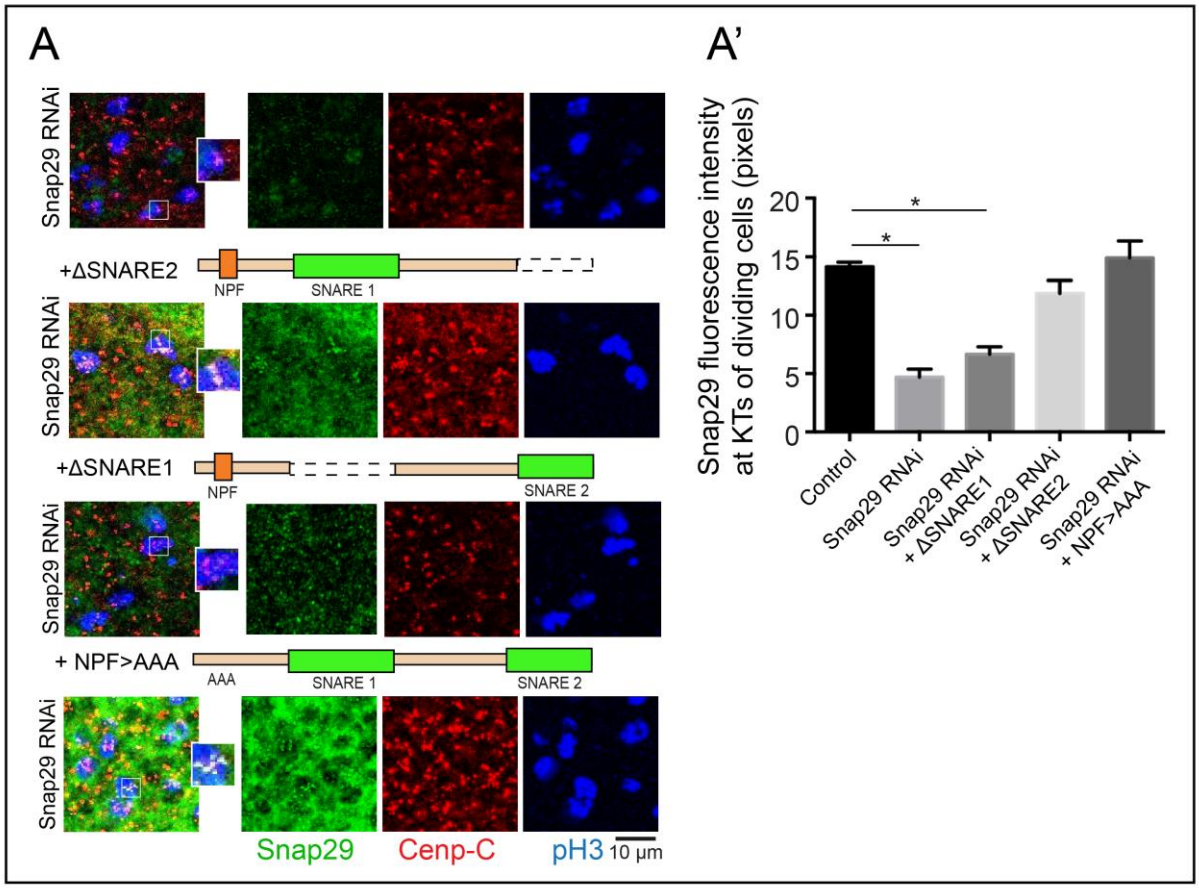

Figure 25. Snap29 localization at KTs requires SNARE 1 domain

(A) Comparable maximum projections of confocal sections of dorsal wing discs in which Snap29 has been downregulated and the indicated Snap29 mutant forms over-expressed. Cartoons of the expressed Snap29 mutant forms are shown above the panels. Anti-pH3 labels mitotic cells and Cenp-C marks KTs. (A') Quantification of Snap29 signal at KTs relative to the experiment in panel A, considering >28 KTs per sample. Note that the expression of a form of Snap29 lacking the SNARE1 domain does not rescue Snap29 localization to KTs in Snap29 depleted tissue. *P*-values are determined by Kruskal-Wallis test with Dunn's multiple comparison analysis. $P^* \leq 0.05$.

In particular, we used two Snap29 constructs lacking the first or the second SNARE domain (termed Delta SNARE1 and Delta SNARE2) and a Snap29 construct with a mutated NPF motif (NPF>AAA). Only in the absence of the SNARE1 domain, Snap29 was not localized to the KT, indicating that SNARE1 domain is required for such localization (Fig. 25A'). Overall,

these data suggest that Snap29 localization at the KT relies on KMN network components and that such localization requires the SNARE1 domain of the protein.

5.1.6 Snap29 controls cell division and tissue architecture

To understand whether Snap29 plays a role during cell division, we performed a time-lapse analysis on S2 cells expressing Histone 2B-GFP and mCherry-α-Tubulin. Upon knock-down of Snap29 (dsSnap29) for 96 hours, cells presented segregation defects, such as lagging chromosomes, failure to form a proper metaphase plate or tripolar spindles, leading to the formation of micronuclei (Movies 1 and 2) (Fig. 26A).

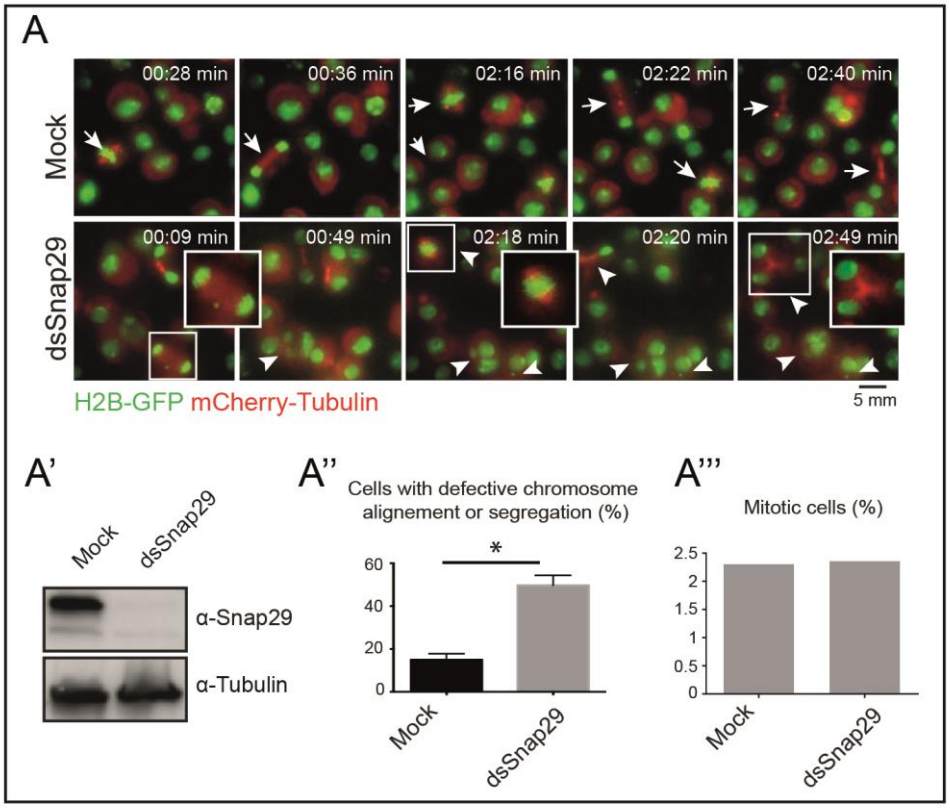

Figure 26. Snap29 depletion affects mitotic progression

(A) S2 cells selected frames of time-lapse imaging of mock or cells treated for 96 hours with dsRNA against Snap29 at indicated mitotic stages. Upon knock-down of Snap29 (dsSnap29) for 96 hours, cells presented segregation defects, such as lagging chromosomes, failure to form a proper metaphase plate or tripolar spindles (high magnifications of insets), leading to

the formation of micronuclei (arrowheads). By contrast, mock cells undergo correct cell division (arrows). (A') Western blot of cells protein extracts from mock and Snap29 depleted cells relative to the experiment in A. Anti-alpha-Tubulin was used as loading control. (A'') Quantification of the mitotic phenotype of mock and dsSnap29 depleted cells, based on time-lapse imaging of an average of >28 individual cells per sample. *P* value is determined by two-tailed t-test considering all defects together. (A''') Mitotic index measure (ratio between mitotic and interphase cells) of dsSnap29 treated cells did not show any difference compared to mock. $P^* \leq 0.05$

Western Blot analysis revealed strong downregulation of Snap29 in dsSnap29 treated cells (Fig. 26A'). Overall, almost 50% of dsSnap29 dividing cells presented aberrant mitosis, compared to 12% of mock dividing cells (Fig. 26A''). Moreover, mitotic index analysis did not highlight differences between mock and ds Snap29 cells, suggesting that Snap29 depletion does not alter the duration of cell cycle (Fig. 26A''').

To further study the mitotic role of Snap29 during tissue development *in vivo*, we depleted Snap29 in the follicular epithelium (FE), the monolayer encasing the germ-line of the adult *Drosophila* ovary. As previously observed in wing imaginal discs, we detected the presence of Snap29 at KTs of dividing cells in FE (Fig. 27A). Upon Snap29 down regulation, the FE appears disorganized and multilayered, suggesting that Snap29 function is required to sustain epithelial tissue architecture (Fig. 27A').

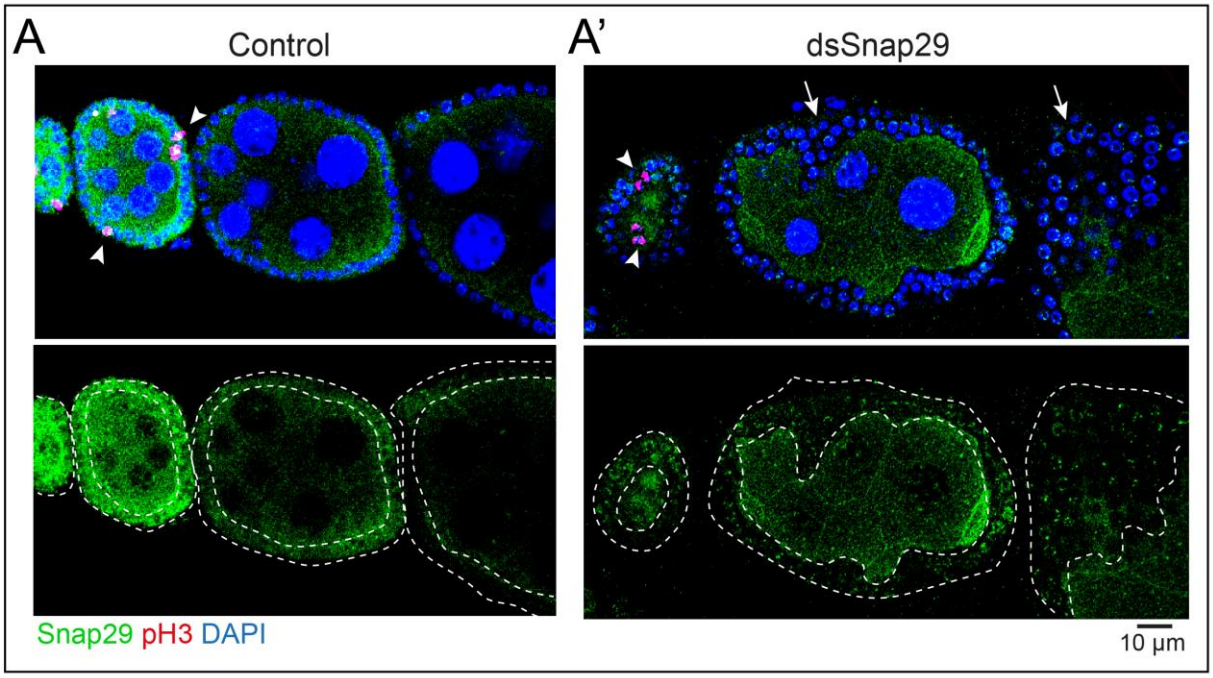

Figure 27. Snap29 depletion affects *Drosophila* tissue architecture

(A) Single confocal sections of *Drosophila* adult ovarioles labeled with anti-pH3, anti-Snap29 (also shown as single channel) and DAPI. (A') Snap29 depletion under the follicular cell-specific GAL4 promoter (traffic jam) shows an invasive follicular epithelium phenotype compared to control (arrows). Follicular epithelium is highlighted by white dashed lines. Arrowheads show that Snap29 signal of dividing cells is reduced in Snap29 depleted tissue compared to control.

We then studied *Snap29B6-21*, a previously characterized *Drosophila* mutant, which generates a truncated form of the protein lacking the SNARE2 domain (Morelli et al. 2014). Eye imaginal discs predominantly composed of cells homozygous for *Snap29B6-21* mutation (mutant eye discs hereafter) show altered tissue morphology (Fig. 28). In addition, compared to control, Snap29 mutant eye discs are composed of many cell undergoing apoptosis. Block of apoptosis by the overexpression of the bacterial inhibitor p35, which *per se* does not alter eye disc architecture, reduces the presence of apoptotic cells and strongly worsens Snap29 mutant phenotype. This indicates that loss of Snap29 in a developing epithelium initiates a process of aberrant tissue formation that is counteracted by apoptosis (Fig. 28).

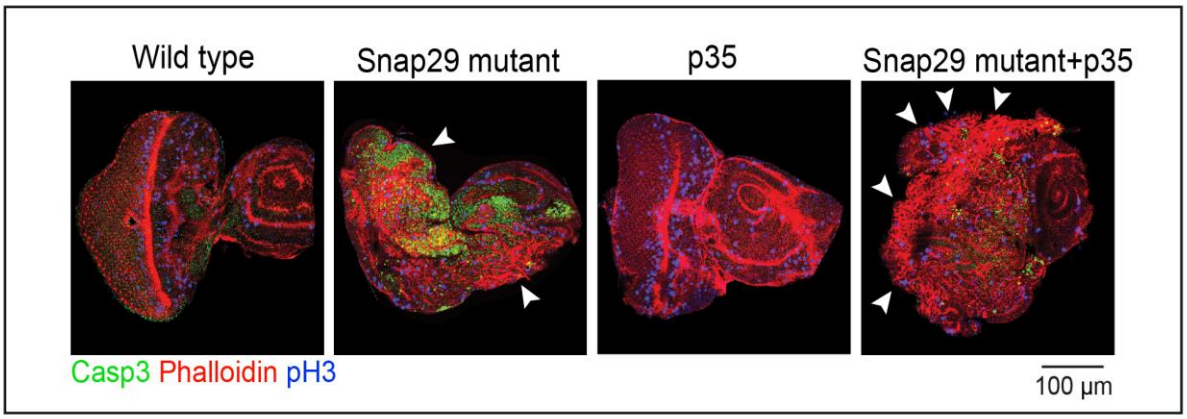

Figure 28. *Drosophila* Snap29 activity supports tissue formation and controls cell division in imaginal discs

Single confocal sections of wild type, Snap29 mutant and of otherwise wild type and Snap29 mutant eye imaginal discs expressing the bacterial apoptosis inhibitor p35. Eye imaginal discs were stained with anti-pH3, Phalloidin and anti-cleaved-Caspase 3.

To test whether such tissue architecture disruption is due to membrane fusion alterations, we tested whether loss of Snap29 could be rescued by overexpression of paralogs that are not involved in cell division. Snap25 is a Snap29 paralog that mediates vesicles fusion during synaptic transmission (Megighian et al. 2010). Interestingly, Snap24 (the *Drosophila* homolog of mammalian SNAP23), a third member of the SNAP protein family, can functionally rescue Snap25 mutant phenotype at the neuromuscular junctions, suggesting a certain level of redundancy among SNAP family members in regulating membrane fusion (Vilinsky et al. 2002). However, we found that the overexpression of Snap25 in Snap29 mutant eye discs, did not determine any rescue of the altered epithelial architecture morphology (Fig. 29A). The amount of Snap25 mRNA upon overexpression was monitored by qPCR and was 5 times more abundant than that observed in Snap29 mutant tissue not overexpressing Snap25 (Fig.

29A'). These data indicate that Snap29 and Snap25 functions in tissue architecture are not redundant.

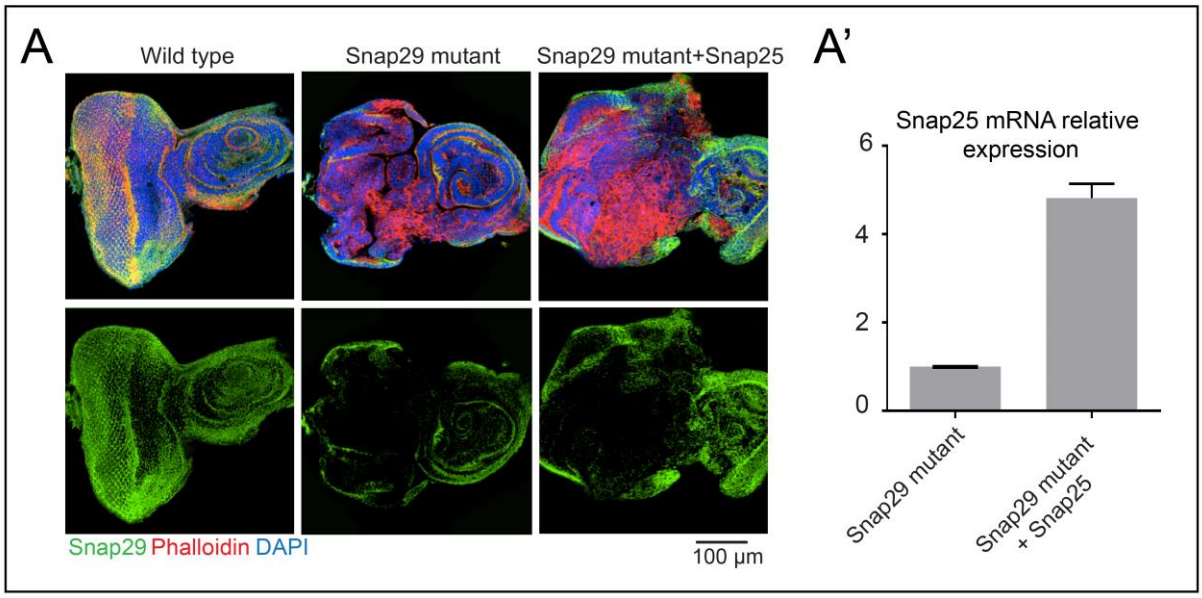

Figure 29. Snap29 and Snap25 functions are not redundant

(A) Single confocal sections of wild type, Snap29 mutant and Snap29 mutant overexpressing Snap25 eye imaginal discs. The overexpression of Snap25 in eye discs does not rescue Snap29 mutant phenotype. (A') qPCR analysis relative to experiment shown in A, revealed that Snap25 mRNA in Snap29 mutant eye imaginal discs overexpressing Snap25 is 5 fold more abundant than Snap29 mutant.

To test whether Snap29 mutant eye discs also display an impairment in cell division, we stained the tissue with pH3 and with the centromeric marker INCENP, which labels the KT during prophase and metaphase and the mitotic spindle midzone from anaphase to cytokinesis (Fig. 30A).

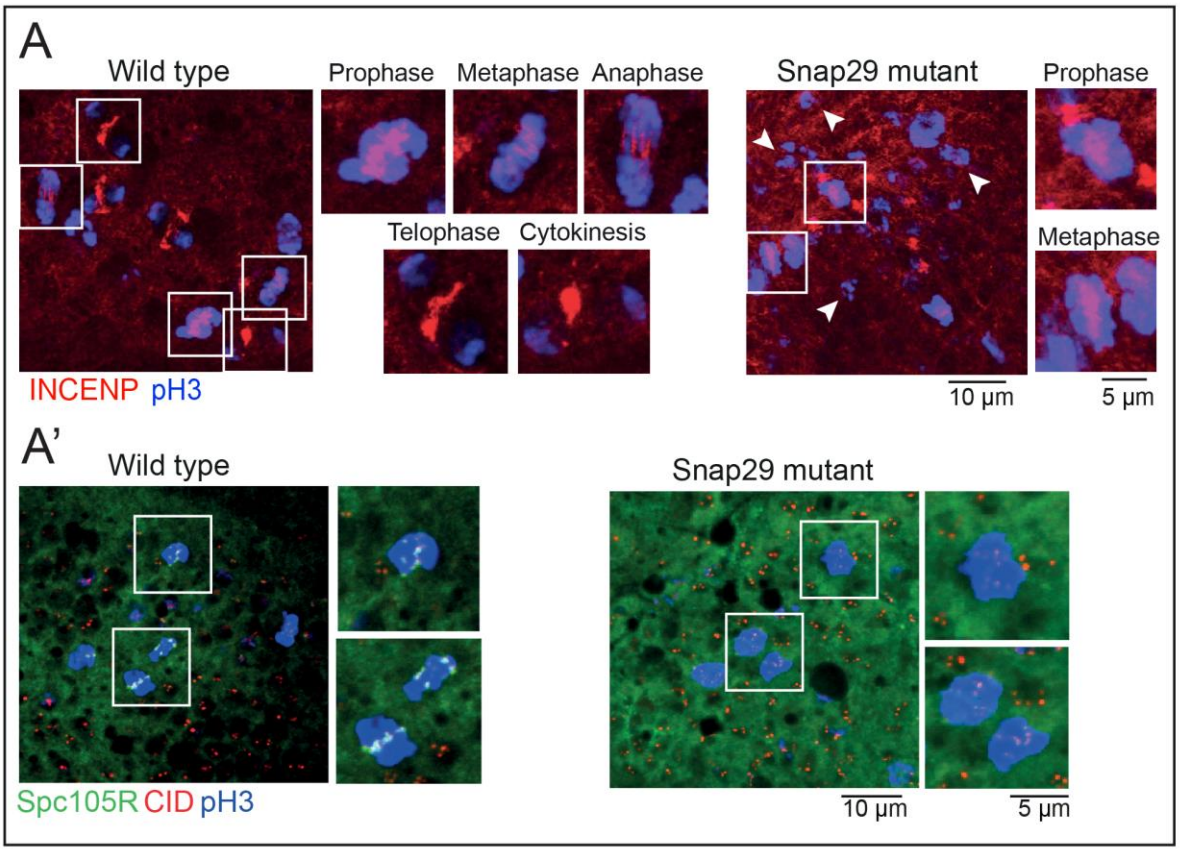

Figure 30. *Drosophila* Snap29 activity controls cell division in imaginal discs

(A) Confocal sections of portions of wild type and Snap29 mutant eye disc tissue. Tissues were stained with anti-pH3 and anti-INCENP, a marker that localizes to the centromere during prophase and metaphase and relocalizes to the spindle midzone during anaphase allowing identification of different mitotic phases (high magnification of insets). Arrowheads point to fragmented DNA. (A') Confocal sections of portions of wild type and Snap29 mutant eye disc tissues stained with the inner KT marker CID and outer KT marker Spc105R. High magnifications of insets show that Spc105R localization at the KT of dividing cells is lost in Snap29 mutant tissue.

In control discs, such labeling allows us to identify unambiguously all mitotic stages of dividing cells in tissue. By analyzing Snap29 mutant discs, we instead observed the presence of pH3-positive foci not clearly attributable to a defined late mitotic stage. Moreover, the staining of Snap29 mutant discs with Spc105R revealed that the outer KT component was absent at KTs of dividing cells when compared to control discs, indicating that the outer KT

assembly might be defective in mutant tissue (Fig. 30A'). Because eye imaginal discs mutant for autophagy genes do not display epithelial architecture defects, such phenotypes are unlikely due to the impairment of Snap29 function during autophagy (Morelli et al. 2014; Takáts et al. 2013; Takáts et al. 2014; Juhász et al. 2007; Itakura et al. 2012). Overall, these data indicate that Snap29 is required to ensure correct cell division, and that such function might be essential to ensure correct tissue architecture.

5.2 Snap29 involvement in CEDNIK pathogenesis

5.2.1 Establishment of genetic models of CEDNIK in zebrafish

Mutations of SNAP29 in humans cause a rare and severe congenital syndrome called CEDNIK (Cerebral Dysgenesis, Neuropathy, Ichthyosis and Keratoderma), which gives rise to neurological and dermatological manifestations with poor life expectancy (Fuchs-Telem et al. 2011; Rapaport et al. 2010; Sprecher et al. 2005). So far, animal models of CEDNIK syndrome were used mainly to investigate dermatological alterations, while others symptoms as neonatal feeding impairment, muscle hypotonia, and neurological defects were just reported by clinicians, but never investigated. In order to model and explore CEDNIK traits, we used the zebrafish *Danio rerio* as *in vivo* model.

To study the role of Snap29 in zebrafish, we first characterized *snap29* mRNA expression during development. To this end, we performed an *in situ* hybridization, which indicates that *snap29* mRNA is expressed ubiquitously during all stages of development from 2.5 hours post fertilization (hpf) and onwards (Fig. 31A). We obtained similar results performing Reverse transcriptase PCR (RT-PCR) of developing embryos and larvae (Fig. 31B).

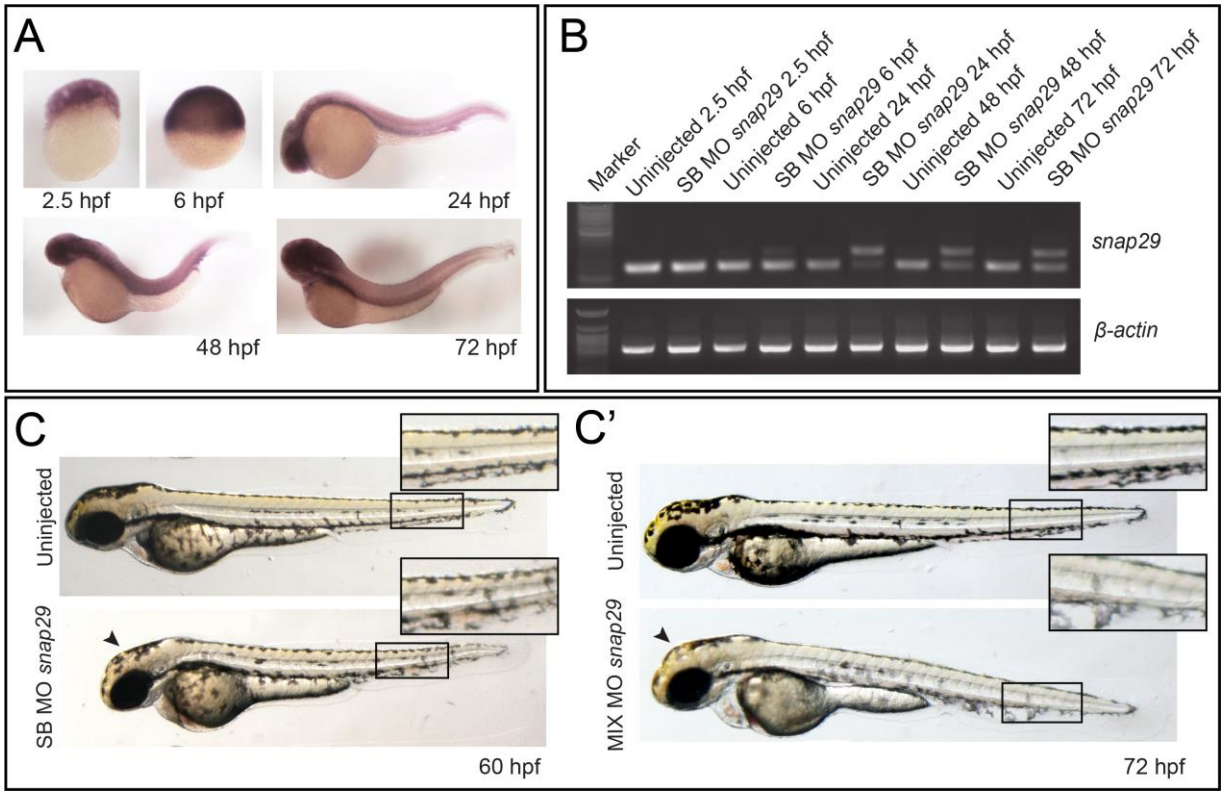

Figure 31. *snap29* mRNA expression and depletion in zebrafish embryos.

(A) *In situ* hybridization with *snap29* labeled anti-sense probe on zebrafish embryos at the indicated developmental stages. (B) RT-PCR performed to assess *snap29* transcript level using genomic DNA extracted from embryos uninjected or injected with a splicing block Morpholino against *snap29* (SB MO *snap29*) at the indicated hours post fertilization (hpf). β-actin was used as internal control. (C-C') 60 and 72 hpf embryos injected respectively with SB MO-snap29 or with a mix of SB and ATG Morpholino (MIX MO *snap29*). Both morphants display lighter pigmentation at the level of the head (arrowheads) and less aligned melanocytes in the tail contour (high magnification of the insets) compared to uninjected embryos.

To deplete *snap29* mRNA and to avoid off-targets effects, we injected a low dosage mixture of splicing block (SB) and ATG Morpholino (MO) against *snap29* (MIX MO). We could monitor the efficacy of *snap29* SB MO by RT-PCR, since it produces a retained intron transcript, longer than wild type *snap29* mRNA (Fig. 31B). Importantly, the analysis of SB MO and MIX MO *snap29* morphants, respectively of 60 and 72 hpf, give rise to similar phenotypes, such as lighter pigmentation at the level the head and less regular distribution of

melanocytes in the tail compared to uninjected embryos (Fig. 31C-C'). Remarkably, the SB MO against *snap29* reproduces the same phenotype previously published in Li et al., 2011. The ability of depleting *snap29* specifically was used to validate and extend the analysis of *snap29* mutant fish (see below).

The zebrafish Snap29 protein and its human homolog have 46% of identical residues, 19.5% of residues with similar properties and possess, as all other species, a NFP motif and two SNARE domains (Fig. 32A). In particular, SNARE 1 and SNARE 2 domains conserve respectively 53% and 57% of amino acids identity. The reported nonsense mutations associated to CEDNIK syndrome (red triangles, Fig. 32A) introduce stop codons that lead to the production of proteins truncated in the first SNARE domain and before the second SNARE2 domain.

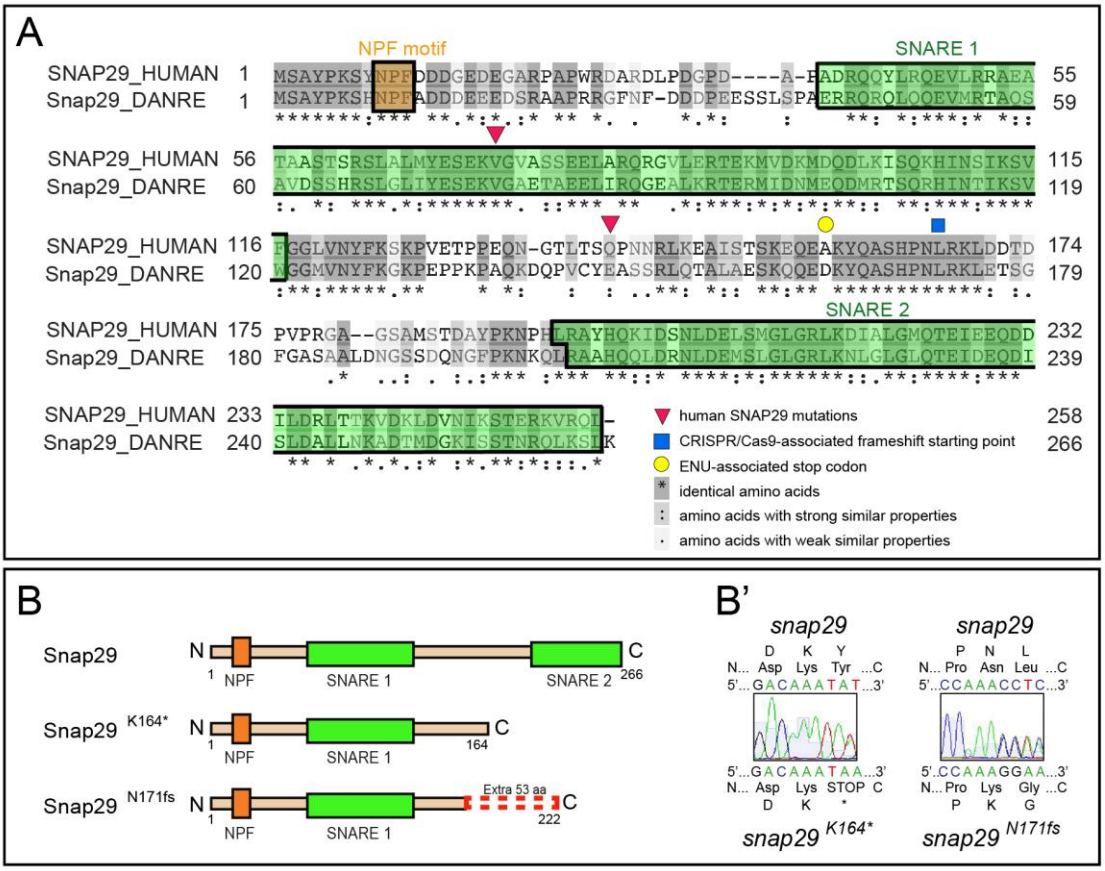

Figure 32. Snap29 conservation from zebrafish to human and Snap29 mutant proteins.

(A) Protein sequence alignment of human and zebrafish Snap29 homologues. NPF motives are highlighted by orange rectangle, while SNARE domains are highlighted by green rectangles. Red triangles refer to two SNAP29 mutations described in CEDNIK patients, green circle refer to the stop codon position generated after ENU treatment in zebrafish, while the blue square refer to the frameshift starting point occurring in CRISPR/Cas9 zebrafish mutant. Amino acids residues are colored according to their conservation between human and zebrafish. (B) Schematic representation of zebrafish Snap29 protein and of the two mutant proteins respectively, ENU mutant Snap29^{K164*} and CRISPR/Cas9 mutant Snap29^{N171fs}. (B') Interpherograms show respectively the nonsense mutation that occurs in *snap29*^{K164*} mutant, in which a stop codon occurs after lysine 164 and the starting point of the frameshift induced by CRISPR/Cas9 INDELs in *snap29*^{P170fs} in the exon 4, which occur from asparagine 170.

To establish a CEDNIK model in zebrafish, we requested an uncharacterized *snap29* ENU mutant available from Zebrafish International Resource Center (ZIRC) and we generated a CRISPR/Cas9 mutant. Both mutants called *snap29*^{K164*} and *snap29*^{N171fs}, respectively introduce stop codons that result in the production of truncated Snap29 proteins lacking the

SNARE 2 domain, similar to one of the human mutations (Fig. 32B). In particular, in *snap29*^{K164*} mutant the stop codon after lysine 164 was caused by a non-sense mutation (T>A), while the stop codon of *snap29*^{N171fs} mutant protein occurs after Indels, which cause a frameshift starting after the codon producing asparagine 171 (Fig. 32B').

To obtain *snap29* mutant homozygous embryos (-/-), we mated parents heterozygous for *snap29*^{K164*} or *snap29*^{N171fs} (+/-). In accordance with Mendelian inheritance, we expected 25% of homozygous embryos for the mutation (-/-), 50% of heterozygous (+/-) and 25% of wild type homozygous embryos (+/+) (Fig. 33A). Macroscopic analysis of 5 days post fertilization (dpf) larvae revealed that in both crosses roughly 25% of the progeny showed the lack of inflated swim bladder, which is the organ that allow fish to float, and lighter pigmentation (Fig. 33B). Genotyping of these animals revealed that they were homozygous respectively for *snap29*^{K164*} and *snap29*^{N171fs}, and both of them do not survive longer than 9 dpf.

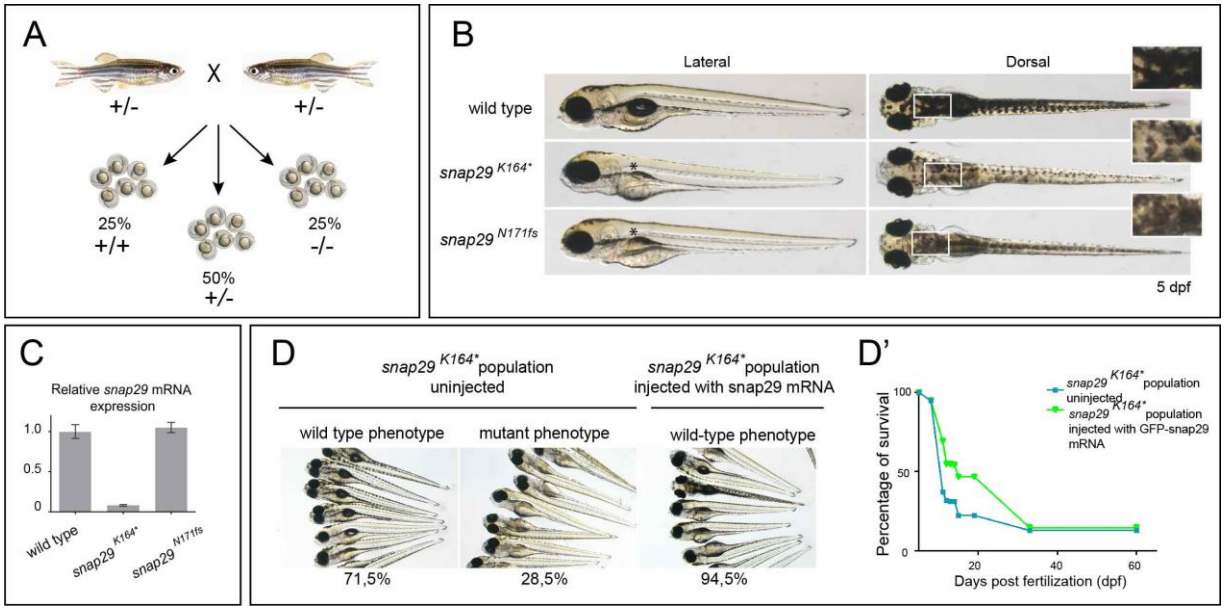

Figure 33. *snap29* mutants generation and rescue.

(A) Schematic representation of adult zebrafish heterozygous for *snap29*^{K164*} or *snap29*^{N171fs} (+/-). The progeny is composed by 25% of wild type homozygous embryos (+/+), 50% of heterozygous (+/-) and 25% of homozygous embryos for mutations (-/-). (B) Lateral and dorsal views of 5 days post fertilization (dpf) larvae of wild type, *snap29*^{K164*} and *snap29*^{P170fs} mutants. Asterisks in the lateral views indicate the lack of swim bladder, while high magnifications of the dorsal views indicate weaker pigmentation of mutants compared to wild type. (C) *snap29* mRNA relative expression measured in wild type, *snap29*^{K164*} and *snap29*^{P170fs} 5 dpf larvae. *snap29*^{K164*} mutants show a reduction of *snap29* mRNA of about 90% compared to wild type, while no reduction is detectable in *snap29*^{P170fs}. Error bars indicate standard error relative to 3 technical replicates. GAPDH was used as internal control. (D) Groups of 5 dpf larvae derived from *snap29*^{K164*} heterozygous mating (i.e. *snap29*^{K164*} population), respectively uninjected and injected with *snap29* mRNA. Larvae were discriminated in wild type phenotype and mutant phenotype according to their normal or weaker pigmentation. *snap29*^{K164*} uninjected population is composed by 71.5% of wild type phenotype larvae and by 28.5% of mutant phenotype larvae. *snap29*^{K164*} injected population present 94% of wild type phenotype larvae, demonstrating that *snap29* mRNA injection rescues the mutant phenotype. (D') Survival curve of uninjected and injected with *snap29* mRNA *snap29*^{K164*} populations at indicated dpf. Percentage of survival refers to zebrafish larvae or adults survived from initial number of fertilized embryos. Injected *snap29*^{K164*} population shows an increase of survival compared to uninjected population until 33 dpf.

Then, we quantified *snap29* mRNA level of both mutants selected according to the phenotype described above and we found that, while *snap29*^{N171fs} homozygous larvae express *snap29* mRNA level comparable to control, *snap29*^{K164*} homozygous larvae display a reduction of more than 95%, suggesting that they are subjected to nonsense-mediated decay (NMD) mRNA degradation (Fig. 33C). Since the first CEDNIK patient report showed a strong reduction of *SNAP29* mRNA (Sprecher et al. 2005), we decided to utilize *snap29*^{K164*} homozygous mutants as CEDNIK model. Moreover, since other reported patients have not been analyzed at the mRNA stability level, *snap29*^{N171fs} mutant might eventually represent a model for these or future patients (Rapaport et al. 2010).

To validate our model, we next tested whether the lack of swim bladder development and the lighter pigmentation previously observed in homozygous larvae were caused by *snap29* mutation. To achieved this, we attempted to rescue the phenotypes by injecting a GFP-tagged zebrafish *snap29* (GFP-snap29*)* mRNA in a population of one-cell embryos derived from the mating of *snap29*^{K164*} heterozygous fish (Fig. 33D). As expected, in the uninjected population, roughly a quarter (28.5%) of 5 dpf larvae displayed the above mentioned phenotypes and the rest (71.5%) of larvae were wild type-like. In contrast, the vast majority (94.5%) of the injected population larvae exhibited a wild type-like phenotype. Moreover, injected population displayed increased survival (Fig. 33D'). By genotyping a portion of the population, we found that homozygous larvae were still present at 14 dpf, but not at 40 dpf. The survival curve analysis suggests that the rescue extends the lifespan of some homozygous larvae up to 33 dpf. Genotyping was performed by extracting genomic DNA from single larvae and fish, amplifying the region of interest and sequencing samples (data not shown). These data indicate that *snap29*^{K164*} zebrafish mutants display a genetic lesion representative of CEDNIK patients. Moreover, we proved that homozygous *snap29*^{K164*} zebrafish mutants

display specific phenotypes that are due to loss of Snap29, since we were able to rescue them temporarily by providing ectopic wild type Snap29.

5.2.2 Characterization of developmental defects of *snap29* mutant

Lighter pigmentation is a trait that has not been reported in CEDNIK patients, so we analyzed it more carefully. To this end, we analyzed melanocytes of *snap29*^{K164*} mutants in detail. Compared to wild type, we did not appreciate any difference in melanocytes number (Fig. 34A).

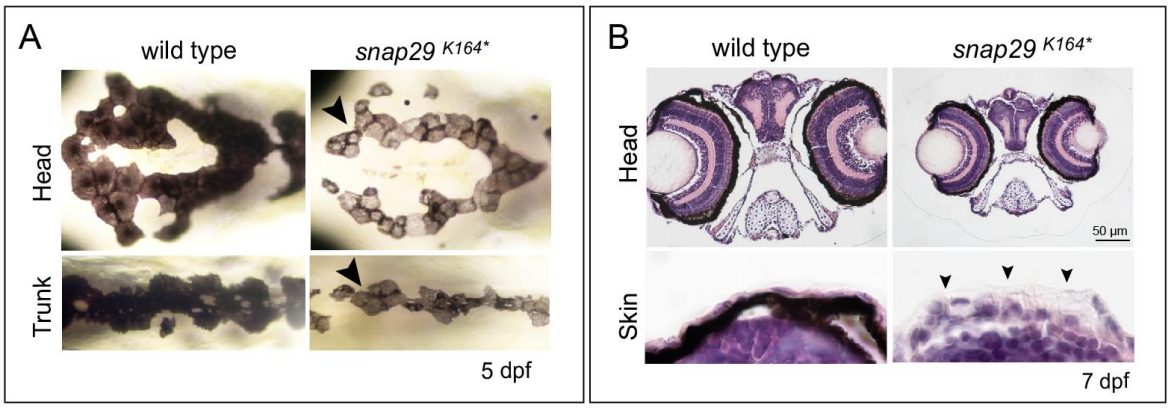

Figure 34. Major defects of *snap29* mutants

(A) Dorsal views of the same regions of head and trunk of wild type and *snap29*^{K164*} mutant at 5 dpf. Arrowheads indicate less pigmented melanocytes in *snap29*^{K164*} mutant compared to wild type. No evident difference in melanocytes number was detected. (B) Hematoxylin-Eosin sections of heads and skin detail of 7 dpf larvae. Note the reduced size of the head and the epidermal thickening (arrowheads) in *snap29*^{K164*}mutant compared wild type.

However, we noticed a reduced amount of melanin accumulated within melanocytes. These data suggest that Snap29 might regulate pigment production, possibly at the level of trafficking to melanosomes, which are lysosomal derivatives. By analyzing the morphology of *snap29*^{K164*} mutant larvae in detail, we observed a prominent microcephaly and skin

thickening (keratoderma), two traits that characterize human CEDNIK syndrome (Fig. 34B). Taken together, we can conclude that Snap29 exerts a role in melanocyte pigmentation in zebrafish and that *snap29*^{K164*} mutant recapitulates relevant features of CEDNIK human syndrome.

Another prominent feature of *snap29*^{K164*} mutant larvae, perhaps related to the inability to feed of CEDNIK infant, is the lack of swim bladder inflation (Fig. 35A-top row). Swim bladder inflation in zebrafish occurs after 120 hpf and is required for free feeding, since it allows buoyancy and active swimming after yolk consumption (Strähle et al. 2012). To test this hypothesis, we administered Rhodamine Dextran-containing food to 6 dpf wild type and *snap29*^{K164*} mutant larvae. We observed that stomachs of *snap29*^{K164*} mutant larvae were empty as they are those of wild type animals that were not provided with food (Fig. 35A-lower row). The inability to feed can be one of the causes determining the precocious lethality observed at 9 dpf occurring in *snap29* mutants.

Since swim bladder is inflated by air gulped from water surface through mouth opening (Lanny et al. 2009), we wondered whether *snap29*^{K164*} mutants present normal buccal cartilages. Alcian Blue staining on ventral cranial cartilages did not highlighted defects in their organization and differentiation, but only a reduction of their size, consistent with the microcephaly of *snap29*^{K164*} mutants (Fig. 35B). These data suggest that *snap29*^{K164*} mutants are not able to feed and that this inability is not caused by defective mouth cartilages organization.

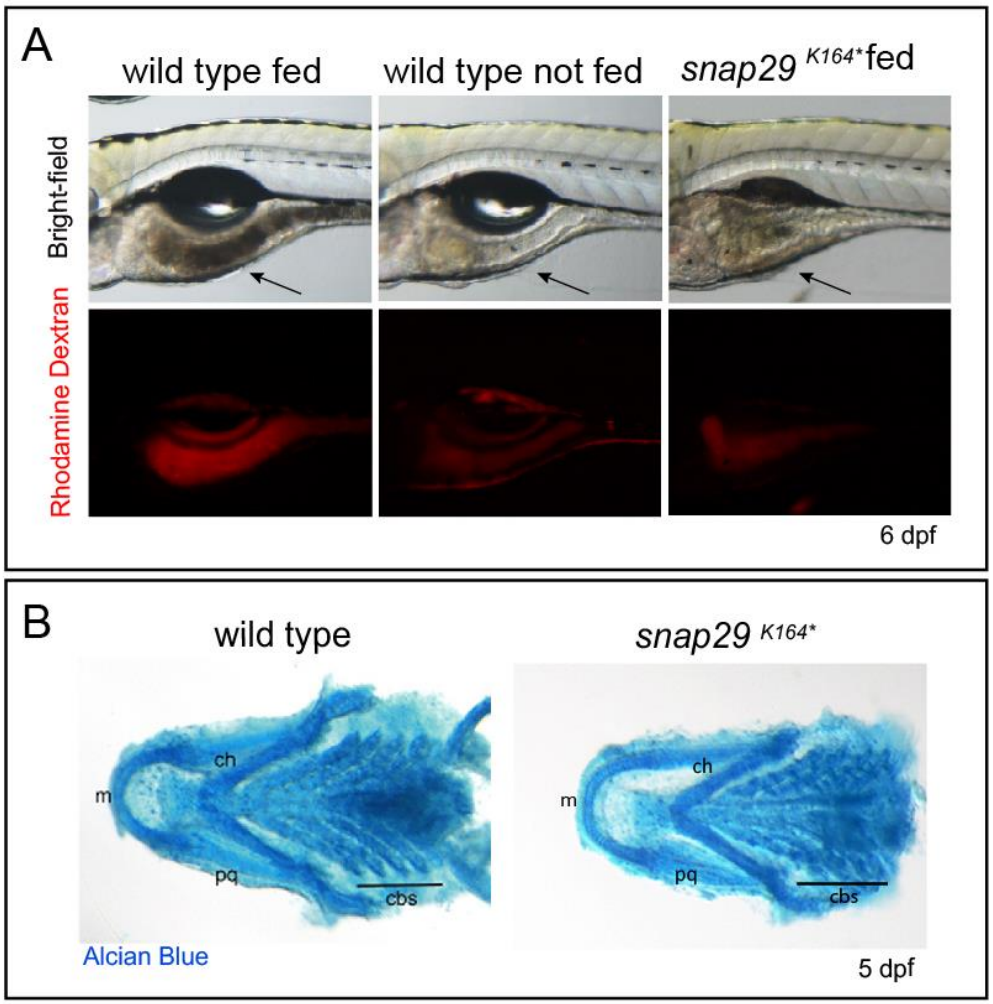

Figure 35. *snap29* mutants do not inflate the swim bladder and do not feed

(A) Lateral views of 6 dpf larvae in which stomachs are indicated by arrows. Larvae were fed with Rhodamine Dextran-containing food that allow detecting the presence of food in the stomachs. The stomach of *snap29*^{K164*} mutant appears empty as not fed wild type larva compared to fed wild type. (B) Ventral views of dissected splanchnocranium of 5 dpf larvae. Cartilages staining with Alcian Blue did not highlight any difference in their organization and/or differentiation between wild type and *snap29*^{K164*} mutant. (m) Meckel's cartilages; (ch) ceratohyal; (pq) palatoquadrate; (cbs) ceratobranchials.

To investigate the inability of *snap29*^{K164*} mutant to swim correctly, we performed a touch-evoked escape response assay, which allows to evaluate the neuromuscular performance underlying sensation and movement. By stimulating tails of 6 dpf mutants with a pipette tip, we observed that 70 milliseconds (ms) after one single touch, wild type larvae were able to

swim away, while *snap29*^{K164*} mutant did not respond equally well (Fig. 36A). Indeed, most of analyzed *snap29*^{K164*} mutants required two or more touches to swim away (Fig. 36A'). This result suggest that the neuromuscular system of mutant fish might be altered.

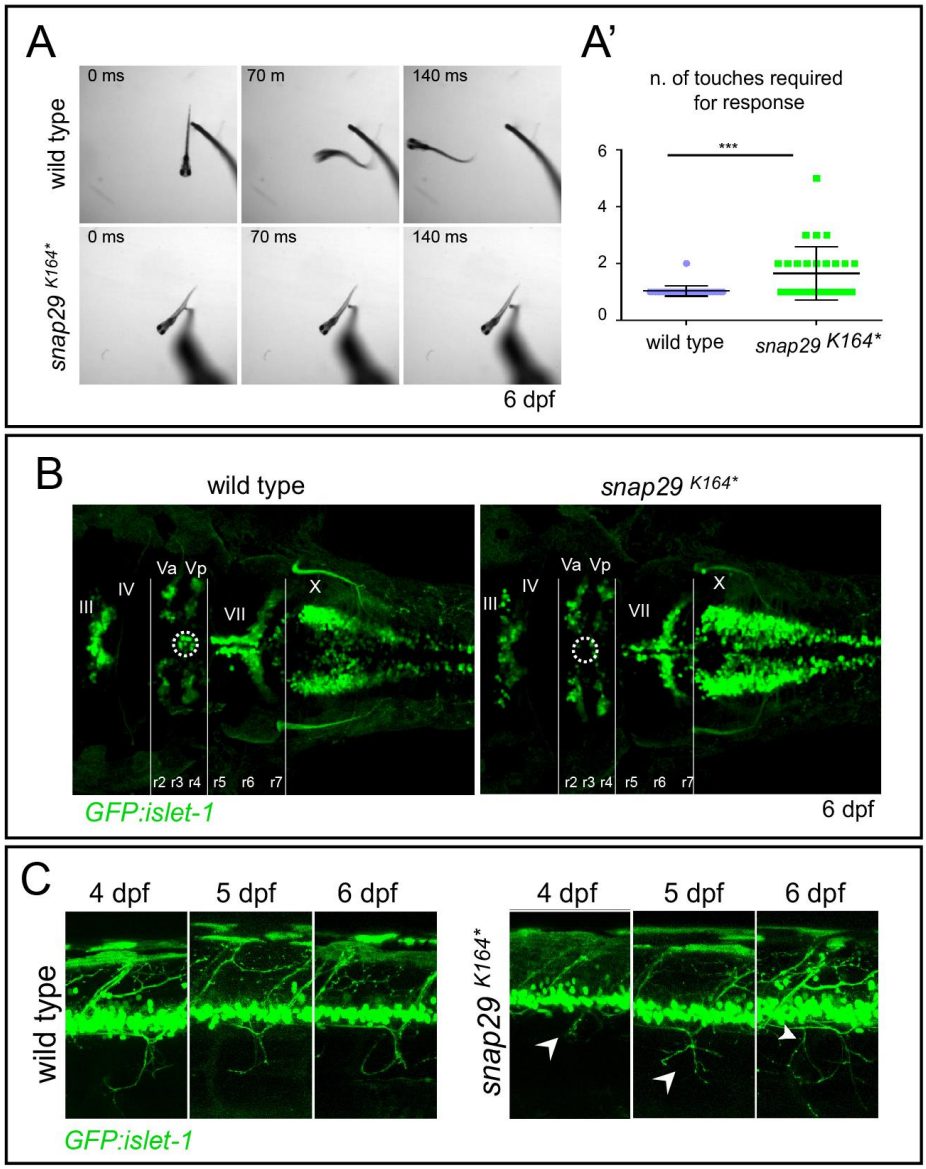

Figure 36. *snap29* mutants display motility impairment and motor neuron defects

(A) Selected frames from the movies of wild type and *snap29*^{K164*} mutant at 5 dpf, recorded for 1 minute after pipette tip stimulus on the tail. (A') Quantification of the number of touches required to provoke larva escape in *snap29*^{K164*} mutants compared to wild type. 6 larvae for each category were considered. In the graph are shown the medians, 25th and 75th percentiles. *P*-value was obtained by Mann-Whitney test. *P**** is 0.0001. (B) Dorsal views of *GFP:islet-1*

(motor neurons reporter) wild type and *snap29*^{K164*} mutant at 6 dpf. (r) rhombomere; (III), (IV), (Va) anterior, (Vp) posterior, (VII), (X) cranial nerves. *snap29*^{K164*} mutant lacks a group of nuclei (white dashed circles) located between the third and fourth rhombomere (r3, r4). (C) Trunk lateral views of *GFP:islet-1* wild type and *snap29*^{K164*} mutant at 4, 5 and 6 dpf. *snap29*^{K164*} mutants present incomplete neuron projections at 4 dpf, and extra branching within the normal motor neuron projection pattern at 5 and 6 dpf (white arrowheads) compared to wild type.

So, to investigate possible neuronal defects in *snap29*^{K164*} mutants, we used the transgenic fish line *Tg*(*islet-1:GFP*), in which GFP is expressed in motor neurons (Uemura et al. 2005). To obtain *snap29*^{K164*} mutant carrying *islet-1:GFP* transgene, we mated *snap29*^{K164*} heterozygous fish with *islet-1:GFP* strain and we derived a *snap29*^{K164*} heterozygous progeny carrying *islet-1:GFP* transgene. By analyzing the brain of 6 dpf larvae obtained from the mating of *snap29*^{K164*} heterozygous fish carrying *islet-1:GFP* transgene, we observed that *snap29*^{K164*} mutants lack a group of nuclei located between the third and fourth rhombomere (Fig. 36B). These nuclei correspond to trigeminal motor nuclei (V) of neurons that innervate different mandibular arch muscles, thus controlling mouth opening (Higashijima et al. 2000). We then analyzed motor neuron projections of *islet-1:GFP snap29*^{K164*} mutants at the level of developing somites in the trunk, and we detected the presence of incomplete neuron projections at 4 dpf, and extra branching within the normal motor neuron projection pattern at 5 and 6 dpf (Fig. 36C).

As previously mentioned, SNAP29 is known to exert its function also during synaptic transmission, but unlike the other SNAP family member SNAP25, it is a negative regulator of neurotransmission (Pan et al. 2005). Interestingly, while *snap29*^{K164*} mutant exhibits extra branching within the normal motor neuron projection pattern, MO against *snap25* causes the opposite phenotype (Wei et al. 2013). To understand whether the phenotype that we observed in *snap29*^{K164*} was caused by defects arisen during early stages of development, we analyzed

behavioral movement of 28 hpf *snap29* morphants and uninjected embryos (*snap29* morphant are referred to SB and ATG MO mix injected embryos) (Fig. 37A). In particular, recording embryos for one minute (Movies 3 and 4) highlighted that *snap29* morphants display more than 4 spontaneous movements within the chorion per minute (i.e. twitches) compared to 2 of uninjected embryos. By contrast, *snap25* morphants show a strong decrease of twitches within the chorion. Overall, these data indicate that neuronal development and synaptic transmission are altered during early development in *snap29* mutant fish.

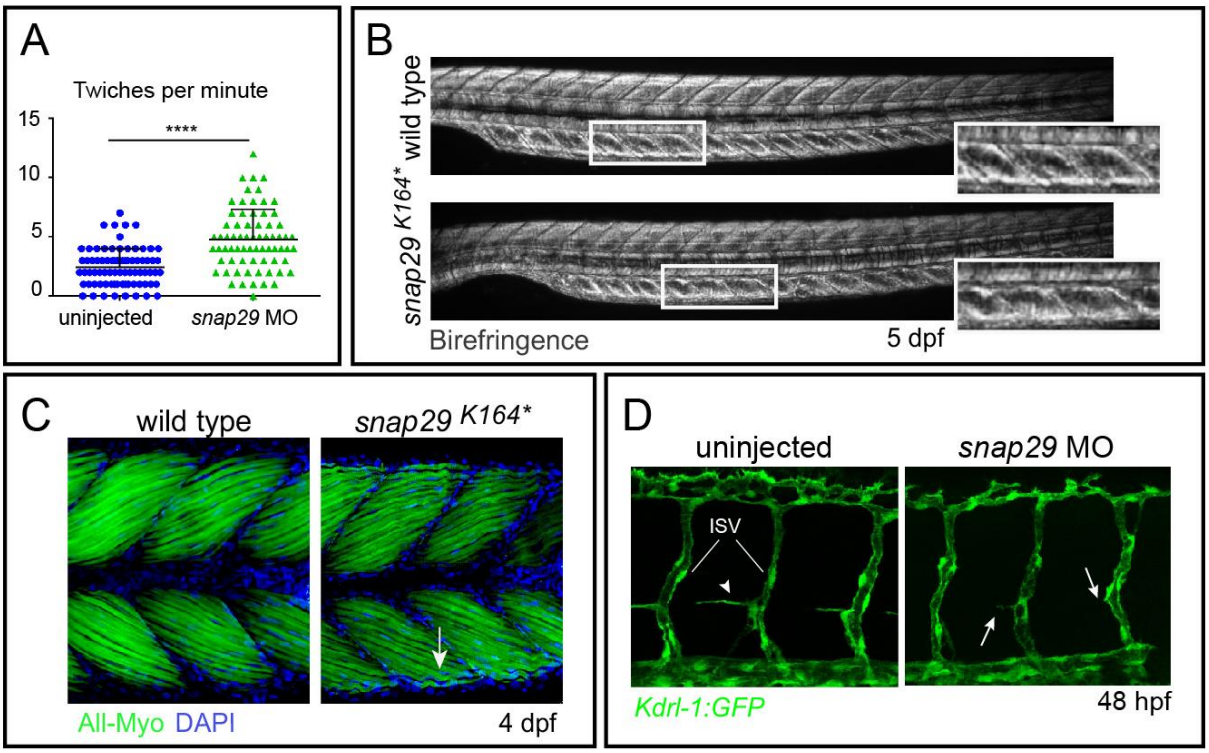

Figure 37. *snap29* mutants present skeletal muscles and blood vessels defects

(A) Quantification of spontaneous movements within the chorion (i.e. twitches) of 28 hpf uninjected and *snap29* morphant embryos recorded for 1 minute. *snap29* morphants are referred to SB and ATG MO mix injected embryos. ≥ 70 embryos were considered for each category. Medians, 25th and 75th percentiles are shown. *P*-value was obtained by Kruskal-Wallis test. *P***** < 0.0001. (B) Birefringence of wild type and *snap29*^{K164*} mutant at 5 dpf. Compared to wild type, *snap29*^{K164*} mutants displayed less bright and organized ventral somites (high magnifications in white boxes). (C) Muscle somites lateral views of 4 dpf wild

type and *snap29*^{K164*} mutant larvae, stained with anti-All myosins, which mark all the heavy chains of Myosin fibers and DAPI. *snap29*^{K164*} mutant present less compacted and ordered filaments, particularly evident in ventral somites (white arrow). (D) Lateral views of 48 hpf *GFP:Kdrl-1* (endothelial cells reporter) uninjected and *snap29* morphants embryos. Compared to uninjected embryos, *snap29* morphants lack endothelial cells migration (white arrows) from intersegmental vessels (ISV).

To test for possible defects in skeletal muscle development, we exploited an optical property called birefringence, in which light is able to rotate as it passes through ordered matter such as muscle sarcomeres (Fig. 37B). Compared to wild type, *snap29*^{K164*} mutants displayed less bright and organized ventral somites. Surprisingly, *snap29*^{K164*} mutants show abnormal blood stream circulation (Movie 5 and 6). Defects in muscle fibers pattern were further confirmed by altered myosin heavy-chains distribution, characterized by less compacted and ordered filaments (Fig. 37C).

Finally, to uncover whether blood stream alterations previously observed in *snap29*^{K164} mutants by birefringence were caused by defective angiogenesis, we injected *snap29* MO in Tg(*kdrl-1:GFP)* embryos, which express GFP in endothelial cells (Fig. 37D). Lateral views of 48 hpf *snap29* morphants embryos show impairment in endothelial cells migration from intersegmental vessels (ISV). This process is called sprouting angiogenesis and allows the formation of an organized blood vessel network from pre-existing vessels (Montero-balaguer et al. 2009).

Taken together, these results show that *snap29*^{K164*} mutant motility is affected by skeletal muscle and motor neuron defects. The presence of mouth innervation problem might also prevent proper feeding.

5.2 Characterization of cellular defects in CEDNIK zebrafish model

What could be the cellular cause for defects found in mutant fish? To determine this, we asked whether the reported cellular functions of Snap29 are altered in the CEDNIK fish model. Considering recent reports that revealed that SNAP29 regulates late step of autophagy in different organisms (Morelli et al. 2014; Takáts et al. 2013; Itakura & Mizushima 2013), we first determined whether autophagy is altered in *snap29* mutant larvae. To this end, we assessed the level of the autophagy marker LC3 of 5 dpf larvae protein extracts by Western blot (Fig. 38A-A'). We observed a mild increase in LC3I and a larger increase in LC3II in homozygous *snap29*^{K164*} mutant compared to wild type (Fig. 38B). Since LC3-II is associated to formed autophagosomes, this result suggests an impairment in late stages of autophagy. Consistent with this, by immunofluorescence, we found the accumulation of the autophagy adapter p62 in the brain of homozygous *snap29*^{K164*} mutants, when compared to wild type. These data suggest that autophagy might be altered in *snap29* mutant fish, in accordance with previous reports.

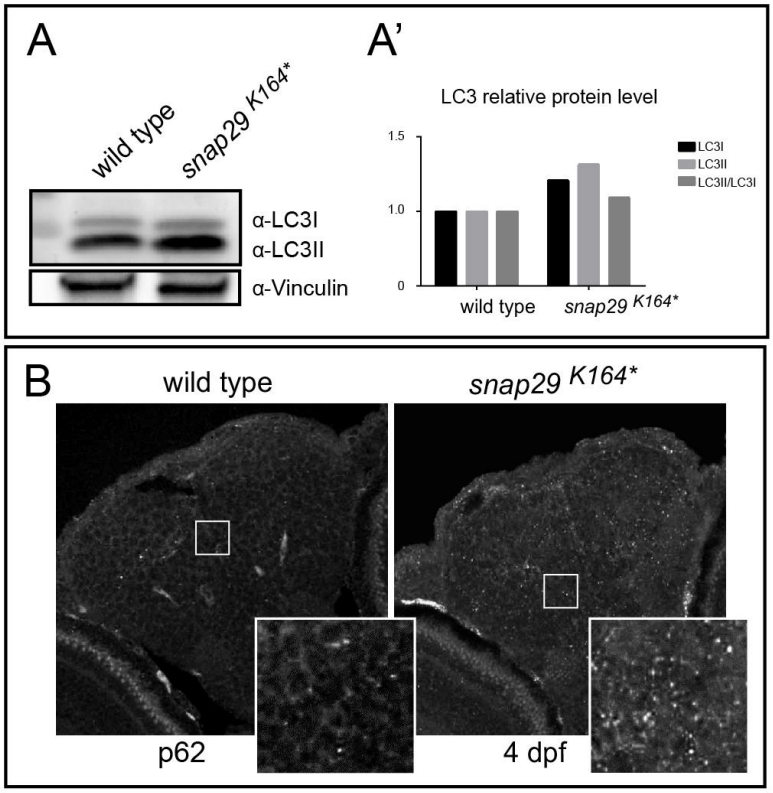

Figure 38. *snap29* mutant tissues show defective autophagy.
(A) Detection of the zebrafish LC3 protein by Western blot in 5 dpf wild type and *snap29*^{K164*} mutant larvae. The antibody recognizes two bands, LC3I and LC3II, respectively at 17 and 15 kDa. Anti-Vinculin was used as loading control. (A') Quantification of LC3I and LC3II bands intensity. Ratio between LC3II and LC3I is also reported. Quantification was performed using Image Lab software. (B) 4 dpf brain paraffin transversal sections of wild type and *snap29*^{K164*} mutant larvae stained with autophagy adaptor marker p62 antibody. *snap29*^{K164*} mutant shows an increase in the accumulation of p62 compared to wild type.

We then tested whether Snap29 acts during cell division in zebrafish, as we have reported in insect and human cells (Morelli et al. 2016). We first wondered whether Snap29 in zebrafish localizes similarly at KT during mitosis, as it does in *Drosophila*. By injecting GFP-*snap29* mRNA in one-cell embryos and by analyzing 24 hpf tails, we observed that GFP-Snap29 localizes to cytoplasmic puncta in interphase and does not localize visibly to the KT of dividing cells during any mitotic phase (Fig. 39A). To determine whether Snap29 might localize to trafficking compartments, we co injected embryos with *RFP-snap29* and *GFP-gm130*, a Golgi apparatus marker (Fig. 39B) (Pouthas et al. 2008). Colocalization analysis

revealed that SNAP29 resides in close proximity to Golgi apparatus, revealing that Snap29 is likely to act in trafficking.

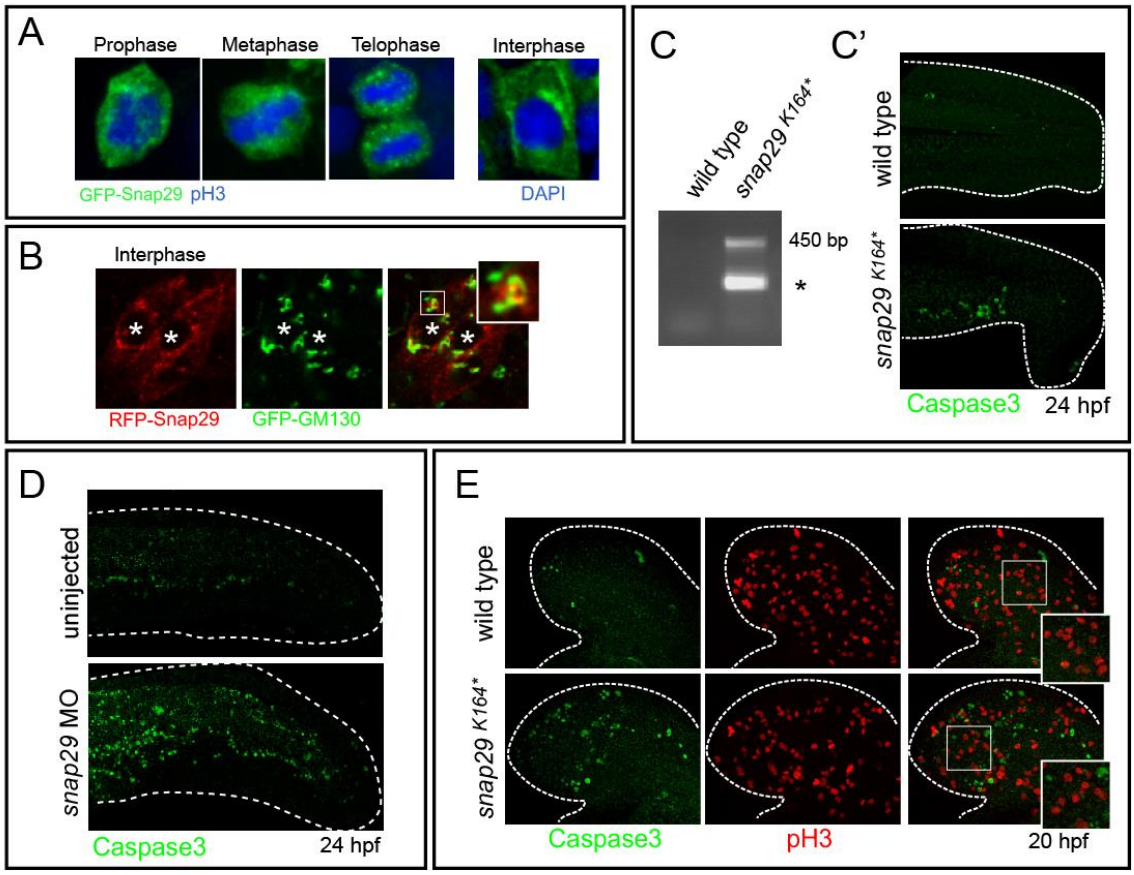

Figure 39. Snap29 promotes cell survival in zebrafish tissue during early development
(A) Comparable maximum projections of cells at indicated stages in the tail of 24 hpf embryo, injected with *GFP-snap29* mRNA and stained with anti-GFP, anti-pH3 and DAPI. No Snap29 was detectable in the nuclei of dividing cells. (B) Maximum projection of a tail portion of 24 hpf embryos, injected with mRNAs of *RFP-snap29* and the Golgi marker *GFP-gm130*. Snap29 resides in close proximity to GM130. (C) PCR performed using genomic DNA extracted from 24 hpf single embryos heads. Primer pair used allows amplification of *snap29*^{K164*} mutant DNA only. The specific amplicon band is of 450 bp. (C') 24 hpf tails of wild type and *snap29*^{K164*} mutant relative to the experiment showed in (C), stained with the apoptosis marker anti-cleaved Caspase 3. *snap29*^{K164*} mutant tail shows a higher number of apoptotic cells compared to wild type. (D) 24 hpf tails of uninjected and *snap29* morphant stained with the apoptosis marker anti-cleaved Caspase 3. *snap29* morphant embryos tail shows a higher number of apoptotic cells compared to wild type. (E) Comparable maximum projections of wild type and *snap29*^{K164*} mutant heads at 20 hpf, stained with anti-pH3 and

anti-cleaved Caspase 3. *snap29*^{K164*} mutant heads shows a high number of apoptotic cells compared to wild type.

We recently reported that SNAP29 controls the fidelity of correct chromosome segregation during cell division (Morelli et al. 2016). To investigate a possible mitotic role of Snap29 in zebrafish tissue homeostasis, as we reported for *Drosophila* tissue (Fig. 29) (Morelli et al. 2016), we analyzed embryos at early stages of development, because of their high proliferative potential. Since during early stages of development macroscopic phenotypes that helped us to discriminate *snap29*^{K164*} from wild type were not still present, we genotyped single embryos by dividing them in two parts (heads and tails). We extracted genomic DNA from single heads and performed a PCR using a primer pair, which allows amplification of *snap29*^{K164*} mutant DNA only, while we processed the corresponding tails for immunofluorescence (Fig. 39C-C'). *snap29*^{K164*} mutant tails show a high number of apoptotic cells, as we previously observed for *snap29* mutant in *Drosophila* while wild type tails had almost none. Analysis of 24 hpf tails of *snap29* morphants revealed similar increase of apoptotic cells to that observed in *snap29*^{K164*} mutants (Fig. 39D). By discriminating embryos on the basis of the presence of high levels of apoptotic cells, we then analyzed heads of *snap29*^{K164*} animals at 20 hpf (Fig. 39E). Roughly 25% of embryos (likely corresponding to the homozygous mutant population) showed a high number of apoptotic cells. However, these did not present visible defects in cell proliferation or chromosome segregation. Overall, these data indicate that in zebrafish Snap29 supports cell survival in early development, a process that is crucial for correct tissue organization and differentiation.

6. Discussion

6.1 The role of Snap29 during mitosis

6.1.1 Snap29 function during mitosis is distinct from its role during autophagy and membrane fusion

Our data uncovered a seemingly moonlighting function for Snap29 during mitosis, which we find mechanistically different from a canonical role in driving membrane fusion (Jahn & Scheller 2006; Sato et al. 2011; Sutton et al. 1998). Indeed, co-immunoprecipitation with the outer KT component Ndc80 revealed that Snap29 is a *Drosophila* KT component, further confirmed by co-localization analysis with the inner KT component CID and with Ndc80. Super-resolution imaging of *Drosophila* KT allowed us to observe that Snap29 resides in the portion of the outer KT, distal to the inner KT protein Cenp-C and proximal to the outer KT protein Spc105R. Snap29 localization at the KT requires NE fenestration, as shown by its nuclear exclusion during early mitotic stages, in which the NE and NPC, respectively marked by Lamin A and WGA, are still intact, following dynamics of recruitment at the KT similar to Spc105R. Together with our immuno-EM data indicating that Snap29 is not associated to membranes in the nucleoplasm or at KTs in promethaphase, these data reveal for the first time that a new function of Snap29 exists, radically different to described canonical SNARE activities.

Considering the trafficking roles of Snap29 and Zw10, we assessed the relationship between Zw10 and the RZZ complex. In the NRZ complex, ZW10 interacts with p31 and syntaxin 18, which in turn is involved in membrane fusion together with Sly1, Sec22 and SNAP23 (Vallee et al. 2006; Hirose et al. 2004). Alternatively during mitosis, RZZ docks to the KT through the binding of ZW10 and Rod respectively to KNL-1 and NDC80 (Caldas et

al. 2015; Cheerambathur et al. 2013). We find that downregulation of RZZ components in S2 cells does not affect Snap29 localization at the KT, suggesting that the localization of the RZZ complex is not required for Snap29 recruitment. The fact that Snap29 is required *in vivo* for recruitment of Spc105R, the KNL1 homolog, suggests that the opposite might be true (i.e. Snap29 is required for RZZ complex localization at the KT).

Recent experiments performed in mammalian neurons highlighted the involvement of the RZZ associated-motor protein Dynein in transport along MTs of autophagosomes fused with late endosomes, before fusion with lysosomes. Since such fusion process involves the formation of a SNARE complex, including SNAP29, syntaxin 17 and VAMP8, and Dynein (Cheng et al. 2015; Takáts et al. 2013; Morelli et al. 2014; Schmitt n.d.), we asked whether during mitosis Snap29 could exploit a similar set of protein to reach the KT. However, in depleted Syntaxin 17 and Vamp7 (the homolog of human VAMP8) *Drosophila* tissue or upon MTs depolymerization, Snap29 localization at the KT results unperturbed, indicating to that the function of Snap29 during autophagy and at the KT are independently regulated.

6.1.2 Snap29 is a *Drosophila* KT component required for proper chromosome segregation

The analysis of *Drosophila* wing imaginal discs depleted of KMN network components, allowed us to establish that Snap29 localization at the KT requires Mis12, Ndc80, Nuf2 and Spc105R. Considering that Snap29 contains two coiled-coil SNARE domains and that the outer KT Ndc80 complex subunits, Mis12, Nnf1 and KNL-1 (the human homolog of *Drosophila* Spc105R) possess coiled-coil regions, we hypothesize that SNARE domains of Snap29 might stabilize protein-protein interactions within the KMN network and thus indirectly, the interactions between the outer KT and MTs (Kiyomitsu et al. 2011; Petrovic et al. 2014; Petrovic et al. 2010). Interestingly, the only Knl-1 complex component

identified in *Drosophila* is Spc105R, conversely to human Knl-1 complex, which is composed by KNL-1 and ZWINT-1 (Petrovic et al. 2014). Since ZWINT-1 interacts with KNL-1 through its coiled-coil domain, we could envisage Snap29 as a potential substitute of ZWINT-1 in *Drosophila.* ZWINT-1 downregulation disrupts RZZ complex localization at the KT, thus avoiding Mad2 recruitment and consequently SAC machinery assembly (Wang et al. 2004; Kops et al. 2005). SAC activity delays cell division to prevent segregation defects, such as chromosomes misalignment at the metaphase plate, leading to high rate of aneuploidy. Similar to the phenotype observed in ZWINT-1 depleted cells, Snap29 downregulation in S2 cells shows chromosomes segregation defects, often resulting in micronuclei generation. However, Snap29 depleted S2 cells did not shown any change in cell division rate compared to mock. The apparent lack of mitotic rate increase in Snap29 depleted cells could be masked by the peculiar ability of *Drosophila* SAC to bypass the prometaphase arrest even in case of mild KT-MT binding perturbations (Buffin et al. 2007). The hypothesis of Snap29 as a potential homolog of ZWINT-1 is further sustained by the lack of recruitment at the KT of Spc105R in *Drosophila Snap29B6-21* mutant tissue. In fact, experiments performed in HeLa cells demonstrated the interdependency between KNL-1 and ZWINT-1 for their recruitment at the KT (Varma et al. 2013).

To identify which Snap29 domain is required for localization to the KT, we performed a structure-function analysis. Interestingly, we found that only the SNARE1 domain is required for localization. Previously published work reported that the N-terminal portion containing SNARE1 domain of the Snap29 paralog Snap25 is essential for the syntaxin binding, consequently priming SNARE complex formation (Fasshauer & Margittai 2004; Sørensen et al. 2006). Thus, the SNARE1 domain might alternate binding of syntaxins for trafficking in interphase with binding with KMN components during cell division.

6.1.3 Snap29 function in tissue architecture is pleiotropic

Drosophila eye imaginal discs, predominantly composed of cells homozygous for *Snap29 B6-21* mutation, as well as follicular epithelium depleted of Snap29, display epithelial architecture alterations that are reminiscent of tumorigenesis. Mutations in several genes affecting autophagy, such as Syntaxin 17 and Vamp7 do not affect epithelial architecture (Morelli et al. 2014; Takáts et al. 2013; Itakura et al. 2012). Thus, impairment in cell divisions in *Snap29B6-21* mutant eye discs could cause the tumor-like phenotype. The presence of pH3-positive foci attributable to fragmented DNA, a sign of aneuploidy, and the high level of apoptosis are consistent with previous evidence demonstrating that aneuploidy and apoptosis are induced in discs by mutations in genes involved in SAC, mitotic spindle assembly and chromatin condensation. However, these mutations were not sufficient to induce tumorigenic overgrowth in absence of ectopic expression of the apoptosis inhibitor p35 (Dekanty et al. 2012). Conversely, Snap29 mutation in eye discs was sufficient *per se* to induce a tumor-like phenotype, albeit ectopic expression of p35 in *Snap29B6-21* mutants determined a worsening of the phenotype. Since impairment of both autophagy and cell division processes are not sufficient to induce dramatic epithelial architecture disruption observed in *Snap29B6-21* mutant eye discs, we hypothesize that it is the combined result of a lack of Snap29 role in mitosis and during interphase.

Intriguingly, SNAP25 was found among Rab3c interactors together with ZWINT-1 in non-dividing neurons, thus suggesting a potential role for ZWINT-1 in membrane fusion process (van Vlijmen et al. 2008). Another member of SNAP protein family, Snap24 (*Drosophila* homolog of human SNAP23), can functionally rescue Snap25 mutant phenotypes at the neuromuscular junctions (NMJ), suggesting a certain level of redundancy among SNAP family members (Vilinsky et al. 2002). In contrast, we find that ectopic expression of Snap25 in *Snap29B6-21* mutant eye discs did not determine any rescue, indicating that Snap29

functions in interphase and during cell division significantly differ from those of the paralog Snap25. Overall, it is possible that Snap29 is part of a network of membrane proteins that during evolution have been coopted to act in cell division, in a process which involves the movement of chromosomes, rather than vesicles. A similar set of data in human cells, published together with this evidence in Morelli, Mastrodonato et al. 2016, revel that, while differences with *Drosophila* exist, such moonlighting function of Snap29 is conserved in mammals.

6.2 The role of Snap29 in CEDNIK pathogenesis

To date, the most investigated CEDNIK traits have been skin defects, attributed only to the impairment of SNAP29 canonical role in membrane trafficking, but central nervous system defects and other possible alterations have not yet been explored in CEDNIK animal models (Schiller et al. 2016; Li et al. 2011).

6.2.1 CEDNIK disease modeling in zebrafish

The analysis of *snap29* mRNA expression by *in situ* hybridization and RT-PCR highlighted the presence of Snap29 already from 2.5 hours post fertilization (hpf) onwards, when zygotic transcription starts to occur (Svoboda et al. 2010). Our results are in contrast to previously reported data reporting that the expression of *snap29* begins only from 48 hpf (Li et al. 2011). However, early *snap29* mRNA expression is in accordance with the fact that injection of both splicing block Morpholino (SB MO) and a low dosage mixture of SB and ATG block Morpholino (MIX MO) against *snap29* in one-cell stage embryos induce at 24 hpf an irregular melanocytes distribution at the level of tail contour. Morpholino is an informative tool for preliminary gene function characterization, but it bears some limitations in disease

modeling. In fact, it induces transient mRNA downregulation and often provokes off-target effects (Bedell et al. 2011). Further validation of MO induced-phenotypes using genetic mutants is the standard to assert the correlation between a gene disruption and its resulting phenotype (Timme-Laragy et al. 2012; Kok et al. 2015). Importantly, the phenotypic characterization of two independent mutants, *snap29*^{K164*} and *snap29*^{N171fs}, that were respectively generated by ENU treatment and CRISPR/Cas9 technology, confirmed the presence pigmentation defects that we observed in *snap29* morphants. We excluded in both mutants any possible off-target effects induced by ENU or CRISPR/Cas9, since we were able to completely rescue their pigmentation defects and partially rescue their precocious lethality.

Even though *snap29*^{K164*} and *snap29*^{N171fs} mutants exhibit similar phenotypes, when we compared their mRNA expression we found reduction only for *snap29*^{K164} mutants. This is likely due to nonsense mediated decay. Indeed, since the premature termination codon of *snap29*^{P171fs} is located too few nucleotides before the last exon-exon junction (You et al. 2007), the mRNA it likely not recognized by NMD and consequently not degraded. Since the only reported analysis of *SNAP29* mRNA level in a CEDNIK patient revealed a dramatic decrease compared to control patient, we chose *snap29*^{K164*} mutant as the most reliable CEDNIK model (Sprecher et al. 2005). However, *snap29*^{N171fs} mutant displays very similar gross phenotypes and might serve as a model for future CEDNIK patients.

Melanosomes, the melanin-containing organelles are lysosome derivatives (Huizing et al. 2008). Interestingly, melanocytes of *snap29*^{K164*} mutants do not show migration problems, but are rather smaller and devoid of melanin. Thus, the phenotype could be explained by the fact that the fusion step involving the docking of vesicles containing enzymes required for melanin biosynthesis to melanosomes might depend upon the formation a SNARE complex including Snap29. Such SNARE complex is known to include syntaxin 13 and VAMP7, which are respectively Qa- and R-SNAREs (Jani et al. 2015). Since the Qb/Qc-SNARE

component of this SNARE complex has not yet been identified, we can envisage that Snap29 could be the third missing SNARE protein. CEDNIK patients are not severely de-pigmented. However, it might be difficult to evaluate mild depigmentation considering the presence of ichthyosis and of keratoderma. Also, it is possible that mechanisms of pigmentation in fish and humans might differ.

6.2.2Snap29 is involved in nervous system development

snap29^{K164*} zebrafish mutants exhibit microcephaly and skin thickening, which are two main human CEDNIK patient manifestations. The poor life expectancy of CEDNIK patients, comprised between 5 and 12 years (Fuchs-Telem et al. 2011), is reflected in the precocious lethality that we observed in *snap29*^{K164*} mutants. Interestingly, for *Snap29* knockout mouse newborns, a feeding impairment was reported (Schiller et al. 2016). Similarly, stomachs of *snap29*^{K164*} mutants at 6 dpf appeared empty compared to wild type. At this developmental stage, larval nourishment does not relay anymore on yolk consumption, but rather requires swimming to feed (Strähle et al. 2012). Swimming and buoyancy in all teleost fish, in turn, requires a functional swim bladder, which need to be filled after 72 hpf by air gulped from water surface (Lanny et al. 2009). Both feeding impairment and the lack of swim bladder inflation prompted us to analyze any possible buccal cartilages, which resulted reduced in size, but comparable to wild type. The lack of buccal cartilages architecture defects led us to investigate possible motility and nervous system defects, to explain the lack of swim bladder inflation and the feeding impairment observed in *snap29*^{K164*} mutants. The reduced touch-evoked responses of *snap29*^{K164*} mutant larvae might correlate with nervous system manifestations including psychomotor retardation, observed in CEDNIK patients (Sprecher et al. 2005), and might explain the bladder and feeding problems. In addition, the absence of trigeminal motor neurons, which control mandibular arch muscles and mouth opening

(Higashijima et al. 2000), suggests a further cause for lack of swim bladder inflation and feeding impairment in *snap29*^{K164*} mutants. In support of this hypothesis, previous observations point to abnormal trigeminal development in another neurocutaneous syndrome called Sturge-Weber (Sanders 2010).

The analysis of motor neurons innervating skeletal muscles in the trunk in the mutant fish, revealed abnormal axon projections branching at different developmental stages. Importantly, SNAP25 and SNAP47 regulate neuronal circuit development and axon branching by mediating membrane fusion events required for neurotransmitters and brain-derived neurotrophic factor (BDNF) release from the presynaptic membrane (Shimojo et al. 2015; Sørensen et al. 2002). Considering the inhibitory role of SNAP29 in synaptic transmission at presynaptic membrane demonstrated in rat hippocampal neurons (Su et al. 2001; Pan et al. 2005), it is possible that the lack of Snap29 results in uncontrolled release of neurotransmitters and BDNF, eventually affecting axon branching. This hypothesis is supported by increase in spontaneous twitches within the chorion observed in 24 hpf *snap29* morphants compared to uninjected embryos. In fact, an opposite phenotype was observed in *snap25* morphants, with a decrease in twitches per minute and a decrease in neuronal axonal branches (Wei et al. 2013). Spontaneous movements have been shown to be required for normal motor neuron development and axonal branching. Indeed their decrease, induced in 24 hpf embryos by the treatment with the anesthetic tricaine, determine motor neuron axonal pathfinding defects (Menelaou et al. 2008). Overall, membrane fusion defects in the nervous system might hamper its development, leading to alterations that are reminiscent of CEDNIK syndrome.

6.2.3 Snap29 depletion affect blood vessels development and skeletal muscle organization

Axonal pathfinding is regulated by signaling molecules such as Slits and Roundabouts (Robo), Netrins and UNC5 receptors as Semaphorins, Plexins and Neuropilins which are also involved in angiogenesis (reviewed by Adams & Eichmann 2010). For this reason, we explored whether defective axonal branching observed in *snap29*^{K164*} mutants could correlate with blood vessel developmental defects. In line with this possibility, the analysis of Tg(*kdrl-1:GFP) snap29* morphants at 48 hpf revealed defective endothelial cell migration from the inter-segmental vessels. Alternatively to being a consequence of altered neuronal pathfinding, defective angiogenesis could also be the result of the impaired recycling of adhesion determinants such as the β1-integrin receptor, as observed in CEDNIK patient-derived fibroblasts (Rapaport et al. 2010). Besides nervous system defects, CEDNIK patients suffer also from neurogenic atrophy, which is a loss of muscle tone cause by wasting of nerves controlling muscles (Sprecher et al. 2005). Accordingly, *snap29*^{K164*} mutants show defective muscle fibers organization, which is likely to affect fish motility. Together, these features of the mutant fish could be useful for future understanding of CEDNIK pathogenesis.

6.2.4 Involvement of autophagy, cell division and Golgi function in CEDNIK pathogenesis?

Similar to autophagosome accumulation previously observed in *Drosophila Snap29B6-21* (Morelli et al. 2014), brains of *snap29*^{K164*} mutants zebrafish accumulate high levels of adapter autophagy p62 foci and total protein extracts of *snap29*^{K164*} mutants show a mild increase of the autophagosome markers LC3I and II, suggesting an impairment in late steps of autophagy. These data indicate that autophagy clearance is reduced in *snap29* mutant fish. Interestingly, mutations in human *EPG5* gene cause a severe neurodevelopmental disease called Vici syndrome, which shares with CEDNIK many clinical manifestations in pediatric patients, such

as microcephaly, brain development abnormalities, reduced conductance and atrophy of the retina and muscle hypotonia (Byrne et al. 2016). Importantly, *EPG5* encodes ectopic P-granules autophagy protein 5 (EPG5), which regulates autophagosome-lysosome fusion step (Cullup et al. n.d.). Moreover, similarly to *snap29*^{K164*} mutants zebrafish, Vici patients exhibit hypopigmentation and muscle biopsy from Vici patients accumulate p62. Thus, further studies are required to establish whether impaired autophagy plays a role in CEDNIK pathogenesis.

Congenital neurodevelopment syndromes like Roberts syndrome and Primary microcephaly (MCPH) are also caused by mutations in genes that regulate cell division (Genin et al. 2012; Musio et al. 2004). Different from our observations in *Drosophila*, but similar to human cells, Snap29 in zebrafish does not localize in the nuclei of dividing cells (this work; Morelli, Mastrodonato et al 2016). However, Snap29 is required to prevent cell division defect and apoptosis in both *Drosophila* and human cells (Morelli, Mastrodonato et al 2016). Consistent with this, *snap29* morphants and *snap29*^{K164*} mutants present a high number of apoptotic cells during early development and in particular the massive cell death occurring in the head of *snap29*^{K164*} mutants can explain the microcephaly that we observed at 7 dpf. Importantly, during *Drosophila* organs formation, when cell death is prevented, alterations that resemble tumor occur. Taken together, these observations suggest that CEDNIK patients might suffer multi-systemic unusually high levels of defective cells that are eliminated, perhaps, preventing appearance tumor-like defects as teratomas, but at the expenses of exhausting the ability of the embryo to compensate for presence of defective cells. Such pathogenic mechanism might apply to other syndromes due to impairment of cell division and KT genes.

Golgi apparatus (GA) is a key compartment, which regulates both autophagy and cell division. During autophagy GA represents, together with ER, a membrane source required for autophagosomes formation (reviewed by Geng & Klionsky 2010; Tooze & Yoshimori 2010).

Moreover, correct GA fragmentation is required for cell entry into mitosis and for the release of proteins from Golgi stacks, which are required for correct mitotic spindle formation and chromosomes segregation (Ayala & Colanzi 2017).

The localization of GFP-Snap29 in zebrafish interphase cells showed a strong signal enrichment in a perinuclear region, colocalizing with the GA marker GM130. This evidence supports a possible involvement of Snap29 in GA homeostasis, in line with a report showing that CEDNIK patient-derived fibroblasts possess a fragmented GA (Gonatas et al. 2006; Mizushima & Komatsu 2011). Interestingly, neurons of patients of several neurodegenerative diseases, as amyotrophic lateral sclerosis (ALS), corticobasal degeneration and Alzheimer's disease show GA defects (Gonatas et al. 2006; Mizushima & Komatsu 2011), indicating that maintenance of GA integrity and function might play a role, yet to be explored, in preventing neuronal CEDNIK manifestations. Overall, these preliminary results highlight a potential involvement of autophagy, GA, trafficking and mitosis in CEDNIK pathogenesis, albeit the mechanisms remain elusive.

7. References

Adams, R.H. & Eichmann, A., 2010. Axon guidance molecules in vascular patterning. *Cold Spring Harbor perspectives in biology*, 2(5), p.a001875. Available at: http://www.ncbi.nlm.nih.gov/pubmed/20452960 [Accessed September 22, 2017].

De Antoni, A. et al., 2005. The Mad1/Mad2 complex as a template for Mad2 activation in the spindle assembly checkpoint. *Current biology : CB*, 15(3), pp.214–25. Available at: http://www.ncbi.nlm.nih.gov/pubmed/15694304 [Accessed September 16, 2017].

Arden, S.D. et al., 2007. Myosin VI is required for targeted membrane transport during cytokinesis. *Molecular biology of the cell*, 18(12), pp.4750–61. Available at: http://www.ncbi.nlm.nih.gov/pubmed/17881731 [Accessed September 16, 2017].

Ayala, I. & Colanzi, A., 2017. Mitotic inheritance of the Golgi complex and its role in cell division. *Biology of the Cell*. Available at: http://doi.wiley.com/10.1111/boc.201700032 [Accessed September 5, 2017].

Baker, R.W. et al., 2015. A direct role for the Sec1/Munc18-family protein Vps33 as a template for SNARE assembly. *Science*, 349(6252), pp.1111–1114. Available at: http://www.sciencemag.org/cgi/doi/10.1126/science.aac7906.

Basto, R. et al., 2004. In vivo dynamics of the rough deal checkpoint protein during Drosophila mitosis. *Current biology : CB*, 14(1), pp.56–61. Available at: http://www.ncbi.nlm.nih.gov/pubmed/14711415 [Accessed December 12, 2014].

Basu, J. et al., 1999. Mutations in the essential spindle checkpoint gene bub1 cause chromosome missegregation and fail to block apoptosis in Drosophila. *The Journal of cell biology*, 146(1), pp.13–28. Available at: http://www.ncbi.nlm.nih.gov/pubmed/10402457 [Accessed September 16, 2017].

Bedell, V.M., Westcot, S.E. & Ekker, S.C., 2011. Lessons from morpholino-based screening in zebrafish. *Briefings in functional genomics*, 10(4), pp.181–8. Available at: http://www.ncbi.nlm.nih.gov/pubmed/21746693 [Accessed September 21, 2017].

Beznoussenko, G. V & Mironov, A.A., 2015. Correlative video-light-electron microscopy of mobile organelles. *Methods in molecular biology (Clifton, N.J.)*, 1270, pp.321–46. Available at: http://www.ncbi.nlm.nih.gov/pubmed/25702127 [Accessed October 31, 2016].

Blow, J.J. & Tanaka, T.U., 2005. The chromosome cycle: coordinating replication and segregation. Second in the cycles review series. *EMBO reports*, 6(11), pp.1028–34.

Bonifacino, J.S. & Glick, B.S., 2004. The Mechanisms of Vesicle Budding and Fusion. *Cell*, 116(2), pp.153–166. Available at: http://www.sciencedirect.com/science/article/pii/S0092867403010791 [Accessed September 15, 2017].

Boucrot, E. & Kirchhausen, T., 2007. Endosomal recycling controls plasma membrane area during mitosis. *Proceedings of the National Academy of Sciences of the United States of America*, 104(19), pp.7939–44. Available at:

http://www.pnas.org/cgi/doi/10.1073/pnas.0702511104 [Accessed November 3, 2017].

Brachner, A. & Foisner, R., 2011. Evolvement of LEM proteins as chromatin tethers at the nuclear periphery. *Biochemical Society Transactions*, 39(6), pp.1735–1741. Available at: http://www.ncbi.nlm.nih.gov/pubmed/22103517 [Accessed September 16, 2017].

Brand, A.H. & Perrimon, N., 1993. Targeted gene expression as a means of altering cell fates and generating dominant phenotypes. *Development (Cambridge, England)*, 118(2), pp.401–15. Available at: http://www.ncbi.nlm.nih.gov/pubmed/8223268 [Accessed September 26, 2017].

Brandizzi, F. & Barlowe, C., 2013. Organization of the ER-Golgi interface for membrane traffic control. *Nature reviews. Molecular cell biology*, 14(6), pp.382–92.

Buffin, E., Emre, D. & Karess, R.E., 2007. Flies without a spindle checkpoint. *Nature Cell Biology*, 9, pp.565–572. Available at: http://eutils.ncbi.nlm.nih.gov/entrez/eutils/elink.fcgi?dbfrom=pubmed&id=17417628&retmode=ref&cmd=prlinks%5Cnpapers2://publication/doi/10.1038/ncb1570.

Byrne, S. et al., 2016. EPG5-related Vici syndrome: a paradigm of neurodevelopmental disorders with defective autophagy. *BRAIN*, 139, pp.765–781. Available at: https://www.ncbi.nlm.nih.gov/pmc/articles/PMC4766378/pdf/awv393.pdf [Accessed September 25, 2017].

Cai, B., Caplan, S. & Naslavsky, N., 2012. cPLA2α and EHD1 interact and regulate the vesiculation of cholesterol-rich, GPI-anchored, protein-containing endosomes. *Molecular biology of the cell*, 23(10), pp.1874–88. Available at: http://www.ncbi.nlm.nih.gov/pubmed/22456504 [Accessed September 24, 2017].

Caldas, G. V. et al., 2015. The RZZ complex requires the N-terminus of KNL1 to mediate optimal Mad1 kinetochore localization in human cells. *Open Biology*, 5(11). Available at: http://rsob.royalsocietypublishing.org/content/5/11/150160.long [Accessed September 18, 2017].

Capalbo, L. et al., 2011. Rab5 GTPase controls chromosome alignment through Lamin disassembly and relocation of the NuMA-like protein Mud to the poles during mitosis. *Proceedings of the National Academy of Sciences of the United States of America*, 108(42), pp.17343–8. Available at: http://www.pubmedcentral.nih.gov/articlerender.fcgi?artid=3198372&tool=pmcentrez&rendertype=abstract [Accessed December 11, 2014].

Capalbo, L. et al., 2012. The chromosomal passenger complex controls the function of endosomal sorting complex required for transport-III Snf7 proteins during cytokinesis. *Open biology*, 2(5), p.120070. Available at: http://www.pubmedcentral.nih.gov/articlerender.fcgi?artid=3376741&tool=pmcentrez&rendertype=abstract [Accessed December 14, 2014].

Carmena, M. et al., 2012. The chromosomal passenger complex (CPC): from easy rider to the godfather of mitosis. *Nature Publishing Group*, 13. Available at: https://www.nature.com/nrm/journal/v13/n12/pdf/nrm3474.pdf [Accessed September 15, 2017].

Carpp, L.N. et al., 2006. The Sec1p/Munc18 protein Vps45p binds its cognate SNARE proteins via two distinct modes. *The Journal of cell biology*, 173(6), pp.927–36.

Cermak, T. et al., 2011. Efficient design and assembly of custom TALEN and other TAL effector-based constructs for DNA targeting. *Nucleic acids research*, 39(12), p.e82. Available at: https://academic.oup.com/nar/article-lookup/doi/10.1093/nar/gkr218 [Accessed September 13, 2017].

Chan, Y.W. et al., 2009. Mitotic control of kinetochore-associated dynein and spindle orientation by human Spindly. *The Journal of cell biology*, 185(5), pp.859–74. Available at: http://www.pubmedcentral.nih.gov/articlerender.fcgi?artid=2711594&tool=pmcentrez&rendertype=abstract [Accessed December 12, 2014].

Cheerambathur, D.K. et al., 2013. Crosstalk between microtubule attachment complexes ensures accurate chromosome segregation. *Science (New York, N.Y.)*, 342(6163), pp.1239–42. Available at: http://www.ncbi.nlm.nih.gov/pubmed/24231804 [Accessed September 18, 2017].

Cheeseman, I.M. & Desai, A., 2008. Molecular architecture of the kinetochore-microtubule interface. *Nature reviews. Molecular cell biology*, 9(1), pp.33–46.

Chen, D. et al., 2007. High-Resolution Crystal Structure and In Vivo Function of a Kinesin-2 Homologue in Giardia intestinalis. *Molecular biology of the cell*, 19(1), pp.308–317.

Cheng, X.T. et al., 2015. Axonal autophagosomes recruit dynein for retrograde transport through fusion with late endosomes. *Journal of Cell Biology*, 209(3), pp.377–386.

Cheung, P.P. & Pfeffer, S.R., 2016. Transport Vesicle Tethering at the Trans Golgi Network: Coiled Coil Proteins in Action. *Frontiers in Cell and Developmental Biology*, 4(March), pp.1–10. Available at: http://journal.frontiersin.org/Article/10.3389/fcell.2016.00018/abstract.

Ciferri, C. et al., 2008. Implications for Kinetochore-Microtubule Attachment from the Structure of an Engineered Ndc80 Complex. *Cell*, 133(3), pp.427–439. Available at: http://www.ncbi.nlm.nih.gov/pubmed/18455984 [Accessed September 16, 2017].

Civril, F. et al., 2010. Structural analysis of the RZZ complex reveals common ancestry with multisubunit vesicle tethering machinery. *Structure (London, England : 1993)*, 18(5), pp.616–26. Available at: http://www.ncbi.nlm.nih.gov/pubmed/20462495 [Accessed December 12, 2014].

Crowell, E.F. et al., 2014. Engulfment of the midbody remnant after cytokinesis in mammalian cells. *Journal of cell science*, 127(Pt 17), pp.3840–51. Available at: http://jcs.biologists.org/cgi/doi/10.1242/jcs.154732 [Accessed November 3, 2017].

Cullup, T. et al., Recessive mutations in EPG5 cause Vici syndrome, a multisystem disorder with defective autophagy. Available at: https://www.ncbi.nlm.nih.gov/pmc/articles/PMC4012842/pdf/emss-50537.pdf [Accessed September 26, 2017].

Dekanty, A. et al., 2012. Aneuploidy-induced delaminating cells drive tumorigenesis in Drosophila epithelia. *Proceedings of the National Academy of Sciences of the United*

States of America, 109(50), pp.20549–54. Available at: http://www.pubmedcentral.nih.gov/articlerender.fcgi?artid=3528526&tool=pmcentrez&rendertype=abstract.

Diao, J. et al., 2015. ATG14 promotes membrane tethering and fusion of autophagosomes to endolysosomes. Available at: https://www.ncbi.nlm.nih.gov/pmc/articles/PMC4442024/pdf/nihms685908.pdf [Accessed September 3, 2017].

Ding, B. et al., 2014. Phosphoprotein of human parainfluenza virus type 3 blocks autophagosome-lysosome fusion to increase virus production. *Cell host & microbe*, 15(5), pp.564–77. Available at: http://www.ncbi.nlm.nih.gov/pubmed/24832451 [Accessed December 11, 2014].

Dooley, K. & Zon, L.I., 2000. Zebrafish: a model system for the study of human disease. *Current opinion in genetics & development*, 10(3), pp.252–6. Available at: http://www.ncbi.nlm.nih.gov/pubmed/10826982 [Accessed September 26, 2017].

Doyon, Y. et al., 2008. Heritable targeted gene disruption in zebrafish using designed zinc-finger nucleases. *Nature Biotechnology*, 26(6), pp.702–708. Available at: http://www.ncbi.nlm.nih.gov/pubmed/18500334 [Accessed September 13, 2017].

Dubuke, M.L. & Munson, M., 2016. The Secret Life of Tethers: The Role of Tethering Factors in SNARE Complex Regulation. *Frontiers in Cell and Developmental Biology*, 4(May), pp.1–8. Available at: http://journal.frontiersin.org/Article/10.3389/fcell.2016.00042/abstract.

Elia, N. et al., Dynamics of endosomal sorting complex required for transport (ESCRT) machinery during cytokinesis and its role in abscission. Available at: https://www.ncbi.nlm.nih.gov/pmc/articles/PMC3064317/pdf/pnas.201102714.pdf [Accessed September 5, 2017].

Erhardt, S. et al., 2008. JCB : ARTICLE. , 183(5), pp.805–818.

Fader, C.M. & Colombo, M.I., 2009. Autophagy and multivesicular bodies: two closely related partners. *Cell death and differentiation*, 16(1), pp.70–8. Available at: http://www.ncbi.nlm.nih.gov/pubmed/19008921 [Accessed December 11, 2014].

Fartasch, M., 2004. The Epidermal Lamellar Body: A Fascinating Secretory Organelle. *The Medical Science*, 122, pp.xi–xii. Available at: http://www.jidonline.org/article/S0022-202X(15)30782-X/pdf [Accessed September 26, 2017].

Fasshauer, D. & Margittai, M., 2004. A transient N-terminal interaction of SNAP-25 and syntaxin nucleates SNARE assembly. *The Journal of biological chemistry*, 279(9), pp.7613–21. Available at: http://www.ncbi.nlm.nih.gov/pubmed/14665625 [Accessed April 11, 2015].

Fuchs-Telem, D. et al., 2011. CEDNIK syndrome results from loss-of-function mutations in SNAP29. *Br J Dermatol*, 164(3), pp.610–616.

Geng, J. & Klionsky, D.J., 2010. The Golgi as a potential membrane source for autophagy. *Autophagy*, 6(7), pp.950–1.

Genin, A. et al., 2012. Kinetochore KMN network gene CASC5 mutated in primary microcephaly. *Human molecular genetics*, 21(24), pp.5306–17. Available at: http://www.ncbi.nlm.nih.gov/pubmed/22983954 [Accessed October 24, 2016].

Giansanti, M.G. et al., 2015. Exocyst-Dependent Membrane Addition Is Required for Anaphase Cell Elongation and Cytokinesis in Drosophila R. Prekeris, ed. *PLOS Genetics*, 11(11), p.e1005632. Available at: http://dx.plos.org/10.1371/journal.pgen.1005632 [Accessed September 4, 2017].

Gillingham, A.K. et al., 2014. Toward a Comprehensive Map of the Effectors of Rab GTPases. *Developmental Cell*, 31(3), pp.358–373. Available at: http://www.sciencedirect.com/science/article/pii/S1534580714006534 [Accessed November 3, 2017].

Glover, D.M., 1989. Mitosis in Drosophila. *Journal of cell science*, 92 (Pt 2)(cdc), pp.137–146.

Gonatas, N.K., Stieber, A. & Gonatas, J.O., 2006. Fragmentation of the Golgi apparatus in neurodegenerative diseases and cell death. *Journal of the Neurological Sciences*, 246(1), pp.21–30.

Goshima, G. & Scholey, J.M., 2010. Control of Mitotic Spindle Length. *Annu. Rev. Cell Dev. Biol*, 26, pp.21–57. Available at: http://www.annualreviews.org/doi/pdf/10.1146/annurev-cellbio-100109-104006 [Accessed September 5, 2017].

Gould, G.W. & Lippincott-Schwartz, J., 2009. New roles for endosomes: from vesicular carriers to multi-purpose platforms. *Nature reviews. Molecular cell biology*, 10(4), pp.287–92. Available at: http://www.nature.com/doifinder/10.1038/nrm2652 [Accessed September 16, 2017].

Guo, B. et al., 2014. O-GlcNAc-modification of SNAP-29 regulates autophagosome maturation. *Nature cell biology*, 16(12). Available at: http://www.ncbi.nlm.nih.gov/pubmed/25419848 [Accessed November 25, 2014].

Güttinger, S., Laurell, E. & Kutay, U., 2009. Orchestrating nuclear envelope disassembly and reassembly during mitosis. *Nature reviews. Molecular cell biology*, 10(3), pp.178–91. Available at: http://www.ncbi.nlm.nih.gov/pubmed/19234477 [Accessed August 25, 2014].

Hamasaki, M. et al., 2013. Autophagosomes form at ER-mitochondria contact sites. *Nature*.

Haren, L. et al., 2006. NEDD1-dependent recruitment of the γ-tubulin ring complex to the centrosome is necessary for centriole duplication and spindle assembly. *The Journal of Cell Biology*, 172(4). Available at: http://jcb.rupress.org/content/172/4/505.long [Accessed September 5, 2017].

Higashijima, S., Hotta, Y. & Okamoto, H., 2000. Visualization of cranial motor neurons in live transgenic zebrafish expressing green fluorescent protein under the control of the islet-1 promoter/enhancer. *The Journal of neuroscience : the official journal of the Society for Neuroscience*, 20(1), pp.206–18. Available at: http://www.jneurosci.org/content/20/1/206.abstract.

Hirokawa, N. et al., 2009. Cytoskeletal motors: Kinesin superfamily motor proteins and

intracellular transport. *Nature Reviews Molecular Cell Biology*, 10. Available at: https://www.nature.com/nrm/journal/v10/n10/pdf/nrm2774.pdf [Accessed September 5, 2017].

Hirose, H. et al., 2004. Implication of ZW10 in membrane trafficking between the endoplasmic reticulum and Golgi. *The EMBO journal*, 23(6), pp.1267–78. Available at: http://www.pubmedcentral.nih.gov/articlerender.fcgi?artid=381410&tool=pmcentrez&rendertype=abstract [Accessed December 12, 2014].

Holt, M. et al., 2006. Identification of SNAP-47, a novel Qbc-SNARE with ubiquitous expression. *The Journal of biological chemistry*, 281(25), pp.17076–83. Available at: http://www.ncbi.nlm.nih.gov/pubmed/16621800 [Accessed December 11, 2014].

Holubcová, Z., Howard, G. & Schuh, M., 2013. Vesicles modulate an actin network for asymmetric spindle positioning. *Nature Cell Biology*, 15(8), pp.937–947. Available at: https://www.nature.com/ncb/journal/v15/n8/pdf/ncb2802.pdf [Accessed September 4, 2017].

Hong, W.J. & Lev, S., 2014. Tethering the assembly of SNARE complexes. *Trends in Cell Biology*, 24(1), pp.35–43. Available at: http://dx.doi.org/10.1016/j.tcb.2013.09.006.

Hood, F.E. et al., 2013. Coordination of adjacent domains mediates TACC3-ch-TOG-clathrin assembly and mitotic spindle binding. *The Journal of cell biology*, 202(3), pp.463–78. Available at: http://www.pubmedcentral.nih.gov/articlerender.fcgi?artid=3734082&tool=pmcentrez&rendertype=abstract [Accessed December 14, 2014].

Höök, P. & Peter, 2010. The mechanical components of the dynein motor. *TheScientificWorldJournal*, 10, pp.857–64. Available at: http://www.ncbi.nlm.nih.gov/pubmed/20454766 [Accessed September 5, 2017].

Howe, D.G. et al., 2013. ZFIN, the Zebrafish Model Organism Database: increased support for mutants and transgenics. *Nucleic Acids Research*, 41(D1), pp.D854–D860. Available at: http://www.ncbi.nlm.nih.gov/pubmed/23074187 [Accessed September 13, 2017].

Hsu, P.D. et al., 2013. DNA targeting specificity of RNA-guided Cas9 nucleases. *Nature biotechnology*, 31(9), pp.827–32. Available at: http://www.nature.com/doifinder/10.1038/nbt.2647 [Accessed September 13, 2017].

Huang, S., Tang, D. & Wang, Y., 2016. Monoubiquitination of Syntaxin 5 Regulates Golgi Membrane Dynamics during the Cell Cycle. *Developmental Cell*, 38, pp.73–85. Available at: http://dx.doi.org/10.1016/j.devcel.2016.06.001 [Accessed September 4, 2017].

Huizing, M. et al., 2008. Disorders of lysosome-related organelle biogenesis: clinical and molecular genetics. *Annual review of genomics and human genetics*, 9, pp.359–86. Available at: http://www.ncbi.nlm.nih.gov/pubmed/18544035 [Accessed September 21, 2017].

Itakura, E., Kishi-Itakura, C. & Mizushima, N., 2012. The hairpin-type tail-anchored SNARE syntaxin 17 targets to autophagosomes for fusion with endosomes/lysosomes. *Cell*, 151(6), pp.1256–69. Available at: http://www.ncbi.nlm.nih.gov/pubmed/23217709

[Accessed December 11, 2014].

Itakura, E. & Mizushima, N., 2013. Syntaxin 17: the autophagosomal SNARE. *Autophagy*, 9(6), pp.917–9.

Izuta, H. et al., 2006. Comprehensive analysis of the ICEN (Interphase Centromere Complex) components enriched in the CENP-A chromatin of human cells. *Genes to Cells*, 11(6), pp.673–684. Available at: http://www.ncbi.nlm.nih.gov/pubmed/16716197 [Accessed September 16, 2017].

Jahn, R. & Scheller, R.H., 2006. SNAREs--engines for membrane fusion. *Nature reviews. Molecular cell biology*, 7(9), pp.631–43.

Jakhanwal, S. et al., 2017. An activated Q-SNARE/SM protein complex as a possible intermediate in SNARE assembly. *The EMBO Journal*, 36(12), pp.1788–1802. Available at: http://emboj.embopress.org/lookup/doi/10.15252/embj.201696270.

Jani, R.A. et al., 2015. STX13 regulates cargo delivery from recycling endosomes during melanosome biogenesis. *Journal of Cell Science*, 128(17), pp.3263–3276. Available at: http://www.ncbi.nlm.nih.gov/pubmed/26208634 [Accessed September 21, 2017].

Jin, S.-W. et al., 2005. Cellular and molecular analyses of vascular tube and lumen formation in zebrafish. *Development*, 132(23). Available at: http://dev.biologists.org/content/132/23/5199?ijkey=6205e4b9043309e9f67b9a60ea87c51db0b94ccb&keytype2=tf_ipsecsha [Accessed September 25, 2017].

Joglekar, A.P., Bloom, K. & Salmon, E.D., 2009. In Vivo Protein Architecture of the Eukaryotic Kinetochore with Nanometer Scale Accuracy. *Current Biology*, 19(8), pp.694–699. Available at: http://www.ncbi.nlm.nih.gov/pubmed/19345105 [Accessed September 16, 2017].

Jongsma, M.L.M., Berlin, I. & Neefjes, J., 2014. On the move: organelle dynamics during mitosis. *Trends in Cell Biology*, pp.1–13.

Jongsma, M.L.M., Berlin, I. & Neefjes, J., 2015. On the move: Organelle dynamics during mitosis. *Trends in Cell Biology*, 25(3), pp.112–124. Available at: http://dx.doi.org/10.1016/j.tcb.2014.10.005.

Juhász, G. et al., 2007. Atg7-dependent autophagy promotes neuronal health, stress tolerance, and longevity but is dispensable for metamorphosis in Drosophila. *Genes & development*, 21(23), pp.3061–6. Available at: http://www.ncbi.nlm.nih.gov/pubmed/18056421 [Accessed October 28, 2016].

Karess, R., 2005. Rod-Zw10-Zwilch: a key player in the spindle checkpoint. *Trends in cell biology*, 15(7), pp.386–92. Available at: http://www.ncbi.nlm.nih.gov/pubmed/15922598 [Accessed December 12, 2014].

Karess, R.E. & Glover, D.M., 1989. rough deal: a gene required for proper mitotic segregation in Drosophila. *The Journal of cell biology*, 109(6 Pt 1), pp.2951–61. Available at: http://www.ncbi.nlm.nih.gov/pubmed/2512302 [Accessed September 11, 2017].

Katsani, K.R. et al., 2008. In vivo dynamics of Drosophila nuclear envelope components. *Molecular biology of the cell*, 19(9), pp.3652–66. Available at:

http://www.molbiolcell.org/cgi/doi/10.1091/mbc.E07-11-1162 [Accessed August 5, 2017].

Kaur, S. et al., 2014. An unmet actin requirement explains the mitotic inhibition of clathrin-mediated endocytosis. *eLife*, 3. Available at: https://www.ncbi.nlm.nih.gov/pmc/articles/PMC3924242/pdf/elife00829.pdf [Accessed November 3, 2017].

Kawaguchi, T. et al., 2009. The t-SNAREs syntaxin4 and SNAP23 but not v-SNARE VAMP2 are indispensable to tether GLUT4 vesicles at the plasma membrane in adipocyte. Available at: http://ac.els-cdn.com/S0006291X09024188/1-s2.0-S0006291X09024188-main.pdf?_tid=5b5899b0-8e35-11e7-bb35-00000aab0f02&acdnat=1504174728_3b715e8a38282461e4506dacf17041ce [Accessed August 31, 2017].

Khodjakov, A. & Rieder, C.L., 1999. The Sudden Recruitment of γ-Tubulin to the Centrosome at the Onset of Mitosis and Its Dynamic Exchange Throughout the Cell Cycle, Do Not Require Microtubules. *The Journal of Cell Biology*, 146(3). Available at: http://jcb.rupress.org/content/146/3/585?ijkey=1a77c208f668c6e9eb06f2568c59975ab3bc3e6f&keytype2=tf_ipsecsha [Accessed September 5, 2017].

Kimmel, C.B. et al., 1995. Stages of embryonic development of the zebrafish. *Developmental dynamics : an official public*, 203(3), pp.253–310.

Kimura, T. et al., 2017. Dedicated SNAREs and specialized TRIM cargo receptors mediate secretory autophagy. *The EMBO Journal*, 36(1), pp.42–60. Available at: http://emboj.embopress.org/lookup/doi/10.15252/embj.201695081.

Kinseth, M. a et al., 2007. The Golgi-associated protein GRASP is required for unconventional protein secretion during development. *Cell*, 130(3), pp.524–34.

Kiyomitsu, T., Murakami, H. & Yanagida, M., 2011. Protein interaction domain mapping of human kinetochore protein Blinkin reveals a consensus motif for binding of spindle assembly checkpoint proteins Bub1 and BubR1. *Molecular and cellular biology*, 31(5), pp.998–1011. Available at: http://www.ncbi.nlm.nih.gov/pubmed/21199919 [Accessed October 24, 2016].

Kline, S.L. et al., 2006. The human Mis12 complex is required for kinetochore assembly and proper chromosome segregation. *The Journal of Cell Biology*, 173(1), pp.9–17. Available at: http://www.ncbi.nlm.nih.gov/pubmed/16585270 [Accessed September 16, 2017].

Kok, F.O. et al., 2015. Reverse genetic screening reveals poor correlation between Morpholino-induced and mutant phenotypes in zebrafish HHS Public Access. *Dev Cell. January*, 12(321), pp.97–108. Available at: https://www.ncbi.nlm.nih.gov/pmc/articles/PMC4487878/pdf/nihms-642648.pdf [Accessed September 21, 2017].

Kondylis, V. & Rabouille, C., 2009. The Golgi apparatus: Lessons from *Drosophila*. *FEBS Letters*, 583(23), pp.3827–3838. Available at: http://www.ncbi.nlm.nih.gov/pubmed/19800333 [Accessed September 16, 2017].

Kops, G.J.P.L. et al., 2005. ZW10 links mitotic checkpoint signaling to the structural

kinetochore. *The Journal of cell biology*, 169(1), pp.49–60. Available at: http://www.pubmedcentral.nih.gov/articlerender.fcgi?artid=1351127&tool=pmcentrez&rendertype=abstract [Accessed December 12, 2014].

Lan, C.-C. et al., 2011. Disease Modeling by Gene Targeting Using MicroRNAs. In *Methods in cell biology*. pp. 419–436. Available at: http://www.ncbi.nlm.nih.gov/pubmed/21951541 [Accessed September 13, 2017].

Lan, W. & Cleveland, D.W., 2010. A chemical tool box defines mitotic and interphase roles for Mps1 kinase. *The Journal of Cell Biology*, 190(1). Available at: http://jcb.rupress.org/content/190/1/21 [Accessed September 24, 2017].

Lanny, C. et al., 2009. Development of zebra fi sh swimbladder : The requirement of Hedgehog signaling in speci fi cation and organization of the three tissue layers. *Developmental Biology*, 331(2), pp.222–236. Available at: http://dx.doi.org/10.1016/j.ydbio.2009.04.035.

Li, M. et al., 2016. Zebrafish Genome Engineering Using the CRISPR–Cas9 System. *Trends in Genetics*, 32(12), pp.815–827. Available at: http://linkinghub.elsevier.com/retrieve/pii/S0168952516301378 [Accessed September 8, 2017].

Li, Q. et al., 2011. Abca12-mediated lipid transport and Snap29-dependent trafficking of lamellar granules are crucial for epidermal morphogenesis in a zebrafish model of ichthyosis. *Disease models & mechanisms*, 4(6), pp.777–85. Available at: http://www.pubmedcentral.nih.gov/articlerender.fcgi?artid=3209647&tool=pmcentrez&rendertype=abstract [Accessed December 11, 2014].

Lieschke, G.J. & Currie, P.D., 2007. Animal models of human disease: zebrafish swim into view. *Nature Reviews Genetics*, 8(5), pp.353–367. Available at: http://www.nature.com/doifinder/10.1038/nrg2091.

Liu, Y. et al., 2016. Insights from the reconstitution of the divergent outer kinetochore of Drosophila melanogaster. *Open biology*, 6(2), p.150236. Available at: http://www.ncbi.nlm.nih.gov/pubmed/26911624 [Accessed September 16, 2017].

Liu, Z. & Zheng, Y., 2009. A requirement for epsin in mitotic membrane and spindle organization. *The Journal of cell biology*, 186(4), pp.473–80. Available at: http://www.pubmedcentral.nih.gov/articlerender.fcgi?artid=2733747&tool=pmcentrez&rendertype=abstract [Accessed December 2, 2014].

Lowe, M., 2011. Structural organization of the Golgi apparatus. *Current Opinion in Cell Biology*, 23(1), pp.85–93. Available at: http://www.ncbi.nlm.nih.gov/pubmed/21071196 [Accessed September 16, 2017].

Lu, Q. et al., 2015. Early steps in primary cilium assembly require EHD1- and EHD3-dependent ciliary vesicle formation. *Nature cell biology*, 17(3), pp.228–240.

Maldonado, M. & Kapoor, T.M., 2011. Constitutive Mad1 targeting to kinetochores uncouples checkpoint signalling from chromosome biorientation. *Nature Cell Biology*, 13(4), pp.475–482. Available at: http://www.ncbi.nlm.nih.gov/pubmed/21394085 [Accessed September 16, 2017].

Malsam, J., Kreye, S. & Söllner, T.H., 2008. Membrane fusion: SNAREs and regulation. *Cellular and molecular life sciences : CMLS*, 65(18), pp.2814–32. Available at: http://www.ncbi.nlm.nih.gov/pubmed/18726177 [Accessed December 8, 2014].

McBride, H.M. et al., 1999. Oligomeric complexes link Rab5 effectors with NSF and drive membrane fusion via interactions between EEA1 and syntaxin 13. *Cell*, 98(3), pp.377–386.

Megighian, A. et al., 2010. Arg206 of SNAP-25 is essential for neuroexocytosis at the Drosophila melanogaster neuromuscular junction. *Journal of cell science*, 123(Pt 19), pp.3276–3283.

Mellone, B.G. et al., 2011. Assembly of Drosophila Centromeric Chromatin Proteins during Mitosis S. Biggins, ed. *PLoS Genetics*, 7(5), p.e1002068. Available at: http://www.ncbi.nlm.nih.gov/pubmed/21589899 [Accessed September 16, 2017].

Menelaou, E. et al., 2008. Embryonic motor activity and implications for regulating motoneuron axonal pathfinding in zebrafish. *The European journal of neuroscience*, 28(6), pp.1080–96. Available at: http://www.ncbi.nlm.nih.gov/pubmed/18823502 [Accessed September 22, 2017].

Mizushima, N. & Komatsu, M., 2011. Autophagy: renovation of cells and tissues. *Cell*, 147(4), pp.728–41. Available at: http://www.ncbi.nlm.nih.gov/pubmed/22078875 [Accessed February 24, 2014].

Montero-balaguer, M. et al., 2009. Stable Vascular Connections and Remodeling Require Full Expression of VE-Cadherin in Zebrafish Embryos. , 4(6).

Morelli, E. et al., 2016. An essential step of kinetochore formation controlled by the SNARE protein Snap29. *Embo Journal*, 35(20), pp.1–40.

Morelli, E. et al., 2014. Multiple functions of the SNARE protein Snap29 in autophagy, endocytic, and exocytic trafficking during epithelial formation in Drosophila. *Autophagy*, 10(12), pp.2251–2268.

Musacchio, A., 2015. The Molecular Biology of Spindle Assembly Checkpoint Signaling Dynamics. *Current Biology*, 25(20), pp.R1002–R1018. Available at: http://linkinghub.elsevier.com/retrieve/pii/S0960982215010453 [Accessed September 16, 2017].

Musacchio, A. & Salmon, E.D., 2007. The spindle-assembly checkpoint in space and time. *Nature reviews. Molecular cell biology*, 8(5), pp.379–93.

Musio, A. et al., 2004. Recapitulation of the Roberts syndrome cellular phenotype by inhibition of INCENP, ZWINT-1 and ZW10 genes. *Gene*, 331, pp.33–40. Available at: http://www.ncbi.nlm.nih.gov/pubmed/15094189 [Accessed October 24, 2016].

Neto, H., Collins, L.L. & Gould, G.W., 2011. Vesicle trafficking and membrane remodelling in cytokinesis. *Biochem. J*, 437, pp.13–24. Available at: http://www.biochemj.org/content/437/1/13.full-text.pdf [Accessed September 5, 2017].

Nichols, R.J., Wiebe, M.S. & Traktman, P., 2006. The Vaccinia-related Kinases Phosphorylate the N' Terminus of BAF, Regulating Its Interaction with DNA and Its Retention in the

Nucleus. *Molecular Biology of the Cell*, 17(5), pp.2451–2464. Available at: http://www.ncbi.nlm.nih.gov/pubmed/16495336 [Accessed September 16, 2017].

Olmos, Y. et al., ESCRT-III controls nuclear envelope reformation. Available at: https://www.nature.com/nature/journal/v522/n7555/pdf/nature14503.pdf [Accessed September 5, 2017].

Pan, P.-Y. et al., 2005. SNAP-29-mediated modulation of synaptic transmission in cultured hippocampal neurons. *The Journal of biological chemistry*, 280(27), pp.25769–79. Available at: http://www.pubmedcentral.nih.gov/articlerender.fcgi?artid=1864940&tool=pmcentrez&rendertype=abstract [Accessed December 11, 2014].

Pankiv, S. et al., 2007. p62/SQSTM1 binds directly to Atg8/LC3 to facilitate degradation of ubiquitinated protein aggregates by autophagy. *The Journal of biological chemistry*, 282(33), pp.24131–45. Available at: http://www.ncbi.nlm.nih.gov/pubmed/17580304 [Accessed September 11, 2017].

Parichy, D.M. et al., 2011. NIH Public Access. , 238(12), pp.2975–3015.

Petr Svoboda, + & & Matyas Flemr, 2010. The role of miRNAs and endogenous siRNAs in maternal-to-zygotic reprogramming and the establishment of pluripotency. *EMBO reports*, 11(11). Available at: http://embor.embopress.org/content/embor/11/8/590.full.pdf [Accessed September 21, 2017].

Petrovic, A. et al., 2014. Modular assembly of RWD domains on the Mis12 complex underlies outer kinetochore organization. *Molecular cell*, 53(4file:///C:/Users/valeria/AppData/Local/Temp/1-s2.0-S109727651400080X-pdf), pp.591–605. Available at: http://www.ncbi.nlm.nih.gov/pubmed/24530301 [Accessed October 24, 2016].

Petrovic, A. et al., 2010. The MIS12 complex is a protein interaction hub for outer kinetochore assembly. *The Journal of cell biology*, 190(5), pp.835–52. Available at: http://www.ncbi.nlm.nih.gov/pubmed/20819937 [Accessed September 16, 2017].

Pohl, C. & Jentsch, S., 2009. Midbody ring disposal by autophagy is a post-abscission event of cytokinesis. *Nature Cell Biology*, 11(1), pp.65–70. Available at: http://www.ncbi.nlm.nih.gov/pubmed/19079246 [Accessed September 16, 2017].

Polgár, J. et al., 2003. Phosphorylation of SNAP-23 in activated human platelets. *The Journal of biological chemistry*, 278(45), pp.44369–76. Available at: http://www.ncbi.nlm.nih.gov/pubmed/12930825 [Accessed December 11, 2014].

Pouthas, F. et al., 2008. In migrating cells , the Golgi complex and the position of the centrosome depend on geometrical constraints of the substratum. , pp.2406–2414.

Przewloka, M.R. et al., 2011. CENP-C Is a Structural Platform for Kinetochore Assembly. *Current Biology*, 21(5), pp.399–405. Available at: http://www.ncbi.nlm.nih.gov/pubmed/21353555 [Accessed September 16, 2017].

Przewloka, M.R. et al., 2007. Molecular analysis of core kinetochore composition and assembly in Drosophila melanogaster. *PloS one*, 2(5), p.e478. Available at:

http://www.pubmedcentral.nih.gov/articlerender.fcgi?artid=1868777&tool=pmcentrez&rendertype=abstract [Accessed April 12, 2015].

Puhka, M. et al., 2012. Progressive sheet-to-tubule transformation is a general mechanism for endoplasmic reticulum partitioning in dividing mammalian cells. *Molecular Biology of the Cell*, 23(13), pp.2424–2432. Available at: http://www.ncbi.nlm.nih.gov/pubmed/22573885 [Accessed September 16, 2017].

Rapaport, D. et al., 2010. Loss of SNAP29 impairs endocytic recycling and cell motility. *PloS one*, 5(3), p.e9759. Available at: http://www.pubmedcentral.nih.gov/articlerender.fcgi?artid=2841205&tool=pmcentrez&rendertype=abstract [Accessed December 11, 2014].

Rizo, J. & Südhof, T.C., 2002. Snares and Munc18 in synaptic vesicle fusion. *Nature reviews. Neuroscience*, 3(8), pp.641–53. Available at: http://www.ncbi.nlm.nih.gov/pubmed/12154365 [Accessed December 11, 2014].

Rohrer, J. & Kornfeld, R., 2001. Lysosomal hydrolase mannose 6-phosphate uncovering enzyme resides in the trans-Golgi network. *Molecular biology of the cell*, 12(6), pp.1623–31. Available at: http://www.ncbi.nlm.nih.gov/pubmed/11408573 [Accessed September 16, 2017].

Rotem-Yehudar, R., Galperin, E. & Horowitz, M., 2001. Association of insulin-like growth factor 1 receptor with EHD1 and SNAP29. *The Journal of biological chemistry*, 276(35), pp.33054–60. Available at: http://www.ncbi.nlm.nih.gov/pubmed/11423532 [Accessed December 11, 2014].

Le Roy, C. & Wrana, J.L., 2005. Clathrin- and non-clathrin-mediated endocytic regulation of cell signalling. *Nature reviews. Molecular cell biology*, 6(2), pp.112–26. Available at: http://www.ncbi.nlm.nih.gov/pubmed/15687999 [Accessed January 22, 2014].

Royle, S.J., 2013. Protein adaptation: mitotic functions for membrane trafficking proteins. *Nature reviews. Molecular cell biology*, 14(9), pp.592–9. Available at: http://www.ncbi.nlm.nih.gov/pubmed/23942451 [Accessed December 12, 2014].

Royle, S.J., Bright, N.A. & Lagnado, L., 2005. Clathrin is required for the function of the mitotic spindle. *Nature*, 434(7037), pp.1152–7. Available at: http://www.pubmedcentral.nih.gov/articlerender.fcgi?artid=3492753&tool=pmcentrez&rendertype=abstract [Accessed December 14, 2014].

Sander, J.D. & Joung, J.K., 2014. CRISPR-Cas systems for editing, regulating and targeting genomes. *Nature Biotechnology*, 32(4), pp.347–355. Available at: http://www.nature.com/doifinder/10.1038/nbt.2842.

Sanders, R.D., 2010. The Trigeminal (V) and Facial (VII) Cranial Nerves: Head and Face Sensation and Movement. *Psychiatry (Edgmont (Pa. : Township))*, 7(1), pp.13–6. Available at: http://www.ncbi.nlm.nih.gov/pubmed/20386632 [Accessed September 22, 2017].

Santaguida, S. et al., 2011. Evidence that Aurora B is implicated in spindle checkpoint signalling independently of error correction. *The EMBO journal*, 30(8), pp.1508–19. Available at: http://www.ncbi.nlm.nih.gov/pubmed/21407176 [Accessed September 16,

2017].

Santoriello, C. & Zon, L.I., 2012. Hooked! Modeling human disease in zebrafish. *Journal of Clinical Investigation*, 122(7), pp.2337–2343. Available at: http://www.ncbi.nlm.nih.gov/pubmed/22751109 [Accessed September 26, 2017].

Sato, M. et al., 2011. Caenorhabditis elegans SNAP-29 is required for organellar integrity of the endomembrane system and general exocytosis in intestinal epithelial cells. *Molecular biology of the cell*, 22(14), pp.2579–87. Available at: http://www.pubmedcentral.nih.gov/articlerender.fcgi?artid=3135482&tool=pmcentrez&rendertype=abstract [Accessed December 11, 2014].

Saurin, A.T. et al., 2011. Aurora B potentiates Mps1 activation to ensure rapid checkpoint establishment at the onset of mitosis. *Nature Communications*, 2, p.316. Available at: http://www.ncbi.nlm.nih.gov/pubmed/21587233 [Accessed September 16, 2017].

Schardt, A. et al., 2009. The SNARE protein SNAP-29 interacts with the GTPase Rab3A: Implications for membrane trafficking in myelinating glia. *J. Neurosci. Res.*, 87(15), pp.3465–3479.

Schiel, J.A. & Prekeris, R., 2013. Membrane dynamics during cytokinesis. *Current opinion in cell biology*, 25(1), pp.92–8. Available at: http://www.ncbi.nlm.nih.gov/pubmed/23177492 [Accessed September 16, 2017].

Schiller, S.A. et al., 2016. Establishment of Two Mouse Models for CEDNIK Syndrome Reveals the Pivotal Role of SNAP29 in Epidermal Differentiation. *The Journal of investigative dermatology*, 136(3), pp.672–9. Available at: http://www.ncbi.nlm.nih.gov/pubmed/26747696 [Accessed October 24, 2016].

Schittenhelm, R.B., Chaleckis, R. & Lehner, C.F., 2009. Intrakinetochore localization and essential functional domains of Drosophila Spc105. *Embo J*, 28(16), pp.2374–2386. Available at: http://dx.doi.org/10.1038/emboj.2009.188%5Cnpapers2://publication/doi/10.1038/emboj.2009.188.

Schlaitz, A.-L. et al., 2013. REEP3/4 Ensure Endoplasmic Reticulum Clearance from Metaphase Chromatin and Proper Nuclear Envelope Architecture. *Developmental Cell*, 26(3), pp.315–323. Available at: http://www.ncbi.nlm.nih.gov/pubmed/23911198 [Accessed September 16, 2017].

Schmitt, H.D., Dsl1p/Zw10: common mechanisms behind tethering vesicles and microtubules. *Trends in Cell Biology*, 20, pp.257–268. Available at: http://ac.els-cdn.com.pros.lib.unimi.it/S0962892410000346/1-s2.0-S0962892410000346-main.pdf?_tid=4cb0c856-9e48-11e7-9182-00000aab0f6b&acdnat=1505942082_4c75732cdd5bfe917259a815cf0200a3 [Accessed September 20, 2017].

Schmitt, H.D., 2010. Dsl1p/Zw10: Common mechanisms behind tethering vesicles and microtubules. *Trends in Cell Biology*, 20(5), pp.257–268. Available at: http://dx.doi.org/10.1016/j.tcb.2010.02.001.

Scholey, J.M., Civelekoglu-Scholey, G. & Brust-Mascher, I., 2016. Anaphase B. *Biology*,

5(4). Available at: http://www.ncbi.nlm.nih.gov/pubmed/27941648 [Accessed September 5, 2017].

Schweitzer, J.K. et al., 2005. Endocytosis Resumes during Late Mitosis and Is Required for Cytokinesis. *Journal of Biological Chemistry*, 280(50), pp.41628–41635. Available at: http://www.ncbi.nlm.nih.gov/pubmed/16207714 [Accessed November 3, 2017].

Screpanti, E. et al., 2011. Direct Binding of Cenp-C to the Mis12 Complex Joins the Inner and Outer Kinetochore. *Current Biology*, 21(5), pp.391–398. Available at: http://www.ncbi.nlm.nih.gov/pubmed/21353556 [Accessed September 16, 2017].

Sengupta, P. et al., 2015. ER trapping reveals Golgi enzymes continually revisit the ER through a recycling pathway that controls Golgi organization. *Proceedings of the National Academy of Sciences*, 112(49), pp.E6752–E6761. Available at: http://www.ncbi.nlm.nih.gov/pubmed/26598700 [Accessed September 16, 2017].

Serio, G. et al., 2011. Small GTPase Rab5 participates in chromosome congression and regulates localization of the centromere-associated protein CENP-F to kinetochores. *Proceedings of the National Academy of Sciences of the United States of America*, 108(42), pp.17337–42. Available at: http://www.pubmedcentral.nih.gov/articlerender.fcgi?artid=3198334&tool=pmcentrez&rendertype=abstract [Accessed December 11, 2014].

Shepperd, L.A. et al., 2012. Report Phosphodependent Recruitment of Bub1 and Bub3 to Spc7/KNL1 by Mph1 Kinase Maintains the Spindle Checkpoint. *CURBIO*, 22, pp.891–899. Available at: http://www.cell.com/current-biology/pdf/S0960-9822(12)00338-7.pdf [Accessed September 24, 2017].

Shimojo, M. et al., 2015. SNAREs Controlling Vesicular Release of BDNF and Development of Callosal Axons. *Cell Reports*, 11(7), pp.1054–1066. Available at: http://dx.doi.org/10.1016/j.celrep.2015.04.032.

Sluder, G., 2014. One to only two: a short history of the centrosome and its. , 1888(July).

Smith, D.A., Baker, B.S. & Gatti, M., 1985. Mutations in genes encoding essential mitotic functions in Drosophila melanogaster. *Genetics*, 110(4), pp.647–70. Available at: http://www.ncbi.nlm.nih.gov/pubmed/3928429 [Accessed September 11, 2017].

Smith, L.L., Beggs, A.H. & Gupta, V.A., 2013. Analysis of Skeletal Muscle Defects in Larval Zebrafish by Birefringence and Touch-evoke Escape Response Assays. *J. Vis. Exp*, 8250925(10). Available at: www.jove.com [Accessed September 25, 2017].

Smoyer, C.J. & Jaspersen, S.L., 2014. Breaking down the wall: the nuclear envelope during mitosis. *Current Opinion in Cell Biology*, 26, pp.1–9. Available at: http://dx.doi.org/10.1016/j.ceb.2013.08.002 [Accessed September 4, 2017].

Smyth, J.T. et al., 2012. Phosphoregulation of STIM1 leads to exclusion of the endoplasmic reticulum from the mitotic spindle. *Current biology : CB*, 22(16), pp.1487–93. Available at: http://www.ncbi.nlm.nih.gov/pubmed/22748319 [Accessed September 16, 2017].

Sørensen, J.B. et al., 2006. Sequential N- to C-terminal SNARE complex assembly drives priming and fusion of secretory vesicles. *The EMBO Journal*, 25(5), pp.955–966. Available at: http://emboj.embopress.org/cgi/doi/10.1038/sj.emboj.7601003 [Accessed

April 11, 2015].

Sørensen, J.B. et al., 2002. The SNARE protein SNAP-25 is linked to fast calcium triggering of exocytosis. *Proceedings of the National Academy of Sciences of the United States of America*, 99(3), pp.1627–32. Available at: http://www.ncbi.nlm.nih.gov/pubmed/11830673 [Accessed September 22, 2017].

Spang, A., 2013. Retrograde traffic from the Golgi to the endoplasmic reticulum. *Cold Spring Harbor perspectives in biology*, 5(6), p.a013391. Available at: http://www.ncbi.nlm.nih.gov/pubmed/23732476 [Accessed September 26, 2017].

Sprecher, E. et al., 2005. A mutation in SNAP29, coding for a SNARE protein involved in intracellular trafficking, causes a novel neurocutaneous syndrome characterized by cerebral dysgenesis, neuropathy, ichthyosis, and palmoplantar keratoderma. *Am J Hum Genet*, 77(2), pp.242–251.

Stanley, H., Botas, J. & Malhotra, V., 1997. The mechanism of Golgi segregation during mitosis is cell type-specific. *Proceedings of the National Academy of Sciences of the United States of America*, 94(26), pp.14467–70. Available at: http://www.ncbi.nlm.nih.gov/pubmed/9405636 [Accessed September 16, 2017].

Strähle, U. et al., 2012. Zebrafish embryos as an alternative to animal experiments — A commentary on the definition of the onset of protected life stages in animal welfare regulations. *Reproductive Toxicology*, 33(2), pp.128–132. Available at: http://dx.doi.org/10.1016/j.reprotox.2011.06.121.

Strambio-De-Castillia, C., Niepel, M. & Rout, M.P., 2010. The nuclear pore complex: bridging nuclear transport and gene regulation. *Nature Reviews Molecular Cell Biology*, 11(7), pp.490–501. Available at: http://www.nature.com/doifinder/10.1038/nrm2928 [Accessed September 11, 2017].

Su, Q. et al., 2001. SNAP-29 : A general SNARE protein that inhibits SNARE disassembly and is implicated in synaptic transmission. , 98(24).

Südhof, T.C. & Rothman, J.E., 2009. Membrane Fusion: Grappling with SNARE and SM Proteins. *Science*, 323(5913). Available at: http://science.sciencemag.org/content/323/5913/474/tab-pdf [Accessed August 31, 2017].

Sun, Y. et al., 2007. Rab6 Regulates Both ZW10 / RINT-1 – and Conserved Oligomeric Golgi Complex-dependent Golgi Trafficking and Homeostasis. , 18(October), pp.4129–4142.

Sutton, R.B. et al., 1998. Crystal structure of a SNARE complex involved in synaptic ˚ resolution exocytosis at 2 . 4 A. , 395(September), pp.347–353.

Suzuki, K. & Verma, I.M., 2008. Phosphorylation of SNAP-23 by IκB Kinase 2 Regulates Mast Cell Degranulation. *Cell*, 134(3), pp.485–495. Available at: http://www.ncbi.nlm.nih.gov/pubmed/18692471 [Accessed August 31, 2017].

Takáts, S. et al., 2013. Autophagosomal Syntaxin17-dependent lysosomal degradation maintains neuronal function in Drosophila. *The Journal of cell biology*, 201(4), pp.531–9. Available at: http://www.pubmedcentral.nih.gov/articlerender.fcgi?artid=3653357&tool=pmcentrez&rendertype=abstract [Accessed November 22, 2014].

Takáts, S. et al., 2014. Interaction of the HOPS complex with Syntaxin 17 mediates autophagosome clearance in Drosophila. *Molecular biology of the cell*, 25(8), pp.1338–54. Available at: http://www.pubmedcentral.nih.gov/articlerender.fcgi?artid=3982998&tool=pmcentrez&rendertype=abstract [Accessed November 22, 2014].

Timme-Laragy, A.R., Karchner, S.I. & Hahn, M.E., 2012. Gene knockdown by morpholino-modified oligonucleotides in the zebrafish (Danio rerio) model: applications for developmental toxicology. *Methods in molecular biology (Clifton, N.J.)*, 889, pp.51–71. Available at: http://www.ncbi.nlm.nih.gov/pubmed/22669659 [Accessed September 21, 2017].

Tooze, S.A. & Yoshimori, T., 2010. The origin of the autophagosomal membrane. *Nature Publishing Group*, 12. Available at: http://www.nature.com.pros.lib.unimi.it/ncb/journal/v12/n9/pdf/ncb0910-831.pdf [Accessed September 26, 2017].

Uemura, O. et al., 2005. Comparative functional genomics revealed conservation and diversification of three enhancers of the isl1 gene for motor and sensory neuron-specific expression. *Developmental Biology*, 278(2), pp.587–606.

Ungar, D. & Hughson, F.M., 2003. SNARE Protein Structure and Function. *Annual Review of Cell and Developmental Biology*, 19(1), pp.493–517. Available at: http://www.ncbi.nlm.nih.gov/pubmed/14570579 [Accessed September 16, 2017].

Vagnarelli, P. et al., 2011. Repo-Man Coordinates Chromosomal Reorganization with Nuclear Envelope Reassembly during Mitotic Exit. *Developmental Cell*, 21(2), pp.328–342. Available at: http://www.ncbi.nlm.nih.gov/pubmed/21820363 [Accessed September 16, 2017].

Vallee, R.B., Varma, D. & Dujardin, D.L., 2006. ZW10 function in mitotic checkpoint control, dynein targeting and membrane trafficking: is dynein the unifying theme? *Cell cycle (Georgetown, Tex.)*, 5(21), pp.2447–51. Available at: http://www.ncbi.nlm.nih.gov/pubmed/17102640 [Accessed September 18, 2017].

Varma, D. et al., 2008. Direct role of dynein motor in stable kinetochore-microtubule attachment, orientation, and alignment. *The Journal of cell biology*, 182(6), pp.1045–54. Available at: http://www.pubmedcentral.nih.gov/articlerender.fcgi?artid=2542467&tool=pmcentrez&rendertype=abstract [Accessed November 17, 2014].

Varma, D. et al., 2006. Role of the kinetochore/cell cycle checkpoint protein ZW10 in interphase cytoplasmic dynein function. *The Journal of cell biology*, 172(5), pp.655–62. Available at: http://www.pubmedcentral.nih.gov/articlerender.fcgi?artid=2063698&tool=pmcentrez&rendertype=abstract [Accessed March 27, 2015].

Varma, D. et al., 2013. Spindle assembly checkpoint proteins are positioned close to core microtubule attachment sites at kinetochores. *Journal of Cell Biology*.

Vas, A.C.J. & Clarke, D.J., 2008. Aurora B kinases restrict chromosome decondensation to telophase of mitosis. *Cell Cycle*, 7(3), pp.293–296. Available at:

http://www.tandfonline.com/doi/abs/10.4161/cc.7.3.5381 [Accessed September 5, 2017].

Vedrenne, C., Klopfenstein, D.R. & Hauri, H.-P., 2005. Phosphorylation Controls CLIMP-63-mediated Anchoring of the Endoplasmic Reticulum to Microtubules. *Molecular Biology of the Cell*, 16(4), pp.1928–1937. Available at: http://www.ncbi.nlm.nih.gov/pubmed/15703217 [Accessed September 16, 2017].

Venkei, Z. et al., 2012. Spatiotemporal dynamics of Spc105 regulates the assembly of the Drosophila kinetochore.

Vilinsky, I. et al., 2002. A Drosophila SNAP-25 Null Mutant Reveals Context-Dependent Redundancy With SNAP-24 in Neurotransmission. , 271(September), pp.259–271.

van Vlijmen, T. et al., 2008. A unique residue in rab3c determines the interaction with novel binding protein Zwint-1. *FEBS letters*, 582(19), pp.2838–42. Available at: http://www.ncbi.nlm.nih.gov/pubmed/18625232 [Accessed December 12, 2014].

Wainman, A. et al., 2012. The Drosophila RZZ complex - roles in membrane trafficking and cytokinesis. *Journal of cell science*, 125(Pt 17), pp.4014–25. Available at: http://www.pubmedcentral.nih.gov/articlerender.fcgi?artid=3482314&tool=pmcentrez&rendertype=abstract [Accessed April 11, 2015].

Wan, X. et al., 2009. Protein Architecture of the Human Kinetochore Microtubule Attachment Site. *Cell*, 137(4), pp.672–684. Available at: http://www.ncbi.nlm.nih.gov/pubmed/19450515 [Accessed September 16, 2017].

Wang, H. et al., 2004. Human Zwint-1 specifies localization of Zeste White 10 to kinetochores and is essential for mitotic checkpoint signaling. *The Journal of biological chemistry*, 279(52), pp.54590–8. Available at: http://www.ncbi.nlm.nih.gov/pubmed/15485811 [Accessed December 12, 2014].

Wei, C. et al., 2013. miR-153 Regulates SNAP-25, Synaptic Transmission, and Neuronal Development. *PLoS ONE*, 8(2).

Wei, J.-H. & Seemann, J., 2017. Golgi ribbon disassembly during mitosis, differentiation and disease progression. *Current Opinion in Cell Biology*, 47, pp.43–51. Available at: http://www.ncbi.nlm.nih.gov/pubmed/28390244 [Accessed September 16, 2017].

Wickner, W., 2010. Membrane Fusion: Five Lipids, Four SNAREs, Three Chaperones, Two Nucleotides, and a Rab, All Dancing in a Ring on Yeast Vacuoles. *Annual Review of Cell and Developmental Biology*, 26(1), pp.115–136. Available at: http://www.ncbi.nlm.nih.gov/pubmed/20521906 [Accessed August 30, 2017].

Wojcik, S.M. & Brose, N., 2007. Regulation of Membrane Fusion in Synaptic Excitation-Secretion Coupling: Speed and Accuracy Matter. *Neuron*, 55(1), pp.11–24. Available at: http://linkinghub.elsevier.com/retrieve/pii/S0896627307004400 [Accessed August 31, 2017].

Woodruff, J.B., Drubin, D.G. & Barnes, G., 2010. Mitotic spindle disassembly occurs via distinct subprocesses driven by the anaphase-promoting complex, Aurora B kinase, and kinesin-8. *The Journal of Cell Biology*, 191(4). Available at: http://jcb.rupress.org/content/191/4/795 [Accessed September 5, 2017].

Wu, X., Xiang, X. & Hammer, J.A., 2006. Motor proteins at the microtubule plus-end. *Trends in Cell Biology*, 16(3), pp.135–143. Available at: http://www.sciencedirect.com/science/article/pii/S0962892406000237 [Accessed September 11, 2017].

Yadav, S. & Linstedt, A.D., 2011. Golgi Positioning. *Cold Spring Harbor Perspectives in Biology*, 3(5), pp.a005322–a005322. Available at: http://www.ncbi.nlm.nih.gov/pubmed/21504874 [Accessed September 16, 2017].

You, K.T. et al., 2007. Selective translational repression of truncated proteins from frameshift mutation-derived mRNAs in tumors. *PLoS biology*, 5(5), p.e109. Available at: http://www.ncbi.nlm.nih.gov/pubmed/17456004 [Accessed October 28, 2016].

Yu, H., 2006. Structural activation of Mad2 in the mitotic spindle checkpoint: the two-state Mad2 model versus the Mad2 template model. *The Journal of Cell Biology*, 173(2), pp.153–157. Available at: http://www.ncbi.nlm.nih.gov/pubmed/16636141 [Accessed September 16, 2017].

Zerial, M. & Mcbride, H., 2001. RAB PROTEINS AS MEMBRANE ORGANIZERS. , 2(February).

Zhao, C., Slevin, J.T. & Whiteheart, S.W., 2007. Cellular functions of NSF: not just SNAPs and SNAREs. *FEBS letters*, 581(11), pp.2140–9. Available at: http://doi.wiley.com/10.1016/j.febslet.2007.03.032 [Accessed September 16, 2017].

Zhen, Y. & Stenmark, H., 2015. Cellular functions of Rab GTPases at a glance. *Journal of Cell Science*, 128(17), pp.3171–3176. Available at: http://jcs.biologists.org/content/joces/128/17/3171.full.pdf [Accessed November 3, 2017].

Zhu, C. et al., 2011. Evaluation and application of modularly assembled zinc-finger nucleases in zebrafish. *Development*, 138(20), pp.4555–4564. Available at: http://www.ncbi.nlm.nih.gov/pubmed/21937602 [Accessed September 13, 2017].

Zhu, Q., Yamakuchi, M. & Lowenstein, C.J., 2015. SNAP23 regulates endothelial exocytosis of von Willebrand Factor. *PLoS ONE*, 10(8), pp.14–22.

Zu, Y. et al., 2013. TALEN-mediated precise genome modification by homologous recombination in zebrafish. *Nature Methods*, 10(4), pp.329–331. Available at: http://www.ncbi.nlm.nih.gov/pubmed/23435258 [Accessed September 13, 2017].